

Master Thesis in Sustainable Nuclear Energy Engineering

HEATREM: design and performance evaluations of an experimental natural circulation loop

Academic year 2024-2025

Professors

Bertani Cristina

Testoni Raffaella

Bonifetto Roberto

Candidate

D'Orazi Lorenzo s318464

Summary

Ab	stract		3
1.	Intro	luction	4
	1.1.	Misconceptions, advantages and challenges	5
	1.2.	Applications: Passive Residual Heat Removal System (PRHRS)	8
	1.3.	Description of existing NC facilities	11
	1.3.1.	ELSMOR	11
	1.3.2.	PASI	13
	1.3.3.	PASTELS	15
	1.3.4.	PROPHET2	16
2.	Conc	eptual design of a new experimental facility	19
	2.1.	Geometry description	19
	2.1.1.	Primary loop	19
	2.1.2.	Secondary loop	21
	2.1.3	Compact Heat Exchanger (CHX)	23
	2.2. Ope	erating conditions	26
3.	Buoy	ancy forces and equations analysis	27
	3.1.	Primary loop	35
	3.2.	Secondary loop	37
4.	Resu	lts	39
	4.1.	Primary loop	40
	4.1.1.	Variation in diameter	40
	4.1.2.	Variation in operative pressure	44
	4.1.3	Variation in heat source and sink height difference	44
	4.1.4	Variation in thermal power	46
	4.1.5.	Variation in HX pressure losses	49
	4.2.	Secondary loop	52
	4.2.1.	Variation in diameter	52
	4.2.2.	Variation in thermal power	59
	4.2.3	Variation in HX pressure losses	62
5.	Comp	parison between ATHLET and MATLAB simulations	76
:	5.1.	Geometry description	77
:	5.2.	Operative conditions	79
:	5.3.	Results	79
6.	Conc	lusions	82
7	Refer	rences	84

Abstract

This master thesis focuses on the conceptual design of an experimental facility to study the passive heat removal by natural circulation, with focus on the decay heat removal from a nuclear reactor.

This study includes the description of the natural circulation phenomena, a literature analysis on the passive heat removal systems already in use in nuclear reactors and the experimental natural circulation facilities already built and operated worldwide, the developments of a simplified steady-state theoretical model to be applied for the preliminary design of an experimental facility named HEATREM (HEAT REMoval) in the Energy Department of Politecnico of Turin, and finally the development of a nodalization of the facility and prediction of its performance by the ATHLET system code (Analysis of THermal-hydraulics of LEaks and Transients).

First of all, a system, consisting of only one loop, was simulated by a lumped parameter steady state model; the model and its implementation in Matlab is described by equations and flow charts. Parametric studies were carried out with this model to investigate the effects of the geometry and operating parameters as pressure, compact heat exchanger pressure losses, loop thermal power, pipe diameter and heat source-sink height difference on natural circulation flow rate and heat source inlet and outlet temperature.

Afterwards, a second loop has been introduced: a compact heat exchanger has been chosen to allow the heat transfer from the primary to the secondary loop. This double-loop system was first modeled by a steady-state simplified model. The results highlighted the capacity for both systems to operate in natural circulation conditions remaining in single phase. The whole system performances have been studied and the effects of the variations of pipes diameter, thermal load and compact heat exchanger pressure losses on the natural circulation flow rate and heat exchanger inlet and outlet temperatures for both primary and secondary loop have been analyzed.

Based on the results of this preliminary study, the geometry and operating conditions of lumped parameter model loop have been chosen and used in the development of a model by ATHLET.

The simulation of the lumped parameter system by ATHLET allowed to better describe the phenomena and the transient behavior during the start-up phase of the facility and the steady-state at the end of its operation.

1. Introduction

A Nuclear Power Plant (NPP) is defined as a thermal power plant, in which the heat source is represented by controlled fission reactions. Due to the exothermic nature of the reaction, the NPP must be continuously cooled with one or more cooling loops (depending on the plant type). Here, operative fluids carry the heat absorbed from the core to a heat sink which removes it. The operation of these systems is fundamental both during nominal operations and after the reactor shutdown. At the reactor shutdown, nuclear fission products continue in releasing heat and, if the heat is not removed in time, it can lead to serious damages and to compromise safety. This heat is known as Decay Heat and it generally corresponds to 6% of the nominal reactor power at the shutdown. As time proceeds its value decreases (*Figure 1*, from the Nuclear Regulatory Commission ANSI/ANS-5.1-1979 "Decay Heat Power in Light Water Reactors", 1979).

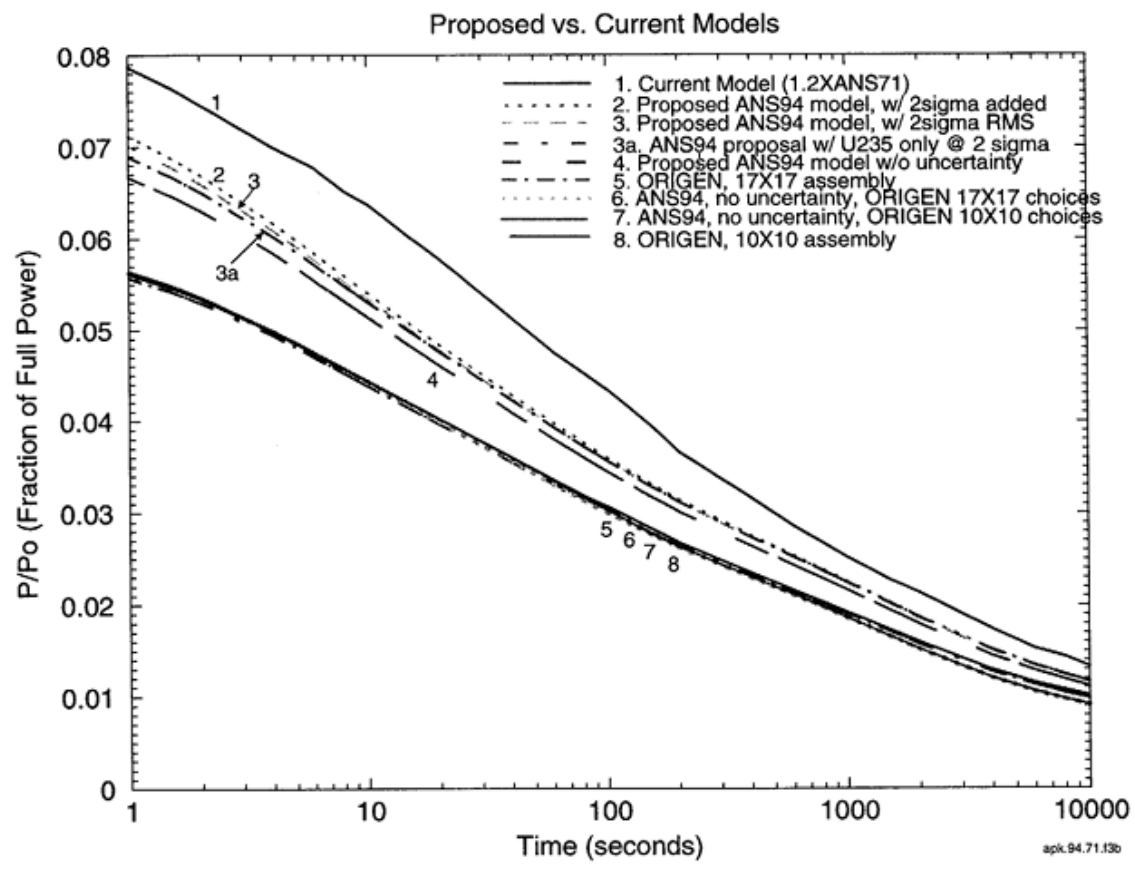


Figure 1. Decay heat distribution models in time.

When the shutdown is actuated in normal conditions, residual and decay heat are transferred directly to the ultimate heat sink by a Normal Residual Heat Removal System (NRHRS), bypassing turbines [1]. In case of emergency conditions, other emergency heat removal systems intervene. NRHRS are active heat removal systems, due to the presence of electrically driven pumps for coolant motion. Since the Fukushima Daiichi NPP accident in 2011, the topic safety of the NPP both in normal and accidental conditions has become more and more relevant. Passive emergency systems have been gradually introduced in NPP design, with the aim of replacing the active ones. These systems work without electric power and are

based on forces available in nature, such as gravity, buoyancy and capillarity. They have been deeply studied since 2011 and nowadays feature in all III⁺ - IV generation reactors.

1.1. Misconceptions, advantages and challenges

The topic has gained large relevance and further studies are necessary. Furthermore, natural circulation is often subject of misconceptions. The most common ones have been discussed here below.

Natural circulation is not a weak phenomenon.

Natural circulation is based on passive phenomena that exclude any electric supply. The lack of pumps is often misinterpreted as weak driving forces in the loop, manifested with low mass flow rates. Natural circulation is driven by gravity and, more important, buoyancy forces and its performance depends on the parameters as density difference and heat source-sink thermal centers height difference. Imposing a correct design can lead to an operative passive loop capable of replacing entirely its active corresponding system. An example is the ESBWR (Economic Simplified Boiling Water Reactor, III⁺ gen.), completely based on passive systems, whose passive cooling system performs with the same heat capacity of the ABWR (Advanced Boiling Water Reactor, III gen.), based on pumped cooling systems [2].

Natural circulation doesn't have a power threshold.

Despite the misleading name, natural circulation is a forced flow since its action is driven by buoyancy forces. The stronger the forces, the stronger the flow and the higher the mass flow rate. Density difference drives the buoyancy force, which means that, as long as a heat source and a heat sink are kept at a certain height difference (with the heat sink located at a higher coordinate with respect to the heat source), the natural circulation can occur. For this reason, NC Loops (NCL) for DHRS (Decay Heat Removal System) are considered the best option, even better than active DHRS. As the decay heat decreases, the temperatures and the mass flow rate of the system change, along with fluid's properties. For safety reasons related to the thermal power to be removed, NCL find applications for DHRS, containment cooling systems and even spent fuel pool applications in some cases, where the thermal load is limited and somehow manageable. Its employment in core cooling during nominal operations must undergo further analysis.

Therefore, the main advantages of natural circulation can be summed as:

1. Elimination of pumps

Due to its passive nature, fluid motion relies no more on electrically driven pumps. This implies lower production costs (due to the lack of components), lower maintenance costs and higher reliability.

2. Simple design

Due to the lack of specific components that may result bulky, these loops don't present many limitations in terms of size and simplicity.

3. Long-term uninterrupted operation and high reliability

In addition to the previous comments, the system is capable of long-term uninterrupted operation, as long as a heat source and a heat sink are provided, kept at different heights and the operative parameters are kept below safety thresholds. For this reason, NC systems have found applications as emergency systems in case of active systems failure [2].

Nevertheless, a NCL encounters many challenges that limit its full application. Recent studies have presented possible solutions which can entirely or partially solve some problems. The main challenges focus on the design, the reduction and control of the pressure losses, the management of instabilities and the identification of proper physical correlations capable of describing completely all transient stages [2].

1. Flexibility in the design

The performances of natural circulation systems are strongly dependent on the design of the loop, specifically on the height difference between the heat source and the heat sink thermal centers. Consequently, once the loop is built, its operation is limited. This important restriction is often added to the space limits that NPP has. Therefore, post-construction changes to increase loop performances are very difficult and invasive. For this reason, an accurate design of natural circulation loop is fundamental since, after the construction, it is very unlikely that further modifications will be possible, limiting the system applications [2].

2. Pressure losses reduction

Pressure losses have always been a challenge for all hydraulic circuits and so for natural circulation loops. The lower the pressure losses in the system, the easier the fluid circulation with higher values of mass flow rates. Logically, simple design and smooth pipes are the main solutions. Further options could be:

- Use large diameters.
 - Increasing pipes diameter leads to slower fluid velocity and smaller pressure losses. Moreover, it allows higher mass inventory and slows transients, especially at the start of the loop operations. The increased coolant inventory in the system reduces the probability of uncovering the core in case of LOCA (Loss Of Coolant Accident), increasing plant safety. However, an increase in the diameter causes a decrease in the mass flow rate (at constant driving force) and an increase in residence time of the fluid in the core, leading to an increase in fluid enthalpy and risk of overpressurization. Furthermore, costs increase with the diameter.
 - Large diameters reduce the pressure losses but specific analysis are required to optimize advantages guaranteeing safety and costs.
- Elimination of components.
 - The presence of mechanical components increases the localized pressure losses in the circuit. Logically, a safe solution is to remove, when possible, those components. In some other cases, a valid option is to substitute them with more innovative components. An example is the employment of natural gravity separators instead of mechanical separators. Separators are used in BWRs in

cooling systems to divide steam from liquid. Although natural gravity separators provide the same effects of mechanical separators, deeper studies are necessary to verify the effects on carryover and carryunder phenomena. These two concepts are related to the presence of liquid drops in steam-only regions and steam bubbles in liquid-only respectively. These events affect safety of components and systems [2].

3. Instabilities

Instabilities represent one of the main challenges of the topic. They are linked with the transients of the system and their effects are very strong at the beginning of the operation of the system, when natural circulation is not at full regime yet. They manifest through oscillations in mass flow rate and temperatures and, if not managed, they can lead to undesired events as Flashing Instability Induced Water Hammer (FIIWH) [7]. Instabilities of many type exist and the most common are:

- Density and Pressure Wave Oscillations (DWO and PWO) [10]
- Flashing [7] [8] [9]
- Geysering [7] [8] [9]
- Direct Contact Condensation phenomena (DCC)

The smoother the oscillations, the easier the operation of the system and the sooner nominal operation is reached. For what concerns the reduction of mass flow rate oscillations, a valid option is the introduction of an orifice at the inlet of the heated section. Although the presence of an orifice deeply affects the instabilities, it also adds localized pressure losses in the circuit reducing the mass flow rate. Instabilities are also strongly linked to the concept of Critical Heat Flux (CHF) that will be discussed later on [2].

4. Verification of valid models for all stages of natural circulation transients

During the transient of a natural circulation system, many phenomena can occur and it is fundamental to have all the correct correlations capable of describing the fluid behavior. While it is easier to describe the system's behavior a long time from its activation, the beginning of operation, where changes are the highest and instabilities dominate, still need validation. This period comprehends the amount of time that cold fluid requires to store the incoming heat till the beginning of natural circulation, and it's called Low Pressure Low Flow (LPLF) regime. This phase can cause pressure oscillations that lead to mechanical failures and undesired phenomena as early CHF. The "quasi-stagnant" fluid in low-pressure conditions at the beginning of the natural circulation process may lead to early reaching of saturation conditions and the arise of instabilities. The main solution is to try to fix the operative pressure inside the system and control the subcooling of the fluid at the heat source inlet [2].

Given that, a natural circulation loop always features specific important elements: one or more heat sources, a heat sink, a connecting pipes system, a riser and a downcomer.

Heat source

It corresponds to the volume in which cold fluid gains heat. This element is fundamental for the magnitude of the driving force and of fluid conditions [2]. For what concerns a NPP, it corresponds to the core (in which the fission reactions occur) for a primary loop and to the heat exchanger for the secondary loop. Regarding experimental facilities, heat sources are often represented by electric heaters.

Riser

It corresponds to the rising pipe that connects the outlet of the heat source to separators (if present) or the loop heat sink. It affects stability in the loop, especially for two-phase flow [2]. This element can be thermally insulated (often in experimental facilities) or not, causing heat dissipation.

Heat sink

It's the region in which the fluid exchanges the gained heat from the source. Depending on the configuration of the loop, heat sinks can be represented by water reservoirs as rivers, lakes, seas or oceans (generally named "ultimate" heat sinks), or heat exchangers (HX), that connect one loop to another. To establish natural circulation, heat sinks must always have higher coordinates than heat sources. As for heat source, this component plays a crucial role in the magnitude of buoyancy forces and in loop stability [2] [3].

Downcomer

It corresponds to the descending pipe that connects separators (if present) or the heat sink to the heat source [2]. As the riser, it can be thermally insulated to avoid heat dissipation.

Detailed studies have proven how loop's performance have strong dependence on specific design parameters as:

- Pipes diameter [3] [4]
- Loop's wall thickness and material [3]
- Loop's aspect ratio [3]
- Initial forced circulation presence [3]
- Subcooling degree level at heater inlet [3]
- Operative pressure [3]
- Heat source heat sink height difference [4]

1.2. Applications: Passive Residual Heat Removal System (PRHRS)

One of the main passive systems is the Passive Residual Heat Removal System (PRHRS), involved in the removal of heat decay produced in core after the shutdown. Many existing NPP already feature PRHRS or other passive systems, or in some other cases these systems are under further evaluations (*Table 1*). Their application can involve short or long operations time: the system operates for 72 hours in the first case, or longer in the second.

Reactor	Type and power	Passive system	Operation time	Comment
HPR-1000	III ⁺ gen., PWR, ∼1200 MW _e .	EPRHR	Short	Used for PRHR
APR+	III-III ⁺ gen., Advanced PWR,	PAFS	Short	Used for emergency auxiliary feedwater system in case of FLB.
	$\sim 1400 \ \mathrm{MW_e}.$	APDHRS	Long	Used for PRHR.
CPR-1000	II gen., PWR,	<i>ACPRHRS</i>	Long	Used for EPRHR.
CF K-1000	$\sim 1000 \ MW_e$.	WCPRHRS	Short	Used for EPRHR.
IPWR	III ⁺ gen, SMR of PWR type, ~220 MW _{th} .	PRHRS	Short	Used for PRHR.
NuScale	III ⁺ gen., modular IPWR, ~60 MW _e per module (up to 12 modules at most).	DRHS	Short	Used for PRHR.
SMART	IV gen., SMR of PWR type, ~100 MW _e .	New ECT	Long	Used for PRHR.

Table 1. Example of passive safety systems already present or under evaluation in existing NPP.

Hydraulic loops involve several classification elements, the most common are:

- Fluid phase (single, two-phase or supercritical phase flow) [2].
- Buoyancy forces generation method (adiabatically or due to thermosyphon effect) [2].
- Heat source heat sink orientation (HHHC, HHVC, VHHC, VHVC) [2].
- Coupling method (series, parallel or combinations of the two) [2].
- Flow type (gravity dominant, friction dominant or intermediate flow) [2][6].

In general, the operation time of these systems is function of many factors but most importantly depends on the characteristics of the heat sink, identified as the component which receives the heat from the heat source and removes it. Different layouts and characteristics have been studied, each having advantages and challenges.

The components of the loop can also find different classifications based on their nature. The most important classification is related to heat sinks, which can be grouped in two main classes:

a) Water tank or pool heat sinks

They use natural or artificial water reservoirs as ultimate heat sink and the heat removal is carried by liquid water. The larger the water heat capacity (associated to a larger water basin volume), the larger the amount of heat that a cooling loop can deliver to the heat sink. This type of heat sinks is associated mostly to short terms operations due to safety issues. As temperature increases, thermal stratification effect may form and the efficiency

of the heat exchange process at pool level may decrease due to the increase of pool temperature. Furthermore, as temperature in pool increases evaporation may occur, reducing the coolant inventory, the efficiency of the heat transfer process and the safety of the plant. In these types of systems, safety is guaranteed as long as the heat exchanger is kept below water surface. If this requirement is not fulfilled, serious damage, overpressurization and a wrong management of the heat can verify. However, if the water reservoir is sufficiently large (in the order of lakes or more), it can be used for longer operations [1].

b) Free air environment heat sinks

They use the atmosphere as ultimate heat sink, exploiting the natural free air convection. Thanks to this, it generally finds applications for long-term operations. However, its efficiency is strongly dependent on the size of the heat transfer area due to the low heat transfer coefficient values and these types of structure are often associated to large cooling towers [1].

The heat sink can be described by many parameters, but the most important are its reliability, the heat transfer properties, the HX area and safety related issues. *Table 2* shows the main advantages and disadvantages of each heat sink type:

Parameter	Water tank heat sinks	Airstream heat sinks
Heat transfer	High convective heat transfer	Small convective heat transfer
efficiency	coefficient.	coefficient.
Reliability	Strongly relies on water tank capacity. Generally used for operations shorter than 72 hours.	Considered as an infinite reservoir, used for long term operations.
HX area	Doesn't require large areas.	Requires large heat transfer surfaces often along with a coooling tower.
Safety	Safety is kept as long as the water level is above the heat exchanger and the effectiveness of the structure is monitored.	If the design is set correctly, the system is capable of operating correctly for unlimited amounts of time.

Table 2. Comparison of the characteristics of water tank and airstream heat sinks.

It is notable how, for what concerns heat transfer efficiency, water tank heat sinks are far better than airstream ones in terms of efficiency and space. However, long term operations represent a serious issue for water tanks since their efficiency reduces drastically, threatening the safety of the plant.

In order to use the listed advantages of water tank heat sinks along with the capability of airstream heat sinks to operate for long terms, recent studies have suggested some possible innovative layouts:

a) Initial use of water cooled condenser (until 72 hours), followed by air cooled condenser (after 72 hours of operation).

- b) Use of a condenser capable to use both water and airstream.
- c) Connection of an airstream condenser to the water tank condenser to allow water cooling and avoid water refill.
- d) Water cooled condenser coupled with sub-atmospheric two phase loop to remove heat from water cooled condenser, discharging it in environment through air cooled condenser.

These options are still purely theorical and under further evaluations. The main issue regarding the list above is related to the correct dimensioning of heat exchanger for the airstream system. The inability of post-construction modifications and the large and precise designs required to ensure its efficiency represent a big challenge [1].

1.3. Description of existing NC facilities

Many existing facilities already focus on natural circulation systems. The application of these passive systems is not always the same, for example while some facilities focus on decay heat removal systems, some others analyze passive containment cooling systems. Among the existing facilities, it was chosen to analyze four significant facilities: ELSMOR [16], PASI [17], PASTELS [18] [19] and PROPHET2 [20].

1.3.1. ELSMOR

ELSMOR (European Licensing of Small MOdular Reactors) is an experimental facility designed and built in SIET, in Piacenza (Italy). The system focuses on natural circulation in decay heat removal systems and the aim of the facility is to assess and verify the safety of these systems in European LW-SMR DHRS thanks to natural circulation systems. The structure features two loops (a primary and a secondary), connected by a plate-type compact heat exchanger (CHX, or Safety-Compact Steam Generator S-CSG). The ultimate heat sink consists in a water pool in which a vertical tube HX is submerged. During all the tests, secondary loop was kept at two-phase natural circulation flow, while primary loop thermohydraulic conditions were varied. The whole structure is shown in *Figure 2* and *Figure 3*.

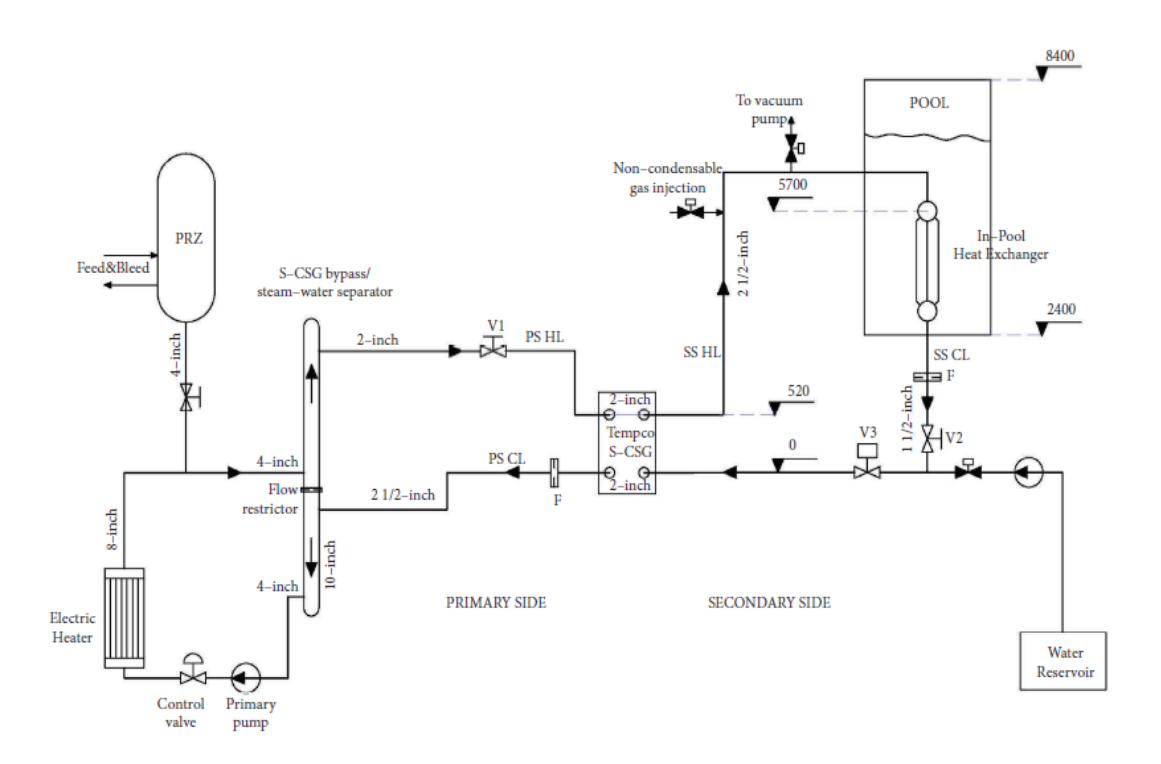


Figure 2. ELSMOR schematic design.

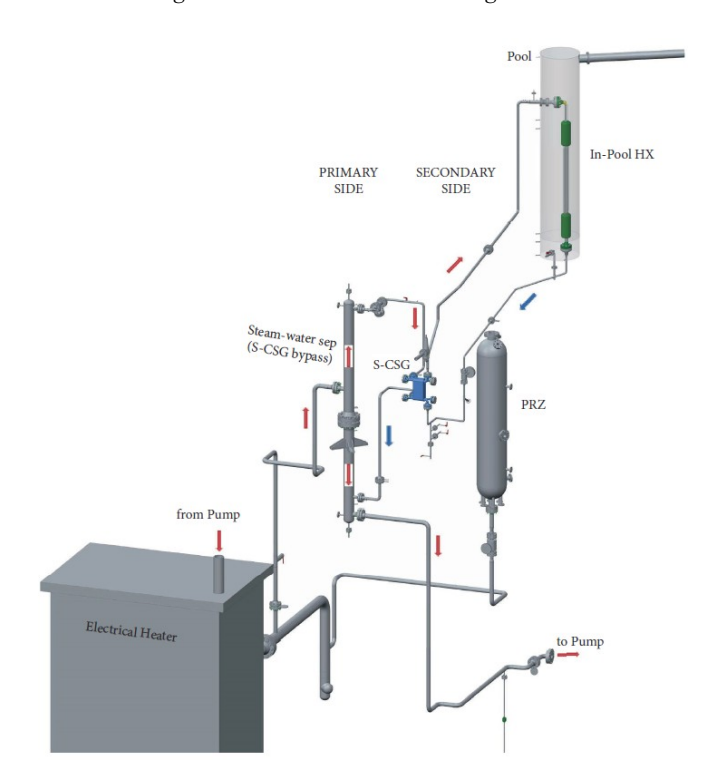


Figure 3. ELSMOR 3-D implant scheme.

Primary loop

The primary loop can operate both in single-phase liquid flow and two-phase flow. In the first case, water is circulated by the primary pump and is split partly through the S-CSG and partly back to the pumps by flow restrictors. The pressure is controlled by a feed and bleed method, where a pressurizer regulates the water extracted or removed based on the operation

conditions. In two-phase flow, the steam-water mixture is sent to steam-water separators which divide the two fluids: the liquid phase is sent back by gravity to primary pumps and the steam is directed to S-CSG.

Secondary loop

As said, the secondary loop operates in two-phase natural circulation flow, driven by the heat supplied by the S-CSG and dissipated through the vertical tube HX in the water tank. The water tank is equipped with a water supply and drainage system to control its level during transients and it's kept open to the atmosphere.

S-CSG

The plate-type compact heat exchanger presents a Chevron type configuration on plates surface that enhances the heat transfer mechanism. The one chosen for this facility is a commercial TEMPCO plate heat exchanger TCBC2102H* 130, which features 130 plates and satisfies the pressure and power requirements.

All pipework and plant components are thermally insulated to limit environmental heat losses. In addition, the plant features three main valves (V1, V2 and V3) capable of establishing natural circulation on the primary side (V3) and of adjusting pressure losses (V1 and V2).

α	4	1'4'		. 0. 1	•	TT 11	2
.>1	<i>i</i> stem	conditions	are s	necitied.	1n	Innie	1
	y Dictili	Comandida	are 5	pecifica	111	Indic	∠ .

Parameter	Value	Unit Measure
Primary side pressure	130	MPa
Secondary side pressure	10	MPa
Power	1	MW
S-CSG plates number	130	-
S-CSG plates Chevron angle	45	O
"Vertical tube HX" tubes number	5	-
Vertical tube HX outer diameter	2	inches
Vertical tube HX length	2	m
Water pool diameter	1	m
Water pool height	5.5	m

Table 3. ELSMOR technical and geometrical parameters.

The tests performed have proven the effects of specific parameters on the loop performance, highlighting that the Filling Ratio (F.R) is the most critical one, followed by the water pool temperature and level, and primary loop conditions.

1.3.2. PASI

The PASI (not an acronym but a nickname for "passive heat removal system") is a test facility designed and constructed at LUT University in Finland for the thermal-hydraulic studies of an open-loop passive containment heat removal system (PRHR-C, Passive Residual Heat Removal for Containment) for nuclear reactors. The facility presents a pressure vessel that simulates containment conditions and a loop composed of a heat exchanger, interconnecting

pipelines and a water reservoir. The system operates at low pressure conditions (from 0.1 to 0.5 MPa) and this can lead to easy boiling oscillations due to large density differences between water and steam. This oscillatory behavior can enhance the heat removal mechanism, but it can cause dynamic loads and fatigue on piping system. The system is triggered whenever the containment atmosphere gets hotter than water in cooling system loop, but the structure is thought to intervene in emergency cases.

The generic structure of the loop presents heat exchangers located in the dome part of the containment, connecting riser and downcomer pipelines between water tank and heat exchanger, and emergency heat removal water tank outside the containment (kept at atmospheric pressure) with a "half-submerged" sparger. The sparger prevents pool cold water direct flow into the riser with subsequent condensation, avoiding the probability of water hammer phenomena. The heat exchanger inside the containment is of "tube bank" type and presents "inversed J"-shaped tubes. When steam is injected inside the containment vessel with a consequent increase in pressure, natural circulation process is activated. During the operation of the facility, steam condensates on the heat exchange tubes and walls of the containment vessel, drained out from the bottom via a condensate drain pipeline and sent to a small drain tank.

The parameters used for PASI design are summed in *Table 4*, while the structure is shown in *Figure 4*.

Parameter	Value	Unit Measure
Containment vessel volume	3.4	m^3
Containment vessel max. pressure	0.5	MPa
Containment vessel max. temperature	170	°C
Number of heat exchanger tubes	15	-
Loop height	8.1	m
Heat exchanger height	2.8	m
Heat exchanger tube outer diameter	38	mm
Riser pipeline outer diameter	114.3	mm
Downcomer pipeline outer diameter	88.9	mm
Height scale compared to a real PCCS	1:2	-

Table 4. PASI technical and geometrical parameters.

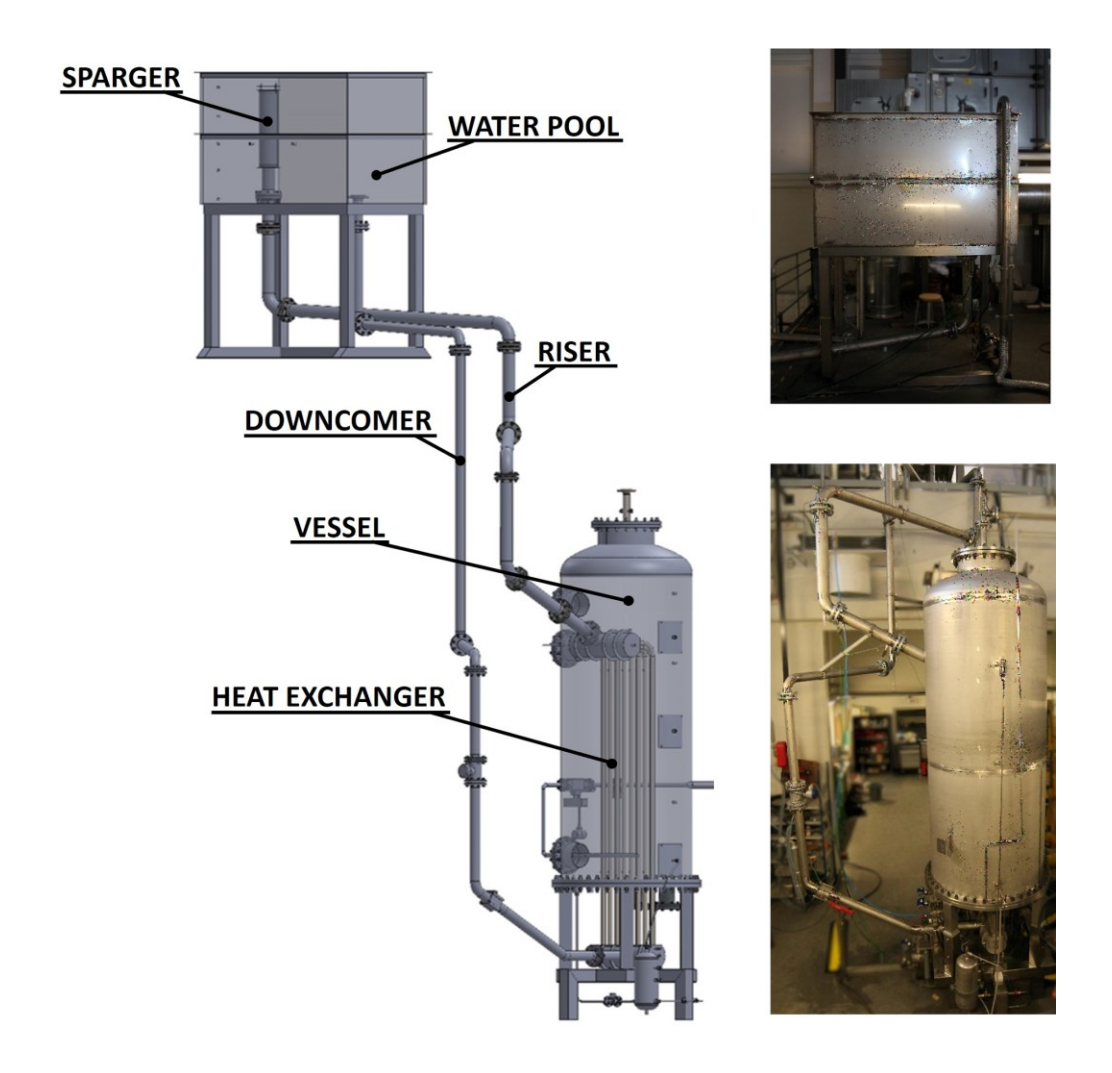


Figure 4. PASI design scheme.

The system tests aim to show the effects of heat-up and cool-down transients, the efficiency of the natural circulation loop in time and the maximum sustainable thermal load. The results show that the system is capable of operating in stable single-phase flow for a certain period, after which the increase in temperature causes the switch to unstable two-phase flow. During the first period, the loop stabilizes on the maximum value of manageable thermal power capable, after which increasing oscillations manifest the arise of flow instabilities. The experiments are ended when water pool temperature reaches saturation values.

1.3.3. PASTELS

PASTELS ("Passive Systems: Simulating the Thermal-hydraulics with Experimental Studies) project has been funded by the European Commission "Euratom H2020" Programme between 2020 and 2024 and it's devoted to the study of passive systems relying on natural circulation. The project consists of two different systems: SACO ("SAfety Condenser" system), which focuses on the decay heat removal process, and CWC ("Containment Wall Condenser"), which focuses on the containment cooling process.

SACO

The SACO test models have been implemented both for full-size PWR secondary loops and for experimental facilities. For what concerns the second case, the system has been inspired by PKL ("Primärkreislauf Versuchsanlage", which in german means "Primary Circuit Test Facility") in Germany. The structure features a "vertical tubes" heat exchanger with four tubes between two manifolds, fully submerged in a water pool. The loop is designed to operate at maximum pressure of 80 bar with 450 kW of thermal load. The dimensions of the experimental facility are expressed in *Table 5*.

Parameter	Value	Unit Measure
Water pool height	7.6	m
Water pool inner diameter	1.4	m
Inner "vertical tube" diameter	34	mm
"Vertical tube" length	5.4	m

Table 5. SACO technical and geometrical parameters.

CWC

Similarly to SACO's discussion, CWC system works along with PASI experimental facility for passive containment cooling systems in an AES-2006 reactor. The input of the tests are the same as *Table 4*.

The tests show the influence of specific parameters on loop performance, such as thermal power, water pool level and temperature distribution for CWC and, for SACO, non-condensable gases volume.

1.3.4. PROPHET2

PROPHET2 is an experimental facility that focuses on natural circulation decay heat removal systems. The aim of the facility is to classify the transients of the start-up process and their characteristics. The structure has been built and tested at the Energy Department of Politecnico of Turin, in Italy. The facility design is inspired by the PROPHET experimental loop, a reduced-height, reduced-pressure test facility inspired by the second Decay Heat Removal system (DHR) of ALFRED reactor.

The loop is closed and capable of operating in both single and two-phase flow. *Figure 5* shows the scheme of the system.

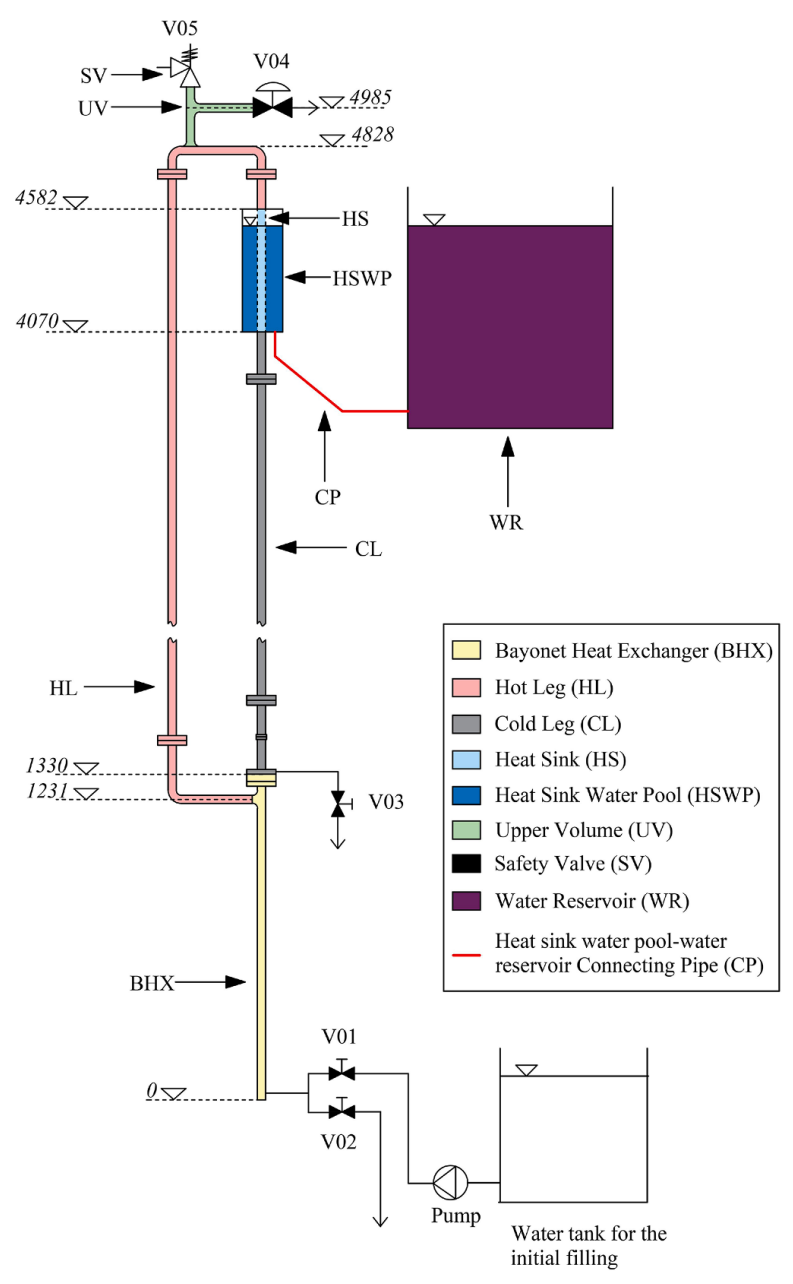


Figure 5. PROPHET2 design layout.

The heat source consists of an electrically heated bayonet heat exchanger (BHX), at the bottom of the loop, while the heat sink (a water pool at the top) features an immersed pipe for the heat exchange. The two structures are connected by a hot leg pipe (HL) and a cold leg pipe (CL). A water reservoir (WR) is attached to the heat sink. The system is tested with a maximum operative pressure of 20 bar.

Table 6 highlights the facility design characteristics.

Parameter	Value	Unit Measure
BHX length	1.328	m
HL length	4.499	m
Heat sink length	0.512	m
Heat sink diameter	0.164	m
CL length	2.740	m
Total loop height	4.828	m
Total loop length	10.275	m
Pipes inner diameter	20.700	mm

Table 6. PROPHET2 technical and geometrical parameters.

2. Conceptual design of a new experimental facility

The elaborate introduces a new experimental facility, set to be in the Energy Department in Politecnico of Turin. The facility will consist of a natural circulation heat removal system, concepted to simulate nominal and emergency operations. The structure is expected to work in both single-phase and two-phase flow. To proceed ordinately, the whole structure has been tested at first imposing a single-phase flow in both loops and the results are discussed on this elaborate. This choice fixes some operative thresholds, but it also avoids the presence of two-phase flow instabilities.

The system analysis begins with a morphological and technical definition of the loops and their components. The model proceeds with a validation of the physics, in which the suitability of the equations is verified. Consequently, all the equations are explained, adjusted and applied to the reference case. Finally, the tests performed are presented and the results are explained and justified. When all the simulations are completed, a new code system is introduced to compare part of the results of the experiments conducted.

2.1. Geometry description

The structure will include two loops (a primary and a secondary) coupled by a compact heat exchanger. Both loops will operate under natural circulation, thanks to the presence of electrical heaters as heat source and a water pool as ultimate heat sink. Both loops will present a VHVC configuration with a series connection.

2.1.1. Primary loop

Let's now focus on the two loops containing the heat source, hereafter called primary loop. Figure 6 shows the simple scheme that has been assumed and highlights the main elements: the heated section (in red), the compact heat exchanger (identified as a parallelepiped small box) and the system of pipes that connects these structures. The shape of the loop is rectangular.

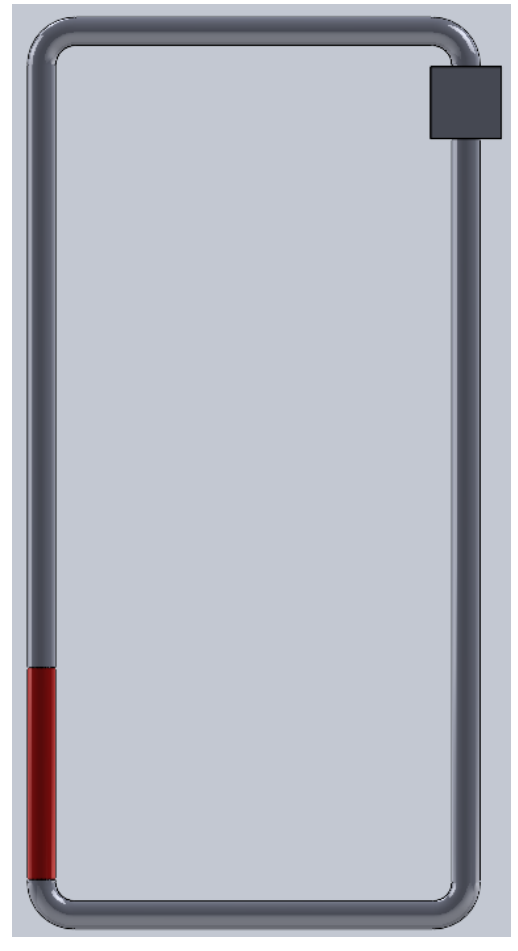


Figure 6. Design of the primary loop.

The pipes are circular, and the tests performed have been conducted assuming a constant diameter in all loop. In some cases, parametric tests have been conducted to show the effects of the different size of diameters on the results. The pipes inner diameters evaluated are: 1.25 inches, 1.5 inches, 2 inches, 2.5 inches and 3 inches (3.508, 4.094, 5.248, 6.268 and 7.792 cm respectively). The measures have been reported in inches since it's the current unit measure used in industrial applications. When the tests required a constant diameter, the choice fell on 2 inches diameter (5.248 cm).

The corners of the loop present 90° turns and have been assumed with a localized pressure loss coefficient of 0.4 for a curvature radius of 10 cm [14]. The pipes haven't been assumed smooth but they present a roughness of 0.05 mm. Adiabaticity has been imposed to neglect any external losses due to radiation or air convection (even though it is not a realistic physical assumption). The height difference between the outlet of the heat source and the inlet of the heat exchanger has been imposed of 4.5 m and the total vertical and horizontal length of the loop are 6 m and 3 m respectively. *Figure* 7 shows loop's real design aspect with quotes in mm.

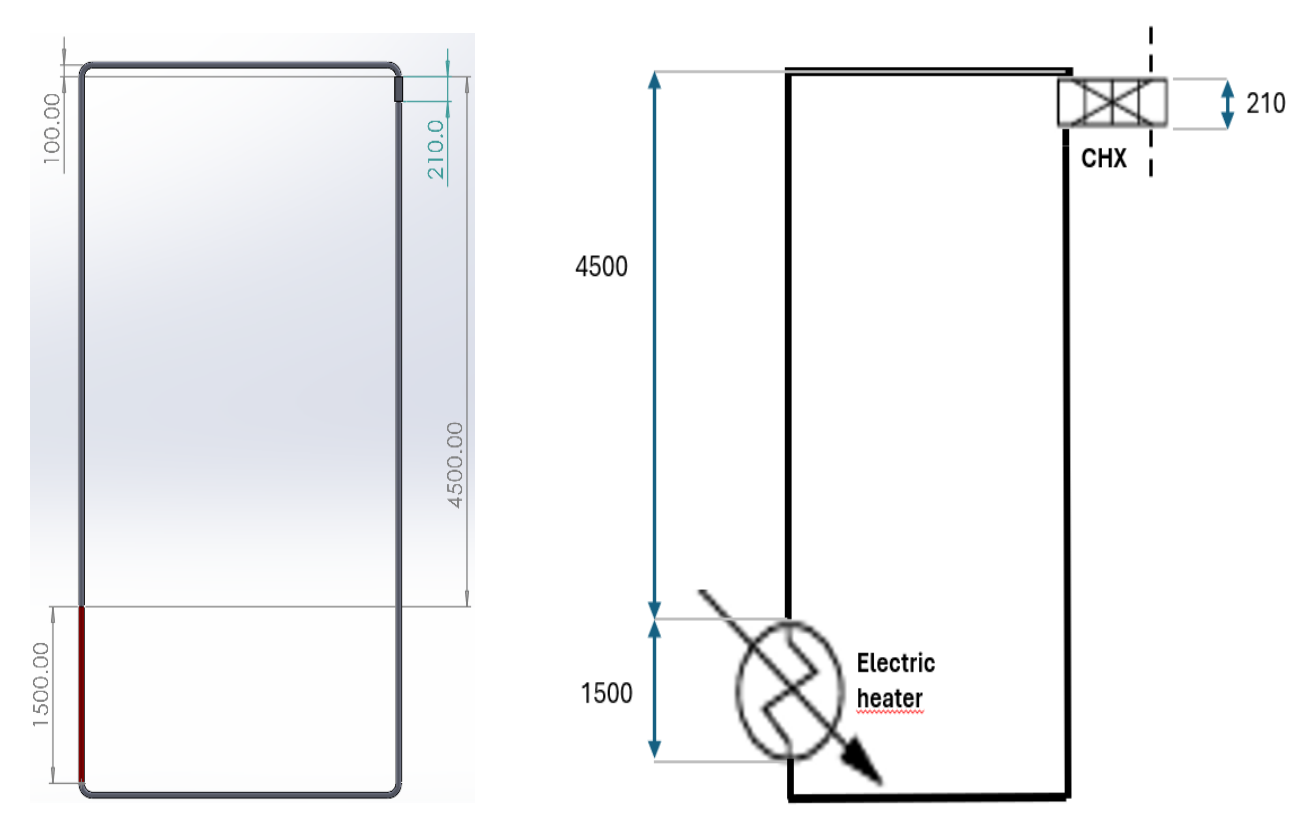


Figure 7. Quoted schemes of the primary loop: a realistic aspect of the loop (on the left) and a schematic design (on the right) based on P&ID symbols [22].

2.1.2. Secondary loop

As said above, the secondary system is linked with the primary through the compact heat exchanger. The geometry is no more simply rectangular shaped and results in being more complex with respect to the previous case. This loop takes the heat from the heat exchanger and discharges it into the ultimate heat sink. We will refer to it as secondary loop from now on. *Figure 8* shows the quoted secondary loop, with the CHX (in red) and water pool (in blue).

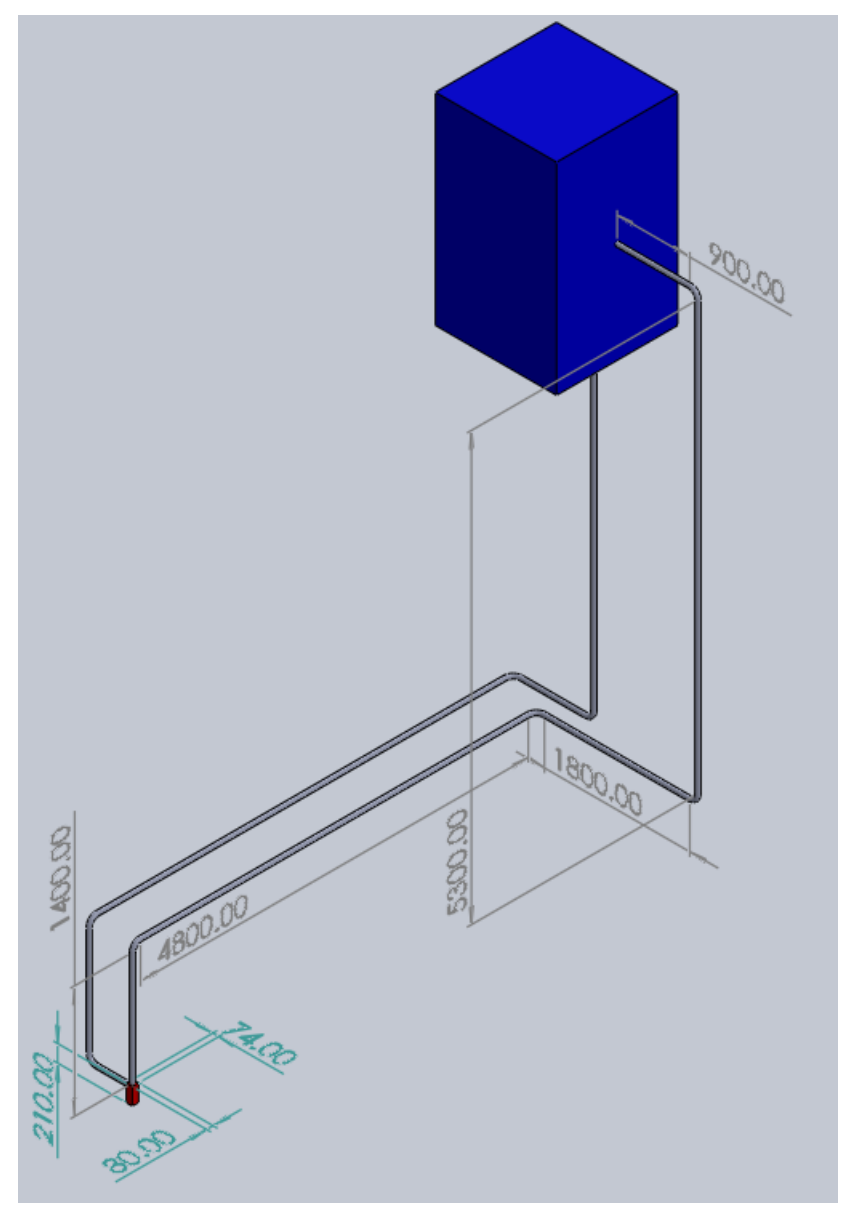


Figure 8. Quoted secondary loop's design aspect.

Pipes diameter is kept equal to the one in primary loop and, as follows, an analysis on the different diameters have been performed also in this case.

The same localized pressure coefficient has been used for the 90° curved turns and the roughness has been kept at 0.05 mm, as in the previous case. The imposed height difference between the heat exchanger and the pool is 7 m and the length of the horizontal pipes has been assumed as 8 m.

The pool dimensions have not been taken into account and an important assumption has been made: the pool can remove all the heat received. In other words, the water flowing through the downcomer to the HX is kept at a constant temperature. This is a very strong assumption since it should require a very large pool and neglects all the effects of temperature stratification in it and the efficiency of the heat transfer process in the HX. However, for an initial analysis of the model it can be considered acceptable.

2.1.3 Compact Heat Exchanger (CHX)

Compact heat exchangers have gained particular interest in new generations NPP. The name comes from the reduced dimensions with respect to standard heat exchangers, but despite that they still guarantee high performance. CHX guarantee compactness, high efficiency and low fabrication costs. Moreover, the diffusion of boding technique endows them with structural integrity, making them well-suited for high-temperatures, high-pressure operating conditions [15]. The choice and the modelling of the compact heat exchanger is the most crucial element of the whole process. Its dimensions and specifics directly affect the performance of the whole process. For this system a CHX has been chosen due to its compactness and the low fabrication costs. Furthermore, the choice has been enhanced by the fact that CHX have gained larger interest for future applications. The main advantage of CHX is that they guarantee high heat exchange performances thanks to the large heat transfer surfaces maintaining reduced dimensions. CHX can be of many types but the most common are plate type and microchannels heat exchangers. The first are very common and after a deep evaluation, it has been decided to proceed with that. For this thesis project a Brazed Plate Heat Exchanger (BPHE) has been chosen and more particularly the surface of the plates presents a 30° Chevron angle pattern. Figure 9 shows the aspect of a BPHE [12].

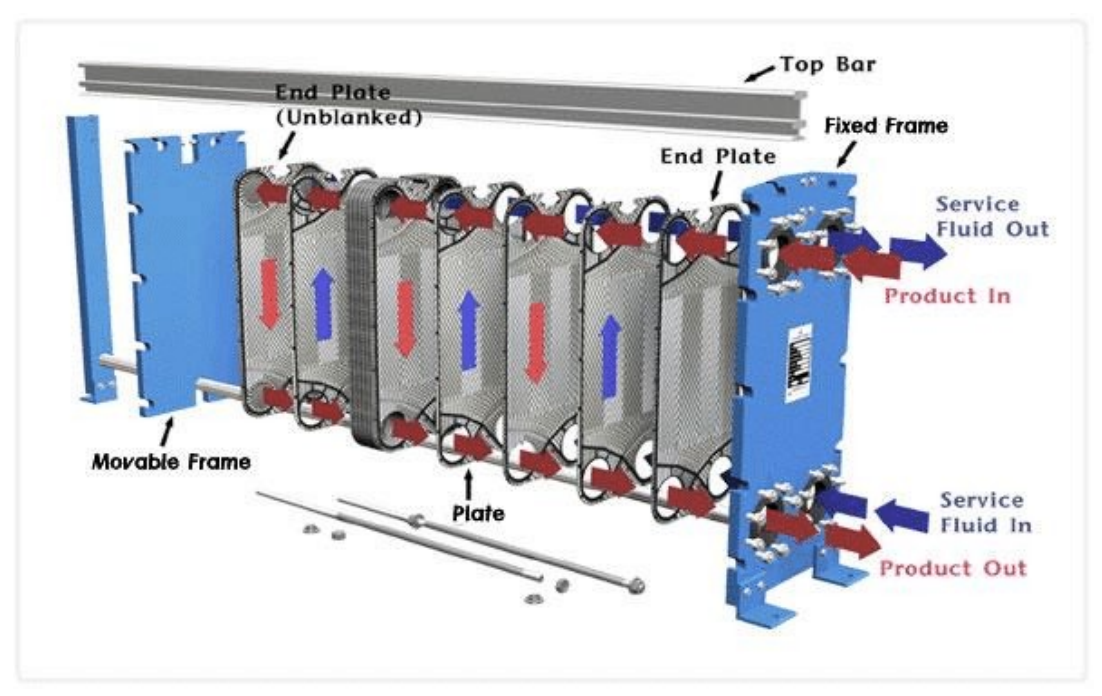


Figure 9. Design scheme of a BPHE.

It is notable how the primary fluid (in red) and the secondary fluid (in blue) are correlated. The system operates in countercurrent flow: the operative fluid of a loop falls alternately in the space between the plates. The pattern of the plates is shown in *Figure 10*, where the Chevron angles are very clear.



Figure 10. Geometry scheme of a Chevron angles-type pattern on plates.

It is notable how the corrugations on the two sides of the plates present different angles. The most common layouts are $30^{\circ}-30^{\circ}$, $60^{\circ}-60^{\circ}$ or in some cases $30^{\circ}-60^{\circ}$. The angle strongly affects the pressure drops and the effectiveness of the heat exchange process in the component. Relative tests have proven that $30^{\circ}-30^{\circ}$ configurations reduce the global friction factor and the pressure drop in the heat exchanger, but cause a reduction in the heat transfer process due to a higher maldistribution of the mass flow rate. The maldistribution increases as the mass flow rate increases. On the other hand, $60^{\circ}-60^{\circ}$ configurations allow a more homogenous distribution of the mass flow and a higher efficiency for the heat transfer mechanism but with higher pressure losses [12]. For our case a 30° - 30° configuration has been chosen since the focus has been placed on the mass flow rate of the loop and so on the reduction of pressure losses in all its components.

Chevron type HX can present two different layouts for what concerns the coupling of two adjacent plates, as shown in *Figure 11* [13].

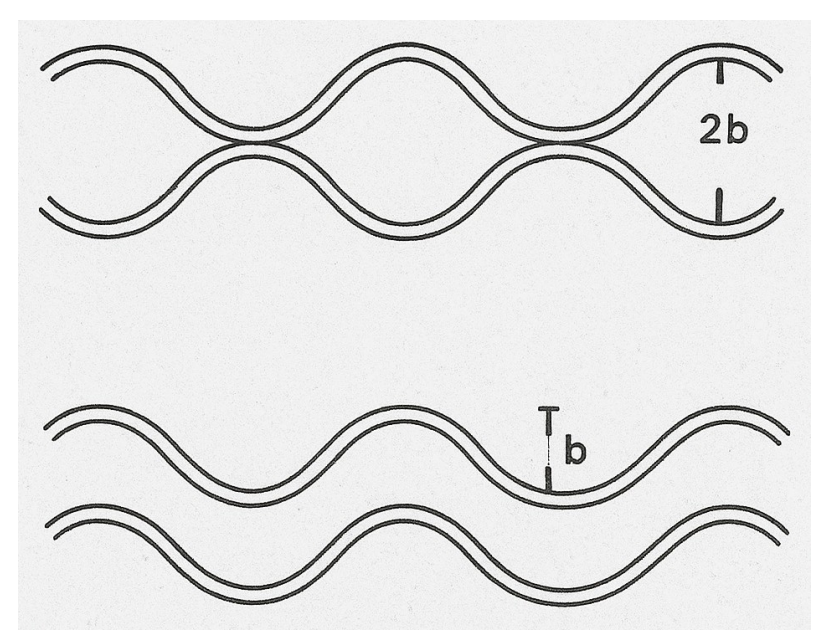


Figure 11. Possible layouts of a plate-type compact heat exchanger.

The figure shows the coupling of two adjacent plates seen from above. For our case, the first configuration has been chosen and the heat exchange between the two systems has been assumed to be as a counter-current microchannels HX. This is a simplifying assumption, since the channels are not perfectly circular and mass flow is allowed to move also between the channels. In other words, water is free to move inside the channels (on the plate width direction) but also between the channels (on the plate height direction). So, water moves inside the microchannels longitudinally (along plate width), but in reality it also moves in the transversal direction with respect to the plane in which the microchannel rely. This last direction corresponds to plate height direction. However, in a preliminary analysis this assumption can be considered acceptable.

The main characteristics and dimensions of the CHX are summed in *Table 7*:

Parameter	Value	Unit Measure
CHX total height	210	mm
CHX total length	74	mm
CHX total thickness	61	mm
N. of plates	25	-
N. of channels per plate	105	-
Plate thickness	1	mm
Degrees angle	30	O
Single channel length per plate	148	mm

Table 7. Compact heat exchanger characteristics.

The thermal conductivity of the plates was assumed $90 \frac{W}{m \cdot K}$, sufficiently high to guarantee good heat transfer properties. For future analysis the evaluations of different materials (and thermal conductivities) and their resistance to the resulting stresses is required. Online researches have shown that the best options are Nichel (Ni) and Titanium (Ti) alloys, which guarantee high conductivity and resistance in aggressive environments despite their elevated

costs. Nevertheless, the main goal was just to define a proper value that could fulfill the heat transfer goal.

The other main problem for this component was the definition of the global pressure losses in it. Since the exact internal geometry of the component is unknown, it is assumed 15 kPa as maximum acceptable value for the overall HX pressure losses. This value comes from the maximum pressure losses in a similar compact heat exchanger extracted from the website of a commercial company (Alfalaval, CBH16-25H brazed plate heat exchanger), and reduced of a factor 2 due to the assumptions of reduced mass flow rate with respect to the one considered in the website. The performance of the loop has been verified with values of pressure drop in the range 1.5 - 15 kPa.

2.2. Operating conditions

The thermal power is provided on the primary loop by electric heaters, capable of providing a maximum of 50 kW. The heat has been assumed distributed uniformly in a pipe of 1.5 m long and the same diameter of the whole loop. No conduction of the solid tubes has been modeled, so all 50 kW are supposed to be delivered to the fluid.

The systems has been studied in two different pressure conditions: a low-pressure case at first, and a high-pressure case then. Regarding the primary loop, the two pressures tested were respectively 8 bar and 150 bar, while the secondary loop was tested at 2 bar and 70 bar respectively. Both cases withstand liquid single-phase flow, keeping the overall temperature below saturation conditions. While the first case is to guarantee single-phase flow even in low pressure conditions, the second case aims to show the behavior at NPP conditions.

3. Buoyancy forces and equations analysis

The buoyancy force is described as the effect of density differences in the loop, which cause different hydrostatic pressures and generates a flow driving force. To proceed with the analysis, it's important to consider the momentum conservation equation, integrated over loop's length (Eq. (1)) [20]:

$$\sum_{k} \frac{L_{k}}{A_{k}} \frac{\partial \dot{m_{k}}}{\partial t} + \oint \frac{\partial}{\partial l} \left(\frac{G_{m}^{2}}{\rho_{m}} \right) dl = -\Delta p_{f,distr} - \Delta p_{f,form} + \Delta p_{buoyancy}$$
(1)

Where L_k is the length of the flow section, A_k the cross section of the flow section, m_k the mass flow rate in the section, G_m is the mass flux (equal to the mass flow rate divided by the respective cross section), ρ_m is the average fluid density at a specific location, $\Delta p_{f,distr}$ the pressure due to distributed friction losses (Eq. (2)), $\Delta p_{f,form}$ the pressure losses due to the form (Eq. (3)) and $\Delta p_{buoyancy}$ are the resultant forces applied due to thermosyphon effects induced by density variations (Eq. (4)). On the left-hand side of the equation, the first element represents the rate of change in time of fluid's inertia, while the second the momentum flux. Developing the right-hand side elements we obtain:

$$\Delta p_{f,distr} = \int_{0}^{L_{loop}} \frac{f \cdot G_m |G_m|}{2 \cdot D \cdot \rho_m} dl \tag{2}$$

$$\Delta p_{f,form} = \sum_{i} K_{j} \left(\frac{(G_{m} | G_{m}|)}{2 \cdot D \cdot \rho_{m}} \right)_{i}$$
(3)

$$\Delta p_{buoyancy} = -\int_{0}^{L_{loop}} \rho_{m} g cos\theta dl \tag{4}$$

Where f is the loop's friction factor, g the gravity acceleration and D the loop diameter. θ is defined as the angle formed with the vertical direction z (assumed positive when upward oriented). It is possible to define the infinitesimal height dz as:

$$dz = cos\theta dl \tag{5}$$

$$-\int_{0}^{L_{loop}} \rho_{m} g cos\theta dl = -\int_{0}^{L_{loop}} \rho_{m} g dz \tag{6}$$

Let's now assume a rectangular loop, defined by four vertices: A (at bottom left), A'(at bottom right), B' (at top right) and B (at top left). The loop is represented in Figure 12.

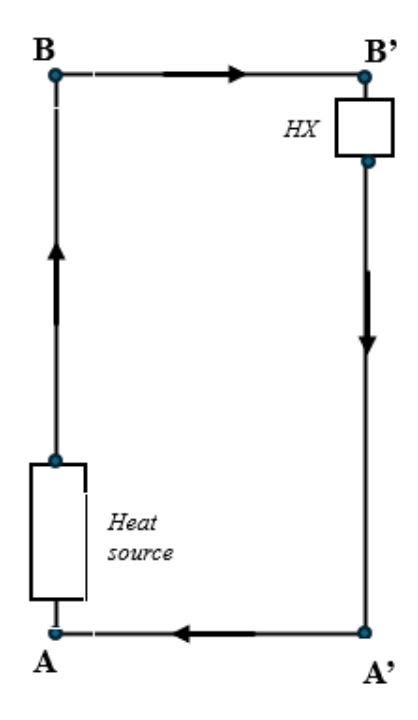


Figure 12. Loop figure for demonstration.

Vertices A and A are placed at the same vertical coordinate, and the same discussion is valid for B and B. The Eq. (6) can be rewritten as:

$$-\int_{0}^{L_{loop}} \rho_{m} g dz = -\left(\int_{A'}^{A} \rho_{m} g dz + \int_{B'}^{A'} \rho_{m} g dz + \int_{B}^{B'} \rho_{m} g dz + \int_{A}^{B} \rho_{m} g dz\right)$$
(7)

Assuming to have the heat source on the right vertical leg and the heat sink on the left vertical leg of the loop, with riser and downcomer adiabatic, the horizontal sections (defined by A-A' and B-B') present constant densities (but with different values). This effect allows to extract them (and gravity acceleration) from the integral and, since their height coordinate is the same, the integral value becomes null. In other words, Eq. (7) becomes:

$$-\int_{0}^{L_{loop}} \rho_{m}gdz = -\left(+\int_{A'}^{B'} \rho_{m}gdz + \int_{A}^{B} \rho_{m}gdz\right) \tag{8}$$

The integration around the whole loop becomes:

$$-\left(\int_{A'}^{B'} \rho_m g dz + \int_{B}^{A} \rho_m g dz\right) = -(\overline{\rho_m})_{A'-B'} \cdot g \cdot (Z_b - Z_a) - (\overline{\rho_m})_{B-A} \cdot g \cdot (Z_a - Z_b) \tag{9}$$

$$\left(\overline{\rho_m}\right)_{A'-B'} = \frac{\left(\int_{A'}^{B'} \rho_m dz\right)}{Z_b - Z_a} \tag{10}$$

$$(\overline{\rho_m})_{B-A} = \frac{\left(\int_B^A \rho_m dz\right)}{Z_B - Z_B} \tag{11}$$

It's possible to rewrite Eq. (9) as:

$$-\int_0^{L_{loop}} \rho_m g dz = \left[(\overline{\rho_m})_{B-A} - (\overline{\rho_m})_{A'-B'} \right] g(Z_b - Z_a)$$
 (12)

Where $(\overline{\rho_m})_{B-A} = \rho_{cold}$ and $(\overline{\rho_m})_{A'-B'} = \rho_{hot}$ are the average densities of the cold and hot sides. $(Z_b - Z_a) = H$ is defined as the difference from the thermal centers [21].

Starting from Eq. (1), it's possible to retrieve the adjusted momentum conservation equation suitable for the study. The system is composed of closed loops, assumed to operate in steady state conditions without any pumps. Under these assumptions, the first term on the left-hand side disappears due to lack of time dependency along with the second due to the closed nature of the loop. Finally, the momentum conservation equation can be summed as:

$$\sum_{k} \frac{f_k \cdot G_m |G_m| \cdot L_k}{2 \cdot D_k \cdot \rho_k} + \sum_{j} K_j \left(\frac{(G_m |G_m|)}{2 \cdot D_j \cdot \rho_j} \right)_j = (\rho_{cold} - \rho_{hot}) \cdot g \cdot H$$
(13)

Expressing the equation with the mass flow rate instead of the mass flux, and recalling that the loop presents constant cross section, we obtain:

$$\left(\sum_{k} \frac{f_k \cdot L_k}{D_k} + \sum_{j} K_j\right) \frac{\dot{m}^2}{2\rho A^2} = (\rho_{cold} - \rho_{hot}) \cdot g \cdot H$$
(15)

The system presents a CHX whose pressure losses have been assumed to appear as form losses.

Posing attention on the mass flow rate from Eq. (15), it is notable how:

- Increasing the height difference *H* between the thermal centers of the source and sink, \dot{m} increases.
- Increasing the pipes cross section A, \dot{m} increases.
- Reducing the pressure losses (localized and distributed), \dot{m} increases.
- Increasing the density difference, \dot{m} increases.

Due to its passive nature, mass flow rates in natural circulation loops tend to be much smaller than in pump-driven ones. For this and for safety reasons, specific analyses aimed to maximize \dot{m} must be done from design to construction.

While in Eq. (15) K is a fixed value depending on the type of component or design of the loop, f_j must be evaluated depending on the type of flow regime, which depends on the value of the Reynolds number, defined in Eq. (16).

$$Re = \frac{\rho \cdot v \cdot D}{\mu} = \frac{4 \cdot \dot{m}}{\pi \cdot D \cdot \mu} \tag{16}$$

Where v is the fluid velocity and μ is the dynamic viscosity. It's important to recall that for a confined flow in a pipe it's possible to identify different regimes depending on the value of the Reynolds number:

- Laminar flow for $Re \leq 2300$.
- *Intermediate flow* for 2300 < Re < 4000.
- *Turbulent flow* for $Re \ge 4000$.

Depending on the type of flow regime, the friction factor was evaluated in the following way:

• Laminar flow \rightarrow Darcy-Weisbach equation (Eq. (17)):

$$f_{laminar} = \frac{64}{Re} \tag{17}$$

• Turbulent flow \rightarrow *Haaland equation (Eq. (18))*

$$\frac{1}{\sqrt{f_{turbolent}}} \approx -1.8 \cdot log_{10} \left[\left(\frac{\frac{\epsilon}{D}}{3.7} \right)^{1.11} + \frac{6.9}{Re} \right]$$
 (18)

Where ϵ is the rugosity of the pipe (imposed at 0.05 mm for stainless steel pipes) and D is the pipe diameter.

• Intermediate flow \rightarrow weighted linear interpolation between the two previous methods. The weight α was found as shown in Eq. (19).

$$\alpha = \frac{Re - 2300}{4000 - 2300} \tag{19}$$

And the friction factor was obtained as Eq. (20):

$$f_{intermediate} = (1 - \alpha) \cdot f_{laminar} + \alpha \cdot f_{turbolent}$$
 (20)

In addition, the energy balance equation has been added. The analysis has taken into account some important assumptions:

Riser and downcomer were assumed to be adiabatic, and air convection and radiative heat dissipation towards the ambient have been neglected.

All the thermal power provided by the electrical heaters is totally delivered to the fluid, this assumption also allowed to define an upper threshold for the expected results since in a more realistic case the thermal power received by the fluid is lower than the one actually provided.

The model initially used a 0-D analysis, which means that the temperature distribution along the heated section was not evaluated.

A rough 1-D script has been developed in the latest part of the thesis path to evaluate the temperature distribution in the heated section. The axial temperature distribution will become

particularly relevant in case of two phase flow and presence of non-condensable gases. The steady state energy balance equation in the heated section for the 1-D study is described in Eq. (21):

$$\frac{\dot{m}_p \cdot c_{p,p}}{A_{pipe}} \frac{\partial T_p}{\partial x} = k_{w,p} \frac{\partial^2 T_p}{\partial x^2} + Q \tag{21}$$

Where $k_{w,p}$ is water thermal conductivity in primary loop at the heat source. The applied model in MATLAB was solved using central difference scheme.

It is important to specify that most of the variables are function of the temperature. Since the study focused on a 0-D model, all of them have been evaluated as function of the average temperature T_{avg} of the loop in analysis (Eq. (22)), as shown in Eq. (23):

$$T_{avg} = \frac{T_{hot} - T_{cold}}{2} \tag{22}$$

$$c_p = c_p(T) = \overline{c_p(T_{avg})} \tag{23}$$

Since all the evaluations have been performed on MATLAB, water properties have been found using XSteam library.

The energy conservation equation applied to the heat exchanger is:

$$Q = \dot{m}_p \cdot c_{p,p} \cdot \Delta T_p \tag{24}$$

$$m_p \cdot c_{p,p} \cdot \Delta T_p = U \cdot A_{tot,CHX} \cdot \Delta T_M \tag{25}$$

Where \dot{m}_p is the mass flow rate in the primary loop, Q is the thermal load provided by electric heaters, $c_{p,p}$ is the specific heat at constant pressure for the primary loop, ΔT_p is the temperature difference between the inlet and the outlet of the heated section (or the inlet and the outlet of the HX), U is the global heat transfer coefficient for the CHX, $A_{tot,CHX}$ is the total CHX heat transfer area and ΔT_M is the log mean temperature difference. ΔT_M between primary and secondary fluid in the case of countercurrent flow is defined by Eq. (26).

$$\Delta T_M = \frac{\Delta T_1 - \Delta T_2}{\ln \frac{\Delta T_1}{\Delta T_2}} \tag{26}$$

$$\Delta T_1 = T_{hot,p} - \bar{T_{hot,s}} \tag{27}$$

$$\Delta T_2 = T_{cold,p} - T_{cold,s} \tag{28}$$

Where $T_{hot,p}$ is the hot fluid at the inlet of CHX on the primary side, $T_{hot,s}$ the hot fluid at the outlet of CHX on the secondary side, $T_{cold,p}$ the cold fluid at the outlet of the CHX on the primary side and $T_{cold,s}$ the cold fluid at the inlet of the CHX on the secondary side. For what concerns the heat exchange at the pool, the equation used is Eq. (29).

$$Q = \dot{m}_s \cdot c_{p,s} \cdot \Delta T_s \tag{29}$$

Where \dot{m}_s is the mass flow rate for the secondary loop, $c_{p,s}$ the specific heat at constant pressure for secondary loop evaluated at the average temperature in the secondary loop and ΔT_s the temperature difference between the inlet and the outlet of the pool (or the outlet and the inlet of the CHX at the secondary side). As already said, the cold temperature for the secondary side was kept fixed at $T_0 = 30^{\circ}C$, reducing the number of unknowns in our problem.

Regarding the CHX, Eq. (25) can be adjusted into a new form, highlighting also the importance of the number of plates and flow passages. The equation is defined as:

$$\frac{\Delta T_p}{\Delta T_M} = \frac{U \cdot A_{tot,CHX}}{\dot{m}_p \cdot c_{p,p}} = \frac{2n}{n+1} \cdot \frac{U \cdot A_{plate}}{\dot{m}_f \cdot c_{p,p}}$$
(30)

Where n is the number of plates, A_{plate} is the heat exchange surface of a single plate and \dot{m}_f the mass flow rate of a single flow passage (defined as the space between two parallel plates). It can be seen how $\frac{n+1}{2}$ is the total number of flow passages and $n \cdot A_{plate}$ is the total heat transfer area $A_{tot,CHX}$. As a consequence, the loop mass flow rate $\dot{m_p}$ can be defined as the product of the number of flow passages and the mass flow rate in a flow passage \dot{m}_f . This equation was fundamental for the evaluation of the temperatures.

Along with the definition of the CHX pressure losses, the global CHX heat transfer coefficient takes into account the convection heat transfer of each plate of the heat exchanger with the primary and secondary fluids, and the thermal conduction through the plate (Eq. (31)).

$$U = \frac{1}{R_{tot}} \tag{31}$$

$$R_{tot} = R_{conv,p} + R_{cond} + R_{conv,s}$$
 (32)

$$R_{tot} = R_{conv,p} + R_{cond} + R_{conv,s}$$

$$R_{conv,p} = \frac{1}{h_p}$$
(32)

$$R_{cond} = \frac{1}{\frac{k_{plate}}{s_{plate}}} = \frac{s_{plate}}{k_{plate}}$$
(34)

$$R_{conv,s} = \frac{1}{h_s} \tag{35}$$

Where h_p and h_s are the convective heat transfer coefficients in primary and secondary side of the CHX respectively, k_{plate} is the thermal conductivity of the plate and s_{plate} is the plate thickness. To calculate the convective heat transfer coefficients, it was necessary to pass from the dimensionless Nusselt number (*Eq. (36)*).

$$Nu = \frac{h \cdot D}{k_{fluid}} \tag{36}$$

Where D is the characteristic length and k_{fluid} is the thermal conductivity of the operative fluid. Nusselt number can be obtained using different correlations depending on the type of flow, and more in particular on the dimensionless Reynolds number (Eq. (16)).

• Laminar flow

$$Nu = 3.66$$
 (37)

• Turbulent flow for Re $< 10000 \rightarrow$ Gnielinski correlation (Eq. (38))

$$Nu = \frac{\frac{f}{8} \cdot (Re - 1000) \cdot Pr}{(1.07 + 12.7 \cdot \left(\frac{f}{8}\right)^{0.5} \cdot \left(Pr^{\frac{2}{3}} - 1\right)}$$
(38)

• Turbulent flow for Re \geq 10000 \rightarrow Dittus-Boelter correlation (Eq. (39)).

$$Nu = 0.023 \cdot Re^{0.8} \cdot Pr^{0.3} \tag{39}$$

Where f is the friction factor and Pr is the Prandtl number. Finally, the pressure increase and water volume expansion due to an increase of the water temperature has been predicted, in order to evaluate the need of including surge tanks in the facility.

All pipes are assumed to be completely filled with water and it was also assumed that the water undergoes an isochoric transformation, so that the increase of temperatures would lead to an increase in pressure that, if not properly checked, can become a serious safety issue.

For the evaluation of the pressure and consequent volume increase for a liquid it was chosen to proceed as follows:

$$\left(\frac{\partial P}{\partial T}\right)_V = \frac{\alpha}{\kappa_T} \tag{40}$$

Where α is the volumetric thermal expansion coefficient and κ_T is the isothermal compressibility coefficient. For our analysis, the two coefficients have been imported from IAPWS95 Python library, depending on temperature values. For our case, these values have been retrieved from average temperatures.

The overall volumetric expansion is evaluated by Eq. (41):

$$\frac{dV}{V} = \alpha \cdot \Delta T \tag{41}$$

To manage the pressure and volume changes, an expansion tank should be introduced. In order to evaluate the needed volume of the expansion tank, it is necessary to calculate the difference of mass contained in the loop between the initial state and the final state:

Initial mass

It has been evaluated by multiplying the total volume of the system and the fluid density at 30° C (Eq. (42)). The volume occupied by the operative fluid in the CHX has been found

considering the volume in a single microchannel and multiplied by the number of channels involved.

$$m_{initial} = \rho(T = 30^{\circ}C) \cdot V_{tot}$$
 (42)

Final mass

The final mass in the loop m_{end} has been found integrating the product of the density and the corresponding cross section in total loop length ($L_{tot} = 18 \text{ m}$), as shown in Eq. (43).

$$m_{end} = \int_0^{L_{tot}} \rho(T, x) \cdot A_{cross}(x) dx \tag{43}$$

The density distribution has been retrieved from temperature distribution, which has been considered as follows:

- Heat source → the temperature distribution has been calculated with a 1-D script for the section.
- Riser \rightarrow due to adiabatic assumption, its temperature distribution has been assumed constant at $T_{hot,n}$.
- CHX \rightarrow the temperature distribution has been evaluated with a linear interpolation between $T_{hot,p}$ (at the inlet of it on the primary side) and $T_{cold,p}$ (at the outlet of it on the primary side).
- Downcomer \rightarrow due to adiabatic assumption, its temperature distribution has been assumed constant at $T_{cold,p}$.

The mass that should enter the expansion tank is:

$$\Delta m = m_{initial} - m_{final} \tag{44}$$

To smooth all the iterative processes, it was necessary the introduction of under-relaxation factors δ . The introduction of these factors avoids excessive differences between two successive iterations that could cause problems in the iterative process (especially at initial stages). For our study the values used were:

$$\delta_q \sim \delta_T \sim 0.3 \tag{45}$$

Where δ_q refers to the iterations for the mass flow rate and δ_T for the temperatures. The example shows their application in our case:

$$x = (1 - \delta) \cdot x_{old} + \delta \cdot x_{new} \tag{46}$$

Where x is the generic variable that will be plugged in the successive iteration, x_{old} is the old value before the iteration and x_{new} is the value obtained after the iteration. Logically, x_{new} is directly connected to x_{old} . Setting the under-relaxation factors this low allows a smoother transition in the results but with a higher number of iterations.

Primary loop 3.1.

The analysis followed an initial evaluation of the primary loop only, assuming the secondary loop at constant temperature T_0 and the HX to behave as an ultimate heat sink. In other words, the hypothesis was:

$$T_{hot,s} = T_{cold,s} = T_0$$

$$\dot{m}_s = 0.2 \, kg/s$$
(47)

$$\dot{m}_s = 0.2 \, kg/s \tag{48}$$

The whole process required an iterative algorithm and, since the total number of iterations was unknown, "while" cycles have been defined. As a threshold, a maximum acceptable relative error of 10⁻³ was imposed as tolerance. The script was built based on two concatenated "while" cycles, one inside the other: in the inner one, the aim was to find the exact values of the temperatures and on the outer one to obtain the correct pressure losses and mass flow rate. The two relative errors have been evaluated as:

$$err_{T} = \left| \frac{T_{cold}^{i} - T_{cold}^{i-1}}{T_{cold}^{i-1}} \right|$$

$$err_{q} = \left| \frac{\dot{m}^{i} - \dot{m}^{i-1}}{\dot{m}^{i-1}} \right|$$

$$(50)$$

Where i indicated the actual iteration and (i - 1) the previous one.

The main difference can be seen in the definition of ΔT_M used for the obtainment of the temperatures, where its formulation turns into:

$$\Delta T_{M} = \frac{(T_{hot,p} - T_{0}) - (T_{cold,p} - T_{0})}{ln \frac{T_{hot,p} - T_{0}}{T_{cold,p} - T_{0}}} = \frac{T_{hot,p} - T_{cold,p}}{ln \frac{T_{hot,p} - T_{0}}{T_{cold,p} - T_{0}}}$$
(51)

The flow chart for the model is shown in *Figure 13*:

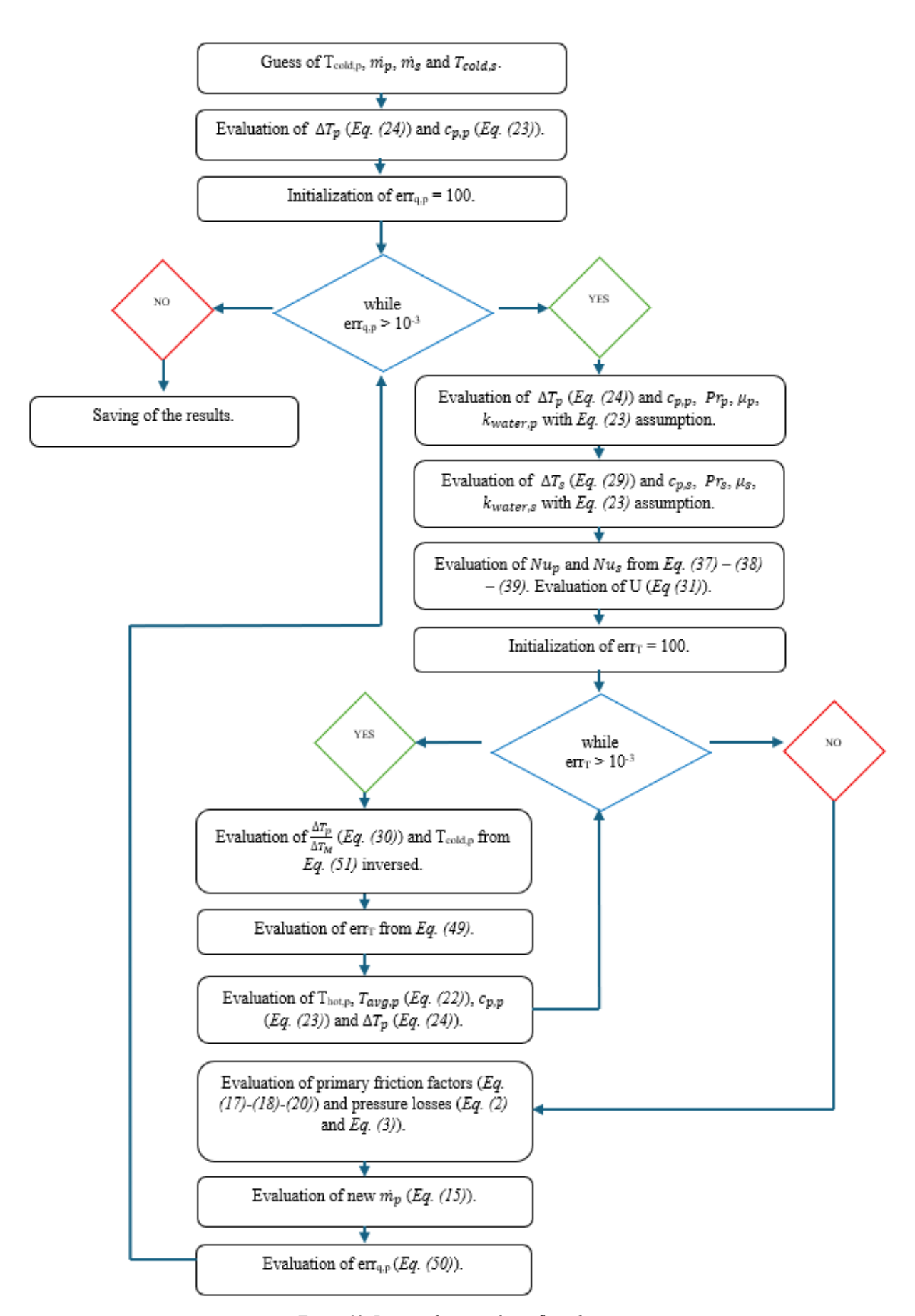


Figure 13. Primary loop resolving flow chart.

For what concerns the calculation of $R_{conv,s}$, it was imposed a constant mass flow rate for the secondary side of 0.2 kg/s which is a value obtained assuming a $R_{conv,s}$ in the same order of $R_{conv,v}$.

3.2. Secondary loop

The way of proceeding is the same as the one described for the primary loops. The best choice was to consider the two loops separately, starting with the secondary due to its easier conditions. It's important to stress that the main assumptions were a uniform temperature along the hot and cold leg and that all the power provided to the electric heaters is delivered to the fluid. Given that, the flow chart correspondent to secondary loop (*Figure* 14) can be assumed to be as follows:

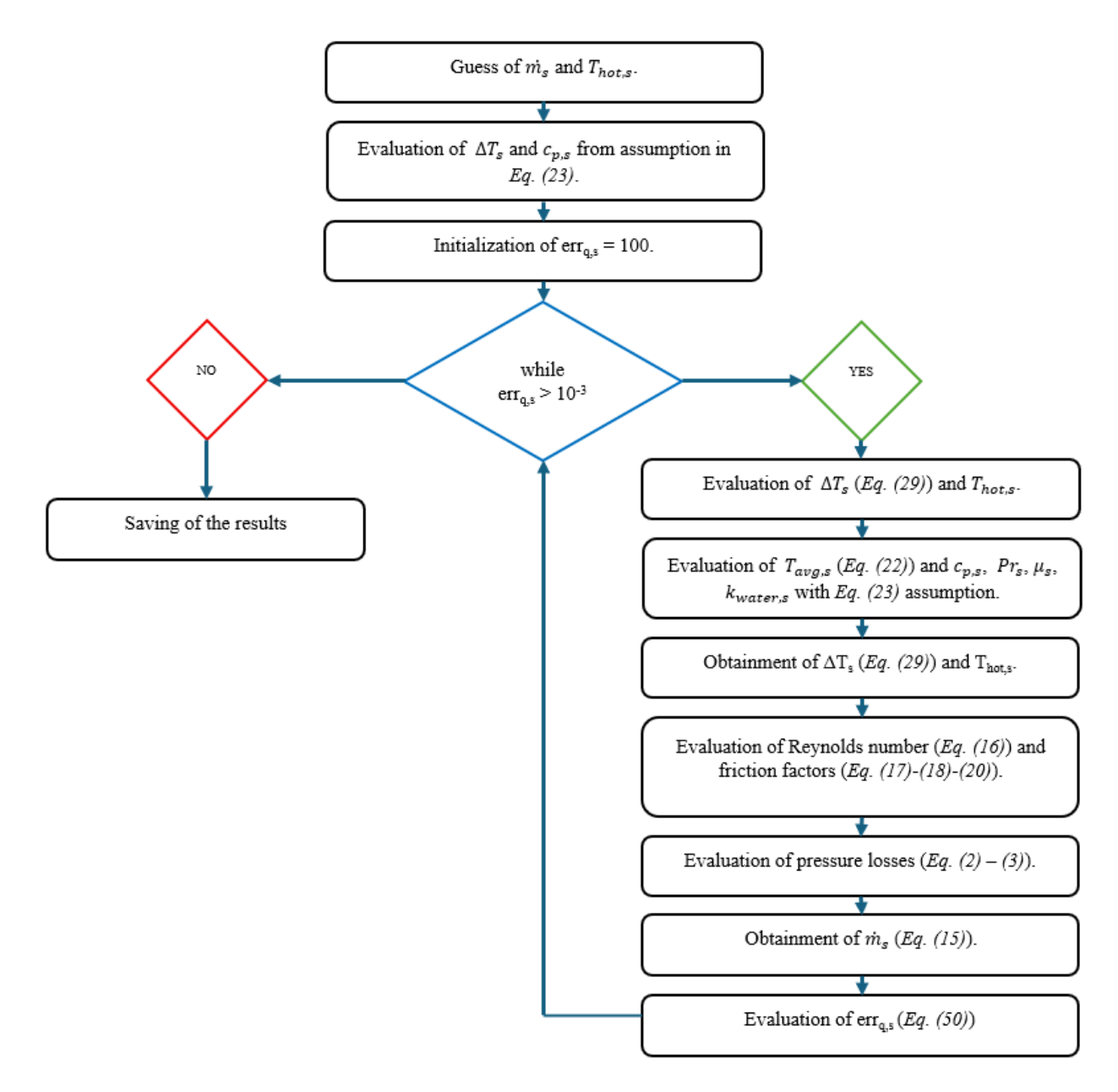


Figure 14. Secondary loop resolving flow chart.

The approach used was to evaluate the secondary temperatures and mass flow rate at first from Figure 14, and then to retrieve primary loop parameters. To obtain these last ones, the flow chart is the same as Figure 13, with the difference that ΔT_M formulation follows Eq. (26) and the secondary mass flow rate \dot{m}_s is no longer arbitrary but obtained by the secondary loop simulations.

4. Results

In this section all the simulations and the results will be presented and discussed, starting from the "primary loop only" and following with "primary and secondary coupling system". The simulations performed have tested the efficiency of the system changing some specific parameters listed below:

- Loop diameter
- Source-sink height difference
- Thermal power
- Pressure
- Heat exchanger pressure losses

As already said, all the simulations aimed to maintain liquid single-phase flow. Before proceeding any further, a brief discussion regarding the Critical Heat Flux CHF [kW/m²] needs to be made: the CHF must be compared with the actual heat flux to discuss how close the conditions are to a thermal crisis. The analysis has been actuated thanks to "The 2006 CHF look up table". The study has been conducted using different diameters (taken from the steel pipe dimensions chart ANSI B36.10 & 36.19), operative pressure and CHX pressure losses (*Table 8*):

Parameter	Value	Unit
Outer diameter	1.25 - 1.5 - 2 - 2.5 - 3	inches
Outer diameter	4.220 - 4.830 - 6.030 - 7.300 - 8.890	cm
Inner diameter	3.508 - 4.094 - 5.248 - 6.268 - 7.792	cm
Operative pressure	5 - 8 - 10 - 15 - 20 - 25	bar
HX pressure losses	1.5 - 2.5	kPa

Table 8. Parameters involved in CHF analysis.

The operative pressure was initially assumed well below the nominal values for a NPP (we will refer to it as "low pressure conditions") to discuss the effects of the thermal load in low pressure loops. It's important to say that all the simulations have been performed both in low pressure (8 bar for primary loop and 2 bar for secondary loop) and high pressure conditions (150 bar for primary loop and 70 bar for secondary loop). The choice to consider two different CHX pressure losses is to show how, increasing its value, the CHF value reduces with mass flow rate. This is caused by the reduction in the mass flow rate and the increase in heat source outlet temperatures. The tested values of the CHX pressure losses are 1.5 kPa and 2.5 kPa. Since the look-up tables don't cover all the ranges of pressure, in some cases a linear interpolation between values has been necessary. It's important to say that the values obtained with these tables were referred to a 8 mm diameter loop. To convert the extracted value to the desired diameter, *Eq.* (52) has been used:

$$CHF\left(D_{exp}, P_{exp}, G_{exp}, X_{\exp}\right) = CHF\left(D = 8 \ mm, P_{exp}, G_{exp}, X_{\exp}\right) \cdot \left(\frac{D_{exp}}{D = 8 \ mm}\right)^{-\frac{1}{2}} \tag{52}$$

$$G_{exp} = \frac{\dot{m}}{A_{riser}} \tag{53}$$

Where D_{exp} is the value of the inner diameter, P_{exp} the nominal pressure, G_{exp} the mass flux (evaluated with Eq. (53)), X_{exp} the quality of the fluid, $CHF(D=8\ mm,P_{exp},G_{exp},X_{exp})$ the values obtained by the tables at fixed parameters, \dot{m} the mass flow rate and A_{riser} the cross section of the riser. The results obtained show the values of the CHF for different diameters at specific values of quality, pressure and mass flux (obtained by the simulations). Table 9 shows the results of the CHF in $\frac{kW}{m^2}$ for 1.5 kPa of CHX losses, and Table 10 for 2.5 kPa. The rows refer to the values of the diameters while the columns to the pressure, with the exception of the last column which expresses the actual heat flux in our circuit.

	5 bar	8 bar	10 bar	15 bar	20 bar	25 bar	$q''\left[\frac{kW}{m^2}\right]$
1.25 in.	1773.861	2115.707	2242.228	2423.696	2539.302	2627.604	54.92
1.5 in.	1617.421	1926.176	2038.664	2209.371	2320.079	2404.281	47.56
2 in.	1404.424	1669.11	1764.826	1918.041	2020.025	2096.983	37.63
2.5 in.	1264.298	1501.791	1586.858	1727.43	1821.711	1893.152	31.28
3 in.	1129.081	1339.792	1414.987	1542.337	1628.672	1693.493	25.44

Table 9. CHF results for different diameters and pressures, at 1.5 kPa of CHX pressure losses.

	5 bar	8 bar	10 bar	15 bar	20 bar	25 bar	$q^{\prime\prime}\left[\frac{kW}{m^2}\right]$
1.25 in.	1281.548	1664.301	1848.563	2108.686	2258.247	2357.628	54.92
1.5 in.	1171.291	1522.4	1690.599	1928.86	2068.156	2162.358	47.56
2 in.	1020.586	1327.858	1473.149	1682.395	1806.442	1891.957	37.63
2.5 in.	920.622	1198.551	1329.77	1518.761	1632.013	1710.841	31.28
3 in.	823.094	1072.1	1189.221	1358.664	1460.854	1532.497	25.44

Table 10. CHF results for different diameters and pressures, at 2.5 kPa of CHX pressure losses.

It's easy to notice how, increasing the pressure losses, the value of the CHF decreases, highlighting once more the importance of the design of the CHX.

4.1. Primary loop

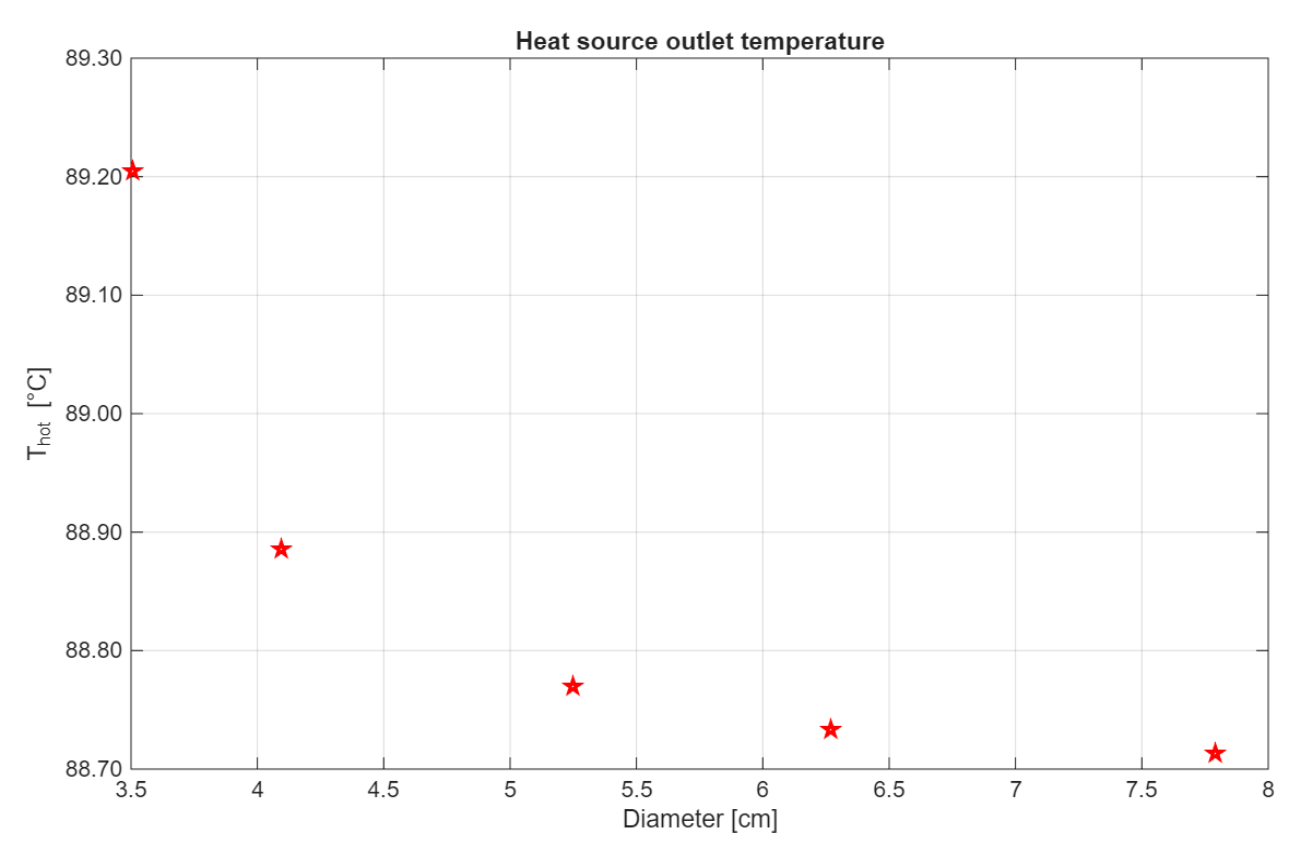
4.1.1. Variation in diameter

In this paragraph we will discuss the results related to the effects of the variation of diameters while the other parameters remain constant. *Table 11* summarizes the values assumed in the calculations:

Parameter	Value	Unit measure
Inner nominal diameter	[3.508 4.094 5.248 6.268 7.792]	mm
Inner nominal diameter	[1.25 1.5 2 2.5 3]	in
Pressure	8 - 150	bar
Loop total height	6	m
Heat source-sink thermal centers height difference	5.145	m
Power	10	kW
HX pressure losses	1.5	kPa
Secondary loop mass flow rate	0.2	kg/s

Table 11. Parameters used in variable diameter analysis.

The results on fluid temperature at the outlet of the heat source, along with the mass flow rate obtained are shown in *Figure 15* and *Figure 16* and refer to an 8 bar primary loop.



Figure~15.~Heat~source~outlet~temperatures~for~different~diameters~at~8~bar.

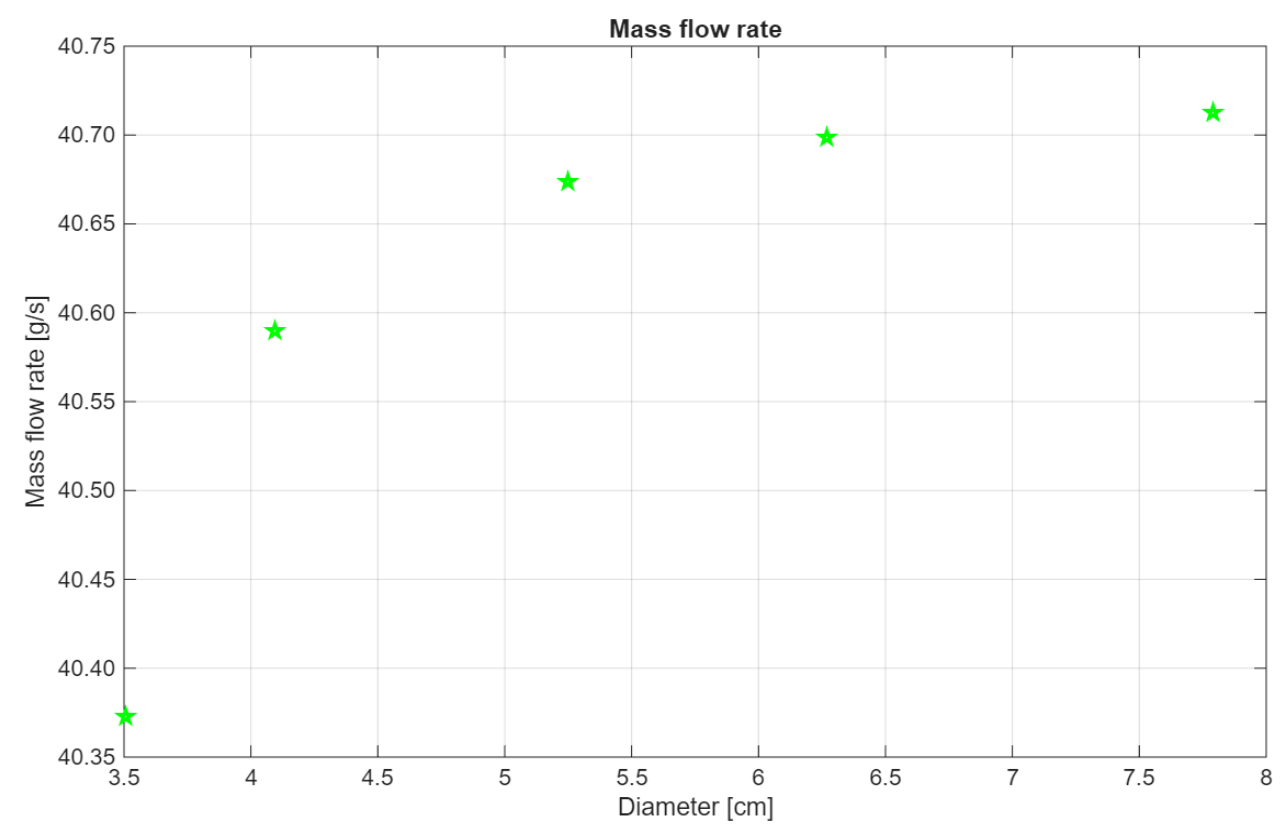


Figure 16. Primary loop mass flow rate for different diameters at 8 bar.

From the graph it's notable how mass flow rate increases with diameter size, while the heat source outlet temperature decreases. As an explanation, smaller diameters caused a lower mass flow rate but a higher temperature jump and vice versa with the higher diameters. However, the effects are small on the overall results. Mass flow rate can also be discussed as a function of the total pressure losses in the loop, as shown in *Table 12*.

1.25 in.	1.5 in.	2 in.	2.5 in.	3 in.
1527.3 Pa	1511.7 Pa	1503.7 Pa	1501.8 Pa	1500.8 Pa

Table 12. Loop's total pressure losses for different diameters.

Since CHX pressure losses and localized pressure losses coefficients are fixed, the differences are caused by the distributed pressure losses and more in particular by friction effects. As friction weakens, the total pressure losses decrease and the mass flow rate increases, as shown with the diameters increase.

The same simulations but for an operative pressure of 150 bar are reported in *Figure 17* and *Figure 18*.

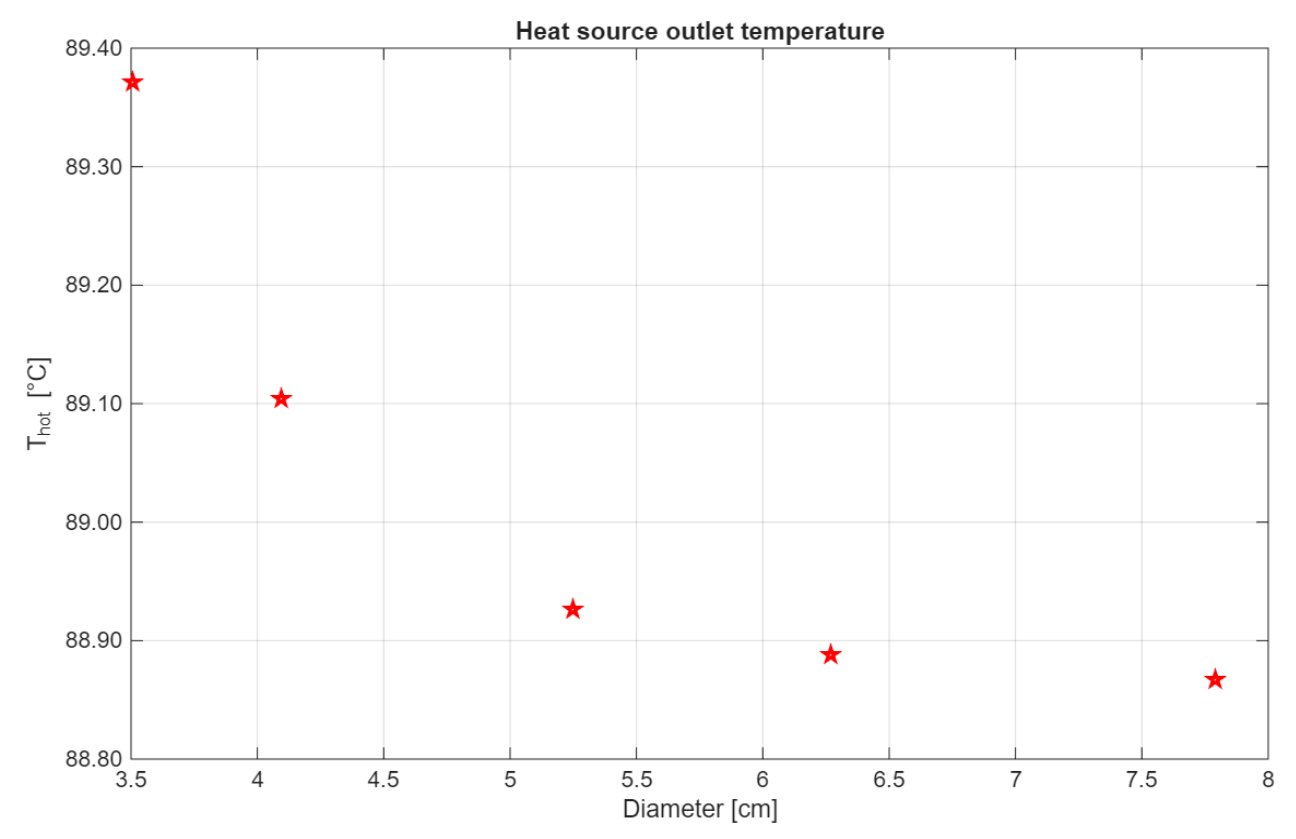
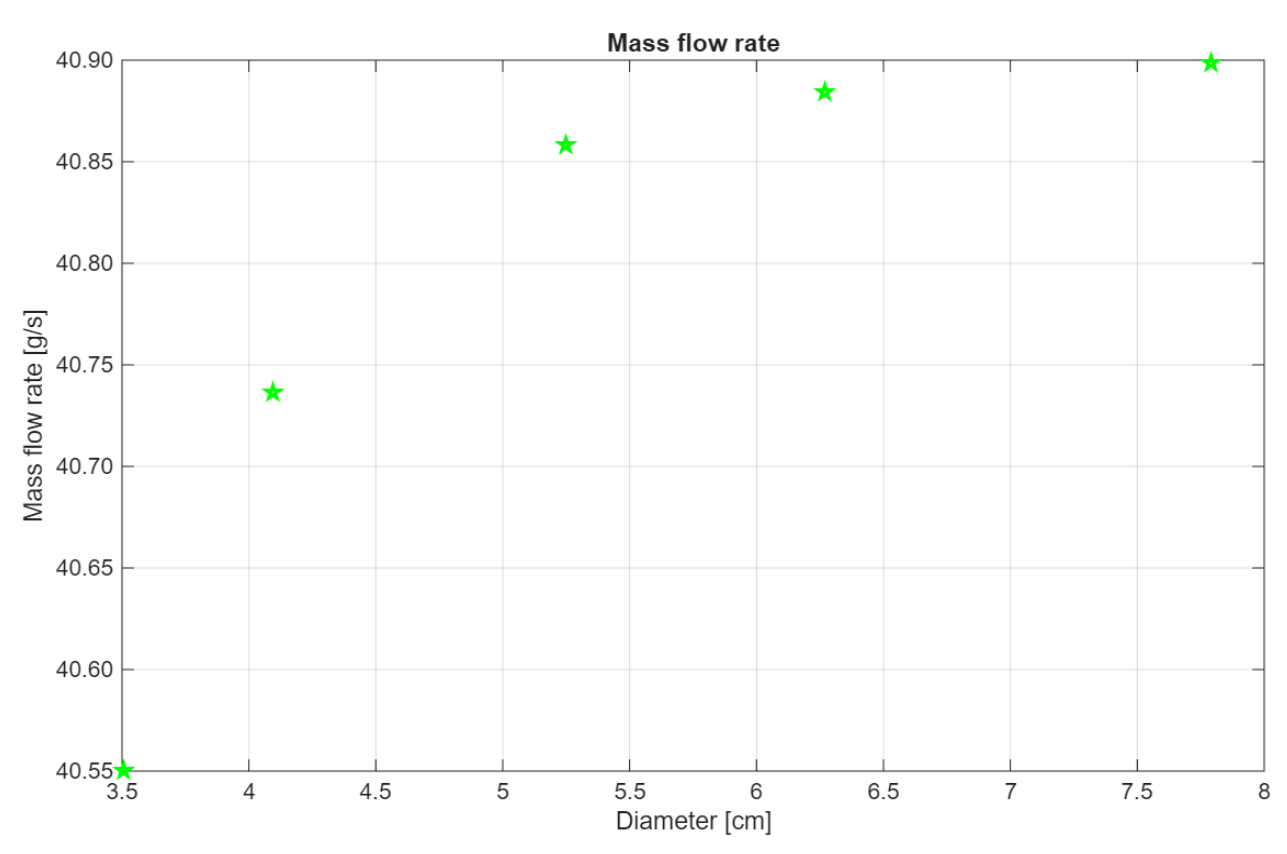


Figure 17. Heat source outlet temperature for different diameters at 150 bar.



Figure~18.~Primary~loop~mass~flow~rate~for~different~diameters~at~150~bar.

The heat source temperatures do not important show changes, along with the mass flow rates (~ 0.35 g/s difference between the two extreme cases, with a difference 0.9%). As a result, it's possible to conclude that loop's diameter has low influence on the final results.

If the attention is paid to the differences between the two pressure cases, it's immediate to notice that the overall solutions do not differ much. In conclusion, pressure doesn't seem to affect deeply the final results.

4.1.2. Variation in operative pressure

In this paragraph the effects of pressure variations are evaluated and discussed. A general idea of the trend of the solution has already been provided in the upper case but it's more accurate to have a proper analysis of the phenomenon. The diameter of the loop, as for the thermal power and the CHX pressure losses, is kept constant. To verify the operation threshold of our single-phase loop, it was decided to proceed with a low-pressure loop study. For this reason, the tested values remained below 30 bar. This choice is justified by the fact that the pressure isn't expected to cause drastic changes to the final results but it simply fixes saturation levels. On the other hand, if it affects the whole results a complete discussion for low and high pressure (~150 bar) analysis would be fundamental. The parameters involved are summed in *Table 13*.

Parameter	Value	Unit measure
Inner diameter	5.248	cm
Inner diameter	2	in
Pressure	[2 5 8 10 15 20]	bar
Loop total height	6	m
Heat source-sink thermal centers height difference	5.145	m
Power	10	kW
HX pressure losses	1.5	kPa
Secondary loop mass flow rate	0.2	kg/s

Table 13. Parameters used in variable pressure analysis.

The results obtained showed infinitesimal variation in all variables: heat source outlet temperature and mass flow rate. The second reaches 88.8 °C and the mass flow rate becomes 40.7 g/s.

The main role of the operative pressure is to fix the maximum thermal load that the loop can take remaining in single phase.

4.1.3. Variation in heat source and sink height difference

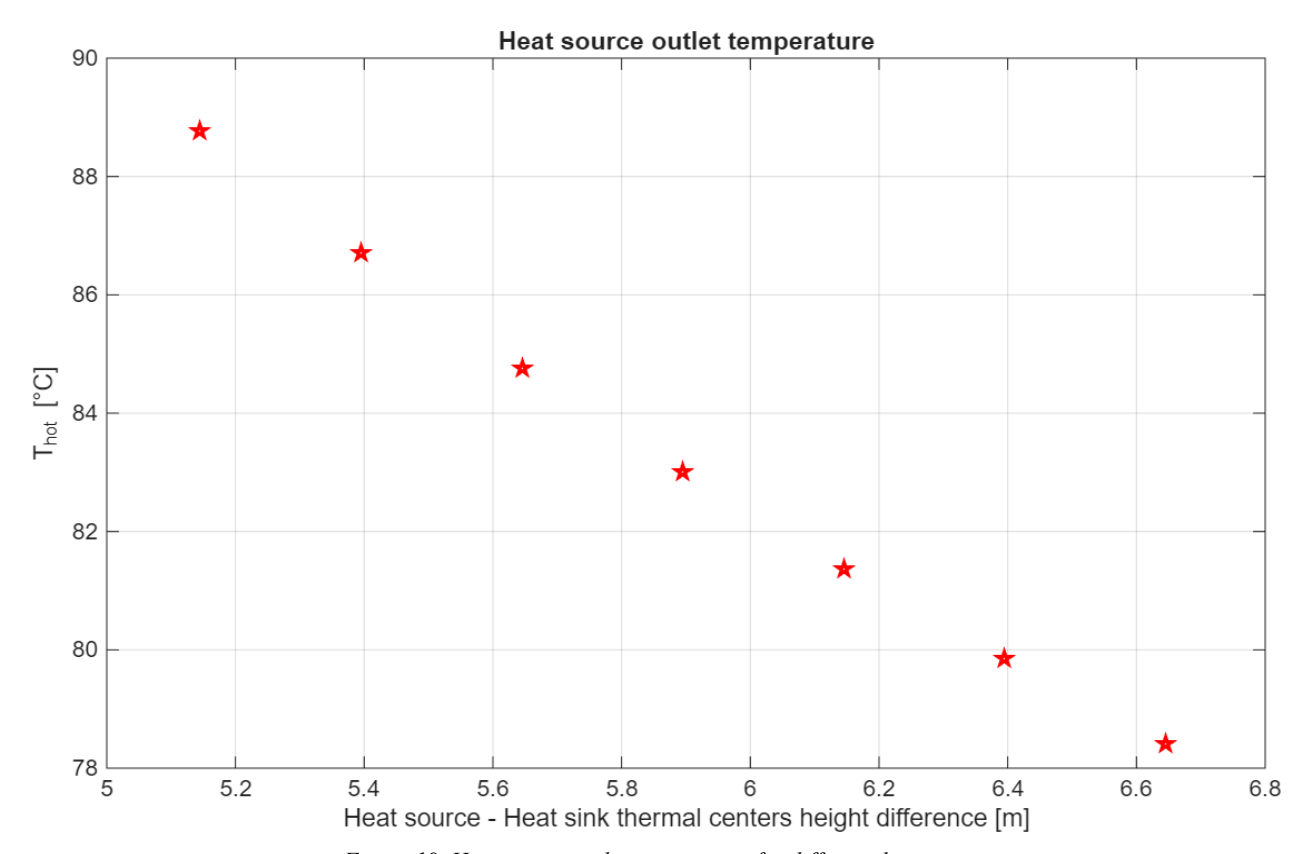
The height difference between the thermal centers of the heat source and the heat sink has a direct impact on the value of the mass flow rate, as shown in Eq. (14), and on the other parameters consequently. In this subsection the loop was evaluated by changing this element (along with the overall loop height) and maintaining all the others fixed, as shown in *Table 14*.

Parameter	Value	Unit measure
Inner diameter	5.248	cm
Inner diameter	2	in
Pressure	8	bar
Loop total height	[6 6.25 6.5 6.75 7 7.25 7.5]	m
Heat source-sink thermal	[5.145 5.395 5.645 5.895	m
centers height difference	6.145 6.395 6.645]	
Power	10	kW
HX pressure losses	1.5	kPa
Secondary loop mass flow rate	0.2	kg/s

Table 14. Parameters used in variable heat source-sink height difference analysis.

Due to limitations linked to the size of the laboratory the maximum loop height cannot exceed 6 m (heat source outlet – heat sink inlet height difference + heated source length) in reality.

The results are shown in Figure 19 and Figure 20.



 $Figure\ 19.\ Heat\ source\ outlet\ temperature\ for\ different\ distances.$

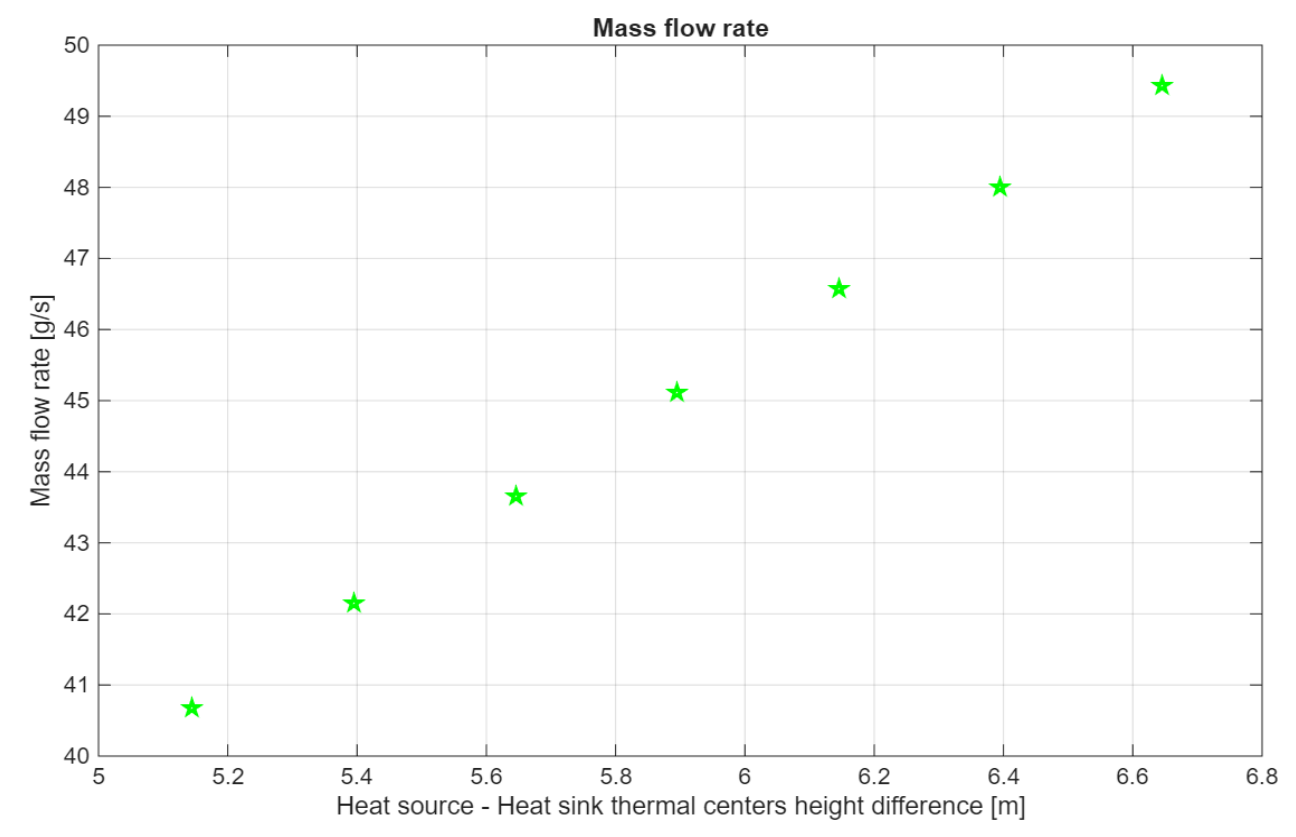


Figure 20. Primary loop mass flow rate for different distances.

The results show increase trend of the mass flow rate with the height difference of the thermal centers of the heat source and the heat sink, and a decrease trend of the temperature jump between inlet and outlet of the heat source. It's important to underline that the increase of the buoyancy effect with the increase of the height of the loop overcomes the effect of the increasing pressure losses caused by longer pipes.

4.1.4. Variation in thermal power

It has already been said that the electric heaters are expected to reach a maximum power load of 50 kW and all the simulations carried out until now have been tested using a much lower load. This subsection analyzes the effects on temperatures and mass flow rate with the increase of thermal power. The parameters considered are summed in *Table 15*.

Parameter	Value	Unit measure
Inner diameter	5.248	cm
Inner diameter	2	in
Pressure	8	bar
Loop total height	6	m
Heat source-sink thermal centers height difference	5.145	m
Power	[10 15 20 25 30 35 40 45 50]	kW
HX pressure losses	1.5	kPa
Secondary loop mass flow rate	0.2	kg/s

Table 15. Parameters used in variable thermal power analysis.

The main restriction is to guarantee that water remains below saturation. As discussed in chapter 4.1.2., the setting of the operative pressure is fundamental for the definition of the saturation temperatures. The loop has been set at quite low pressure (8 bar) to verify threshold conditions. The results are shown in *Figure 21*, *Figure 22* and *Figure 23*.

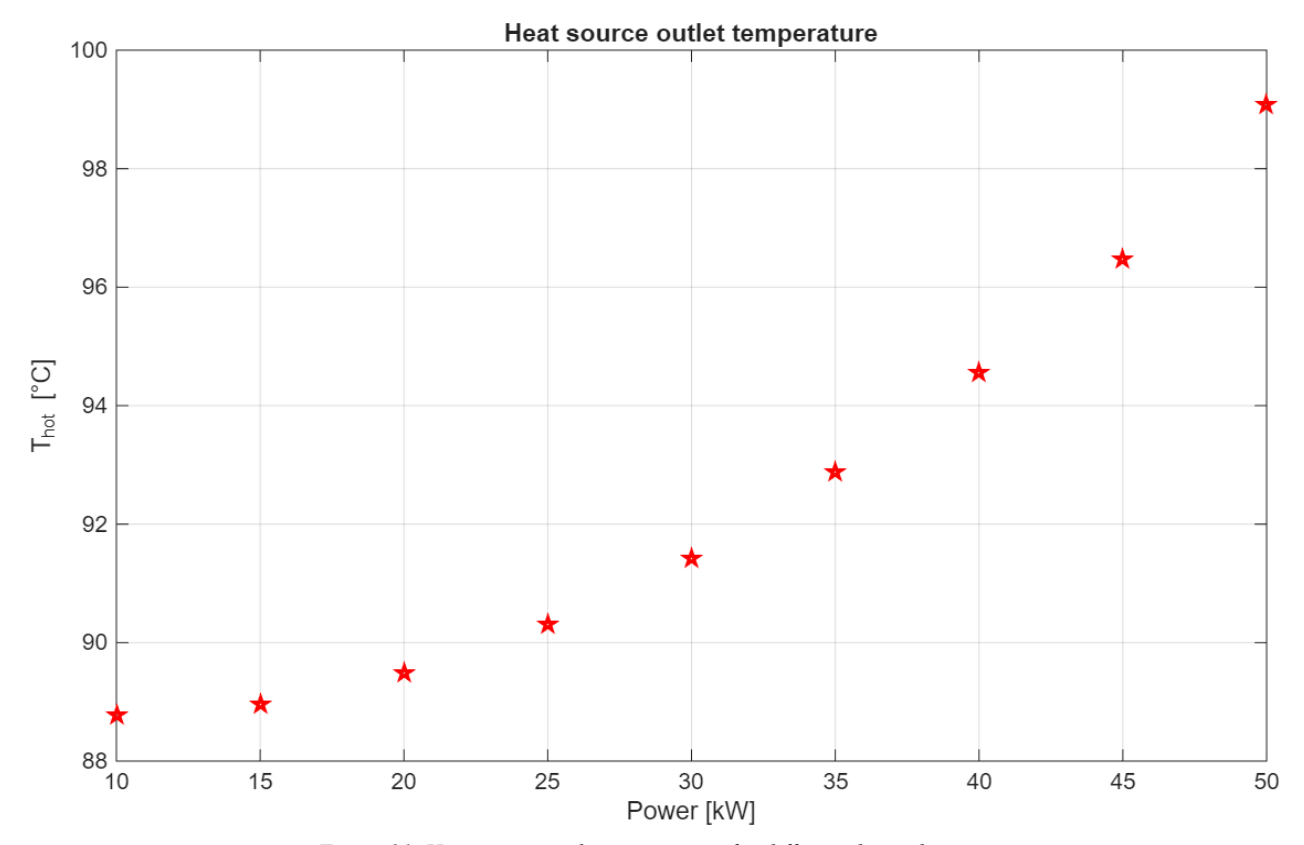


Figure 21. Heat source outlet temperature for different thermal power.

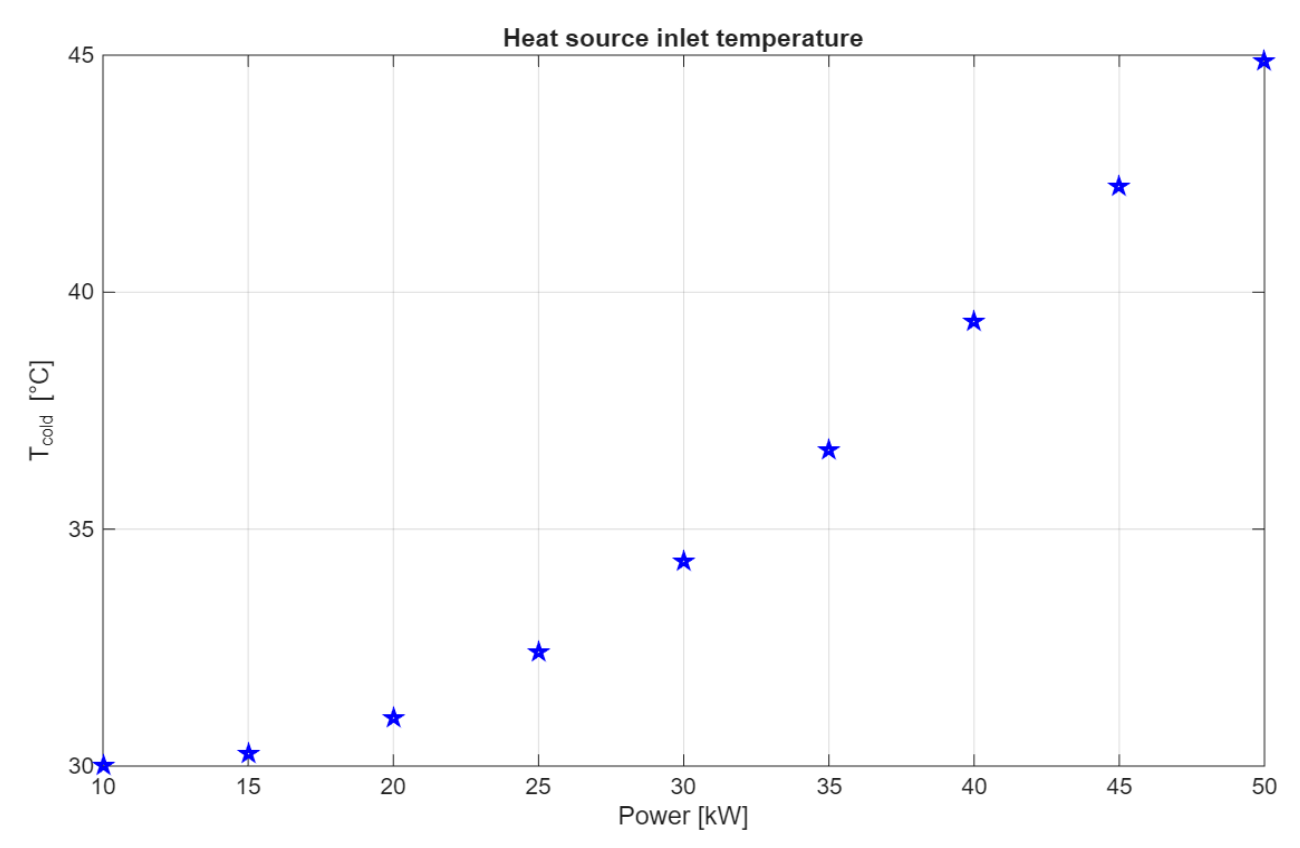


Figure 22. Heat source inlet temperature for different thermal power.

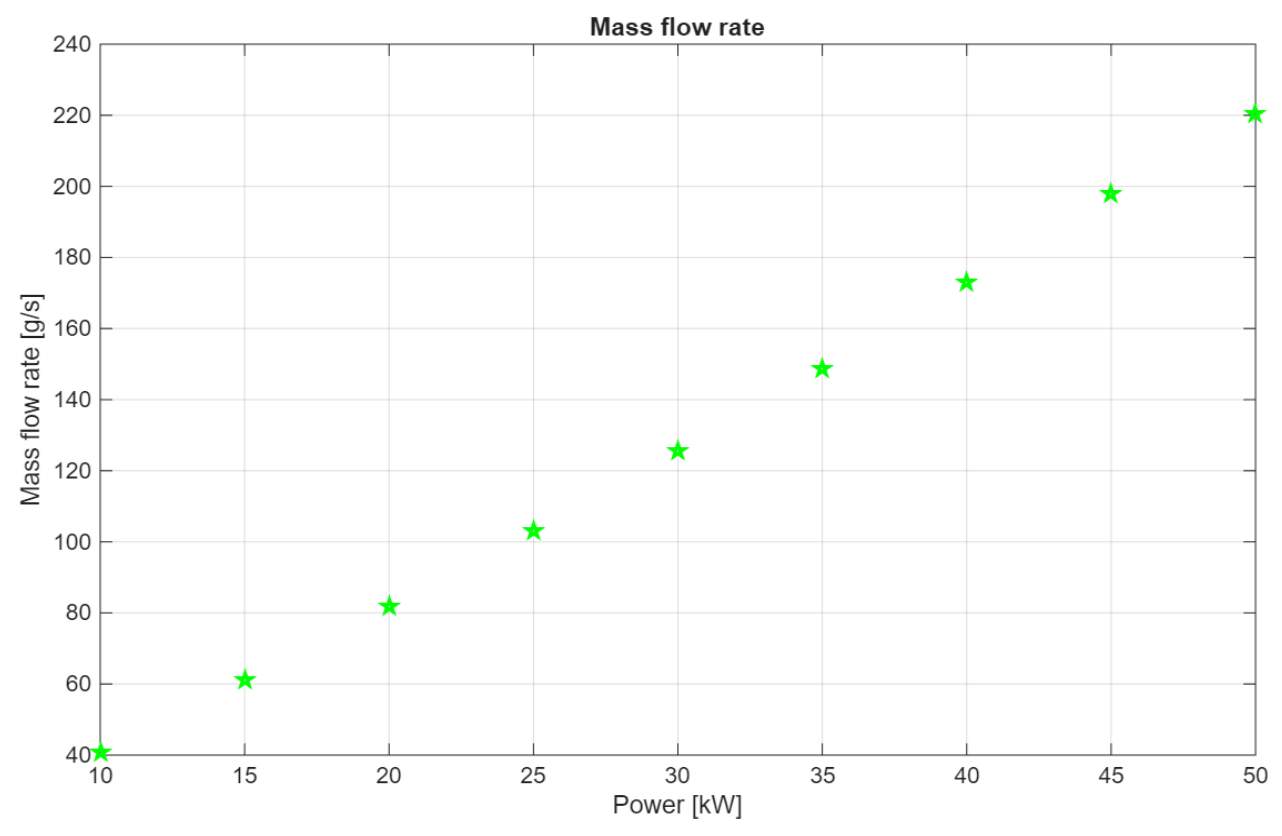


Figure 23. Primary loop mass flow rate for different thermal power.

The trends of the curves are rising: higher power causes higher temperatures and mass flow rate.

Considering the evaluations done regarding the variation of operative pressure, studying the system at 150 bar would only avoid the possibility of falling near saturation conditions without affecting particularly the results. In other words, the higher the operative pressure the higher the water subcooling, that allows to avoid saturation in the hottest spots of the loop.

4.1.5. Variation in HX pressure losses

Since the actual value of the compact heat exchanger pressure losses are unknown a priori, different scenarios have been considered, with different pressure losses assumed in the CHX. The data imposed are presented in *Table 16*.

Parameter	Value	Unit measure
Inner nominal diameter	5.248	cm
Inner nominal diameter	2	in
Pressure	150	bar
Loop total height	6	m
Heat source-sink thermal centers height difference	5.145	m
Power	10	kW
HX pressure losses	[1.5 3 5 10 15]	kPa
Secondary loop mass flow rate	0.2	kg/s

Table 16. Parameters used in variable CHX pressure losses analysis.

The results are shown in Figure 24 and Figure 25.

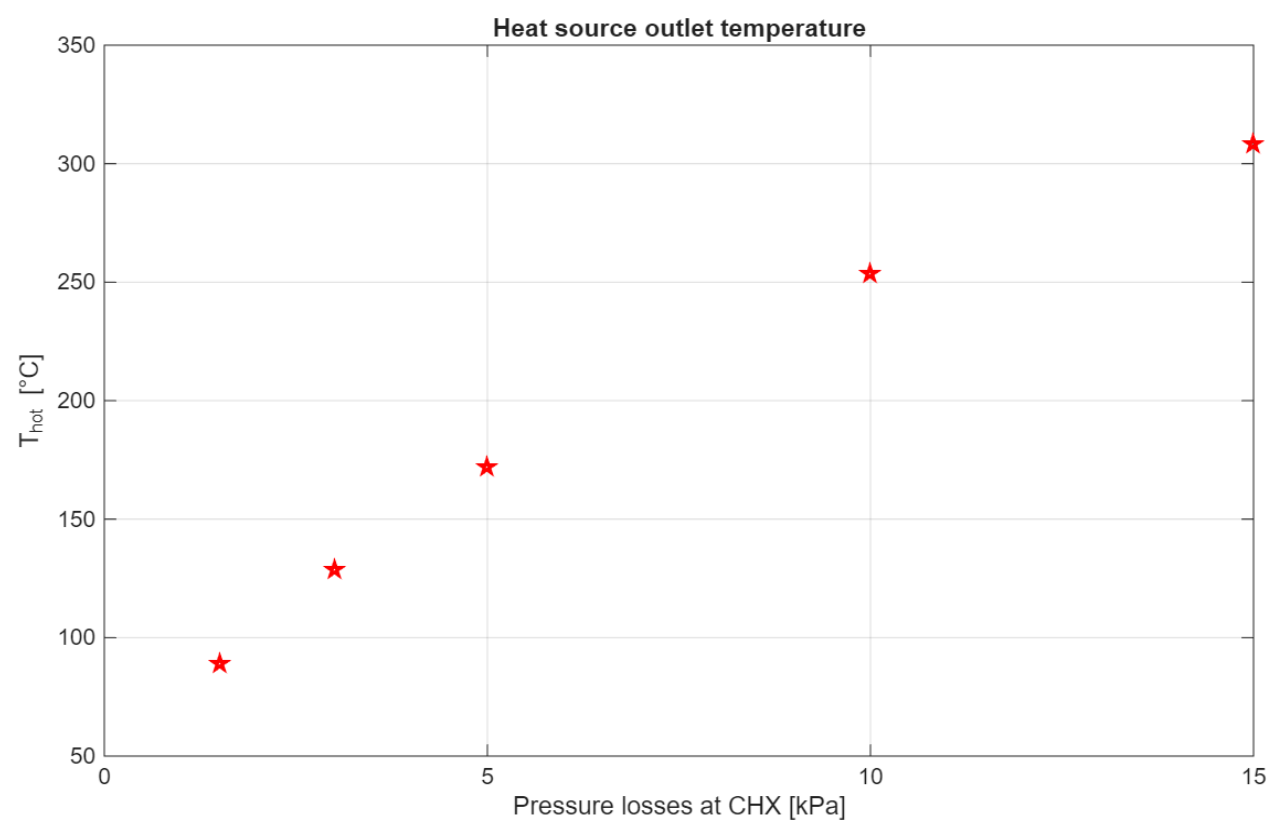


Figure 24. Heat source outlet temperature for different CHX pressure losses.

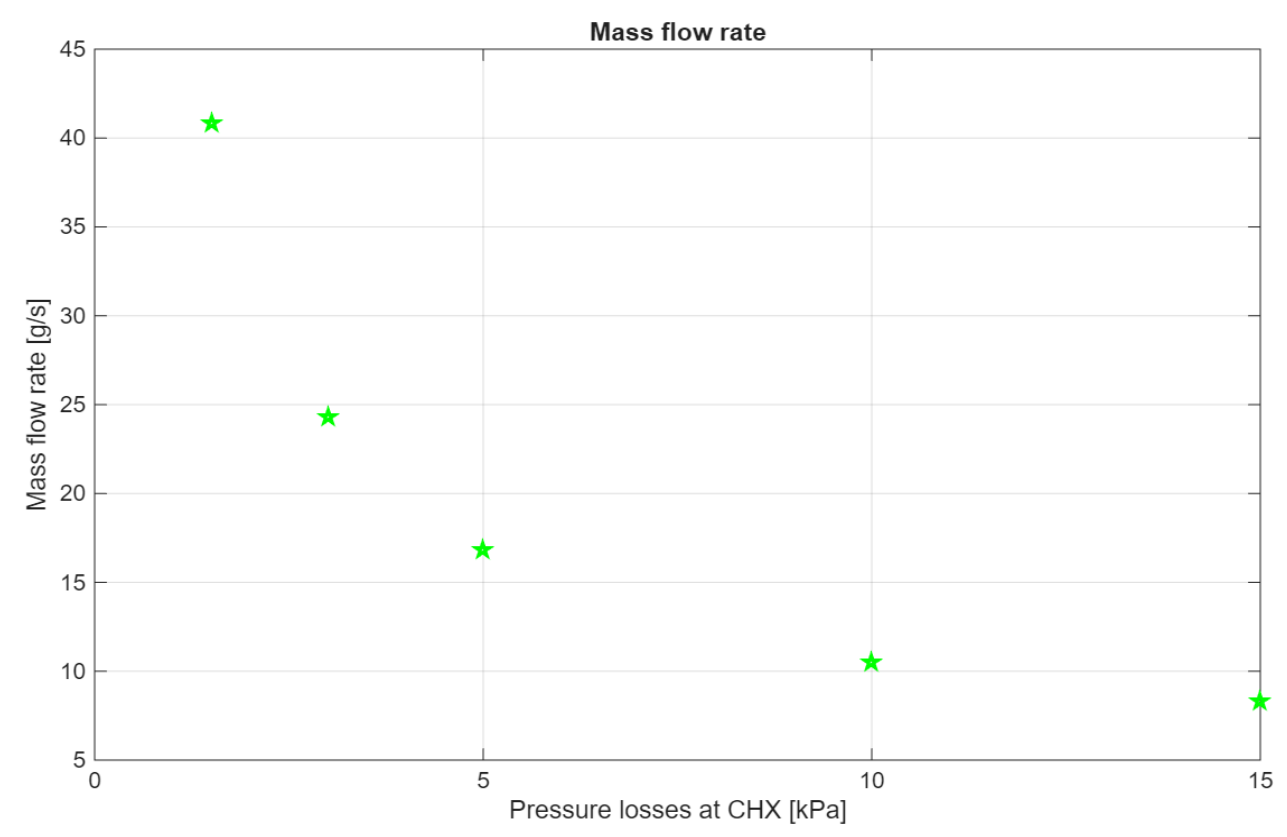


Figure 25. Primary loop mass flow rate for different CHX pressure losses.

As the pressure losses increase, the hydraulic resistance increases and therefore the mass flow rate decreases. Low mass flow rates cause longer residence time in the heat source of the operative fluid, which ends up in higher temperatures at heat source outlet. For what concerns water temperature at heat source inlet, its values remain almost constant at 30 °C.

Despite the other cases, this analysis has been performed with an operative pressure of 150 bar. This choice was justified by the necessity to fix a pressure value that guaranteed a sufficiently high saturation temperature in the loop and avoided the possibility of steam production. For the worst case (a pressure loss imposed at 15 kPa) a minimum of 100 bar is required for the loop, with a respective saturation temperature at 311 °C (slightly above the 308 °C reached by the simulation).

Fixing the thermal load and the height difference between the heat source and the heat sink, the major variations seem to be caused by diameter and CHX pressure loss coefficient changes. For this reason, it's important to discuss the effects of the combination of CHX pressure losses applied to different values of diameter. *Table 17* shows the parameters imposed for the simulations.

Parameter	Value	Unit measure
Inner diameter	[3.508 4.094 5.248 6.268 7.792]	cm
Inner diameter	[1.25 1.5 2 2.5 3]	in
Pressure	150	bar
Loop total height	6	m
Heat source-sink		
thermal centers height	5.145	m
difference		
Power	10	kW
HX pressure losses	[1.5 3 5 10 15]	kPa
Secondary loop mass flow rate	0.2	kg/s

Table 17. Parameters used in variable diameter and CHX pressure losses analysis.

The plots of mass flow rate and temperatures are shown in Figure 26 and Figure 27.

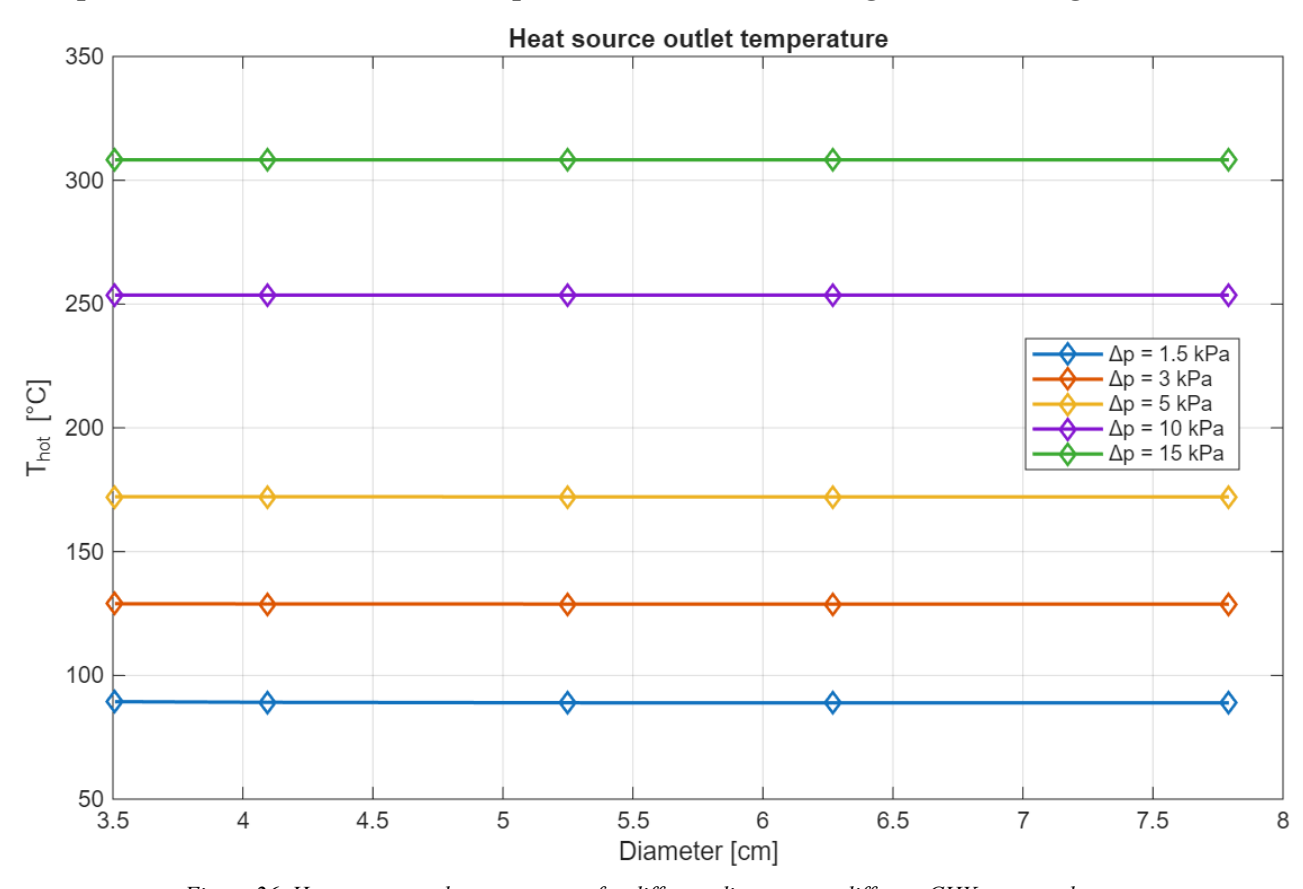


Figure 26. Heat source outlet temperature for different diameters at different CHX pressure losses.

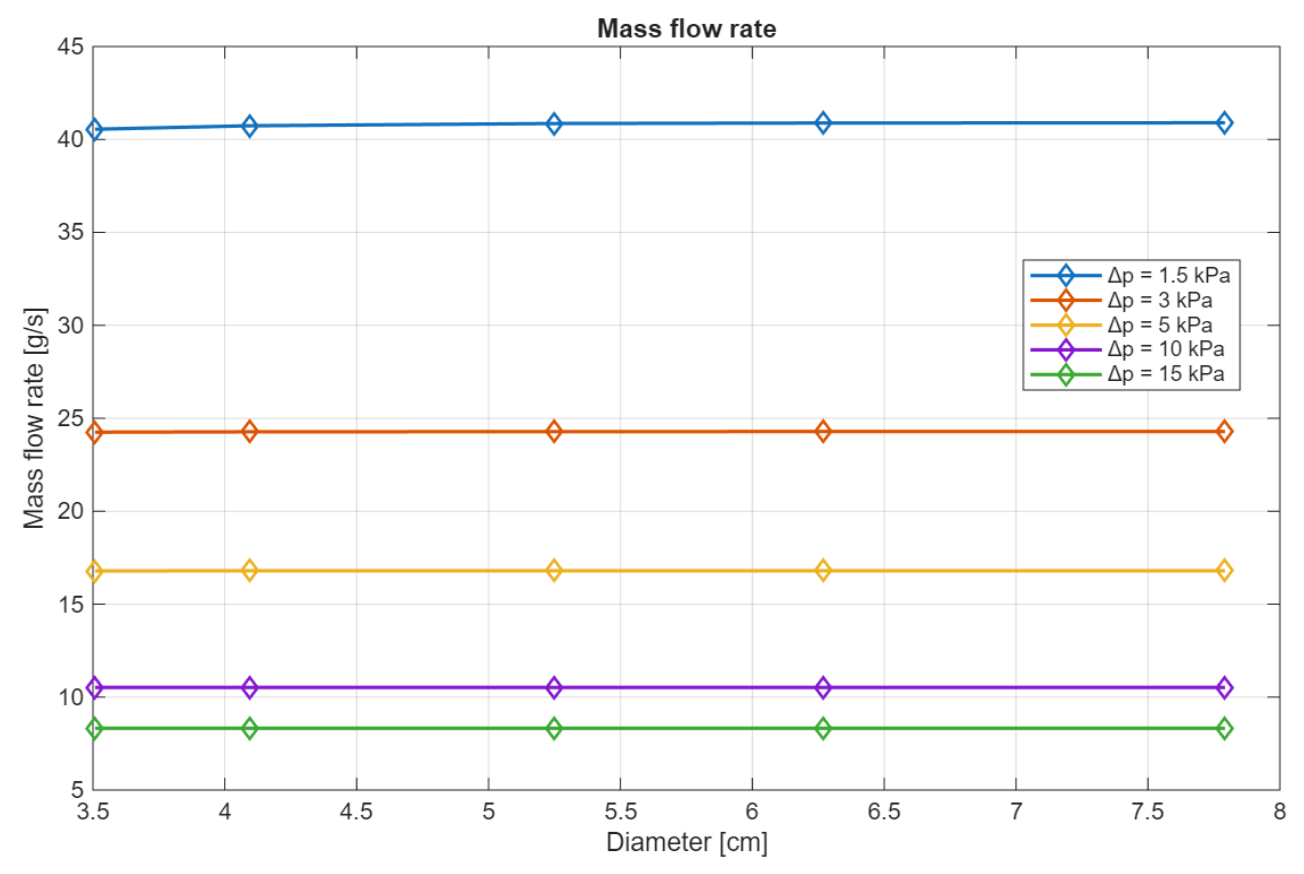


Figure 27. Primary loop mass flow rate for different diameters at different CHX pressure losses.

It's evident how the effect of the pressure loss coefficient is dominant and leads to large differences in all the graphs. The effects of the diameters are slightly visible.

4.2. Secondary loop

A parametric analysis has been performed on the global structure, evaluating the behavior of both primary and secondary loops in terms of mass flow rate and temperatures. The two systems are coupled by the CHX. Similarly to the previous tests, the model studied the effects induced by the variations of:

- Loop pipes diameter.
- CHX pressure losses.
- Thermal power.

The effects of the variation of operative pressure have been neglected due to the discovery of its infinitesimal effect on results. For what concerns the variation of the thermal centers of heat source and sink height distance, the choice has been to maintain it constant for both primary and secondary loop due to structural limitations.

4.2.1. Variation in diameter

The structure of the model is like the one of chapter 4.1.1.. The analysis assumed that both primary and secondary loops had equal diameter size. *Table 18* shows the values of the parameters involved.

Parameter	Value	Unit measure
Primary/Secondary inner diameter	[3.508 4.094 5.248 6.268 7.792]	cm
Primary/Secondary inner diameter	[1.25 1.5 2 2.5 3]	in
Primary loop pressure	8 – 150	bar
Primary loop total height	6	m
Heat source-sink thermal centers height difference	5.145	m
Power	10	kW
HX pressure losses	1.5	kPa
Secondary loop pressure	2 - 70	bar
Secondary loop source- sink height difference	7	m

Table 18. Parameters used in variable diameter analysis.

As for the primary loop model, the effects of diameter variations have been tested for both low pressure (8 bar at primary loop and 2 bar at secondary) and high pressure (150 bar at primary and 70 bar at secondary) systems.. The value of the thermal load and the CHX pressure losses are of fundamental importance.

The results in a low-pressure system are shown in *Figure 28, Figure 29, Figure 30, Figure 31* and *Figure 32*.

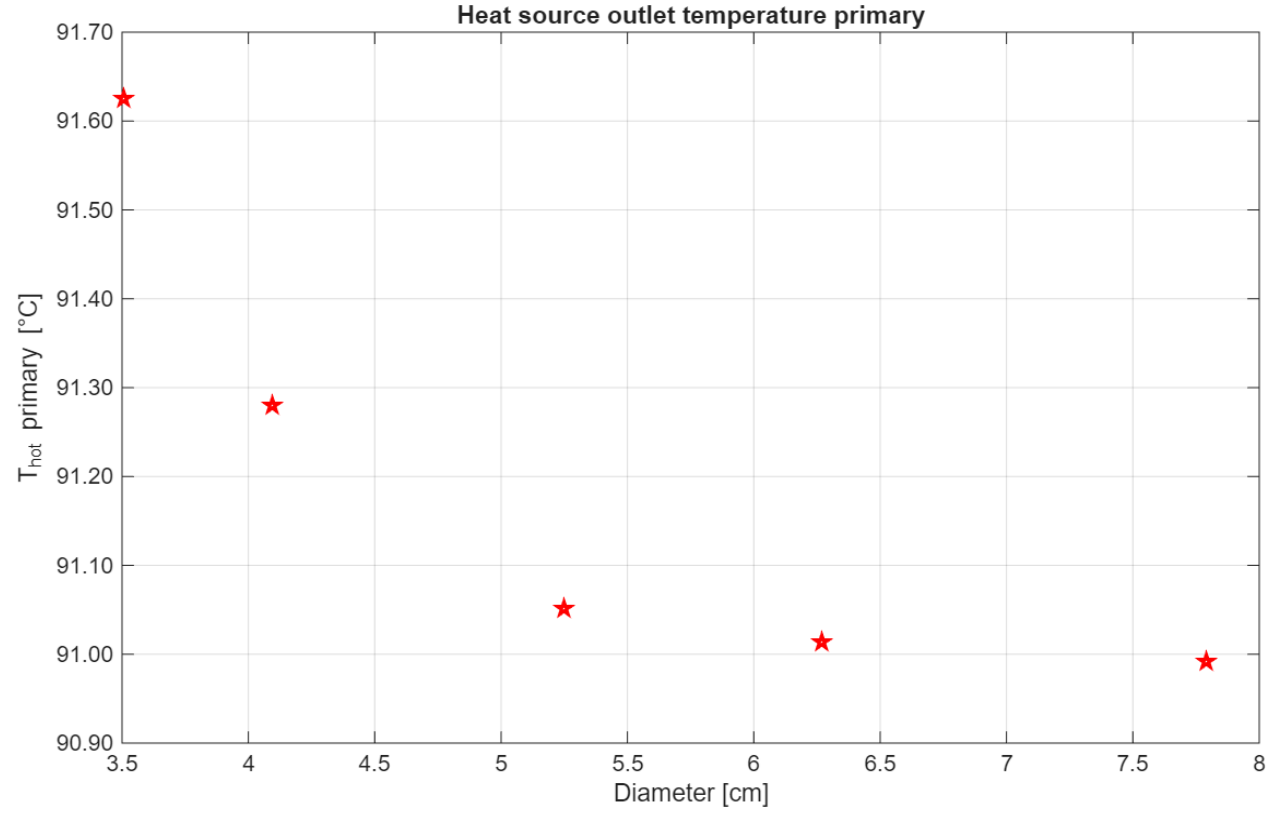


Figure 28. Heat source outlet temperature for different diameters at 8 bar.

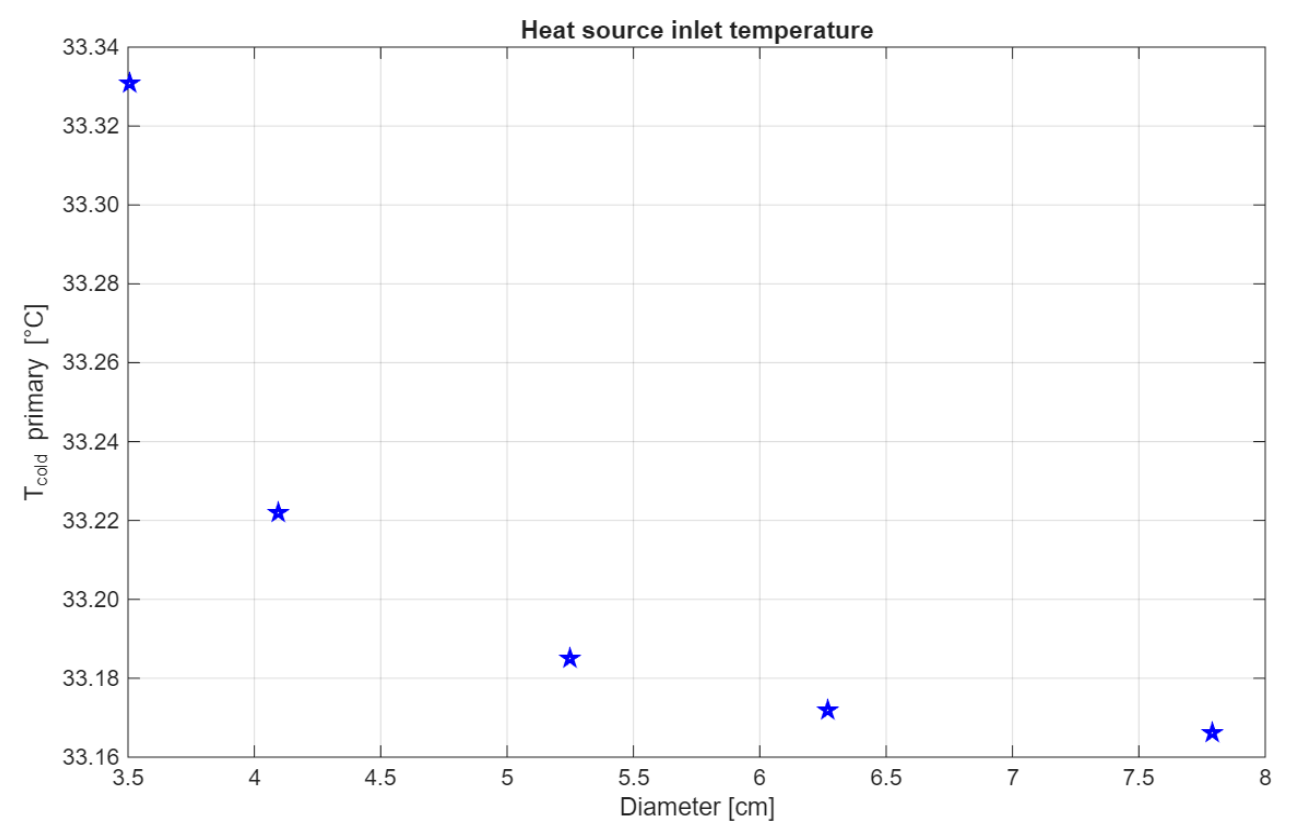


Figure 29. Heat source inlet temperature for different diameters at 8 bar.

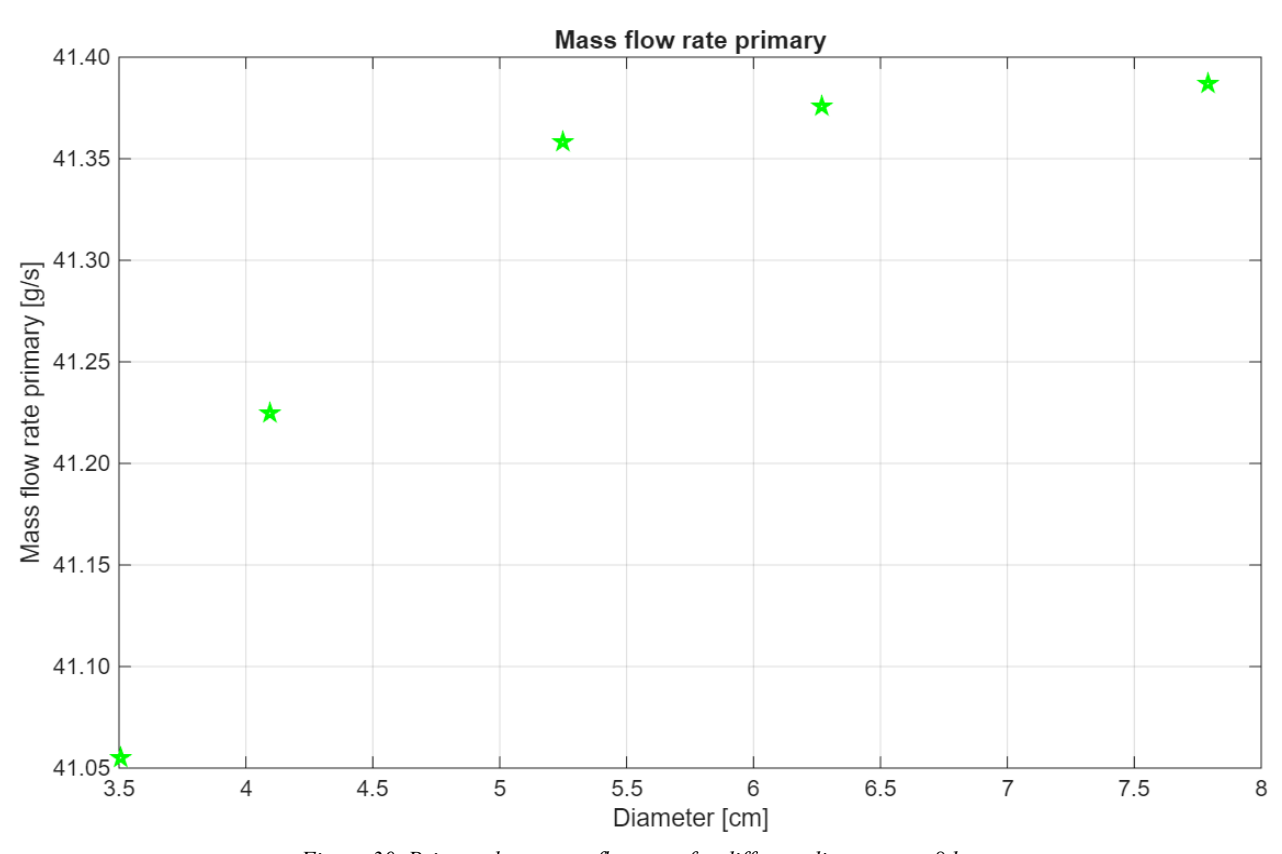


Figure 30. Primary loop mass flow rate for different diameters at 8 bar.

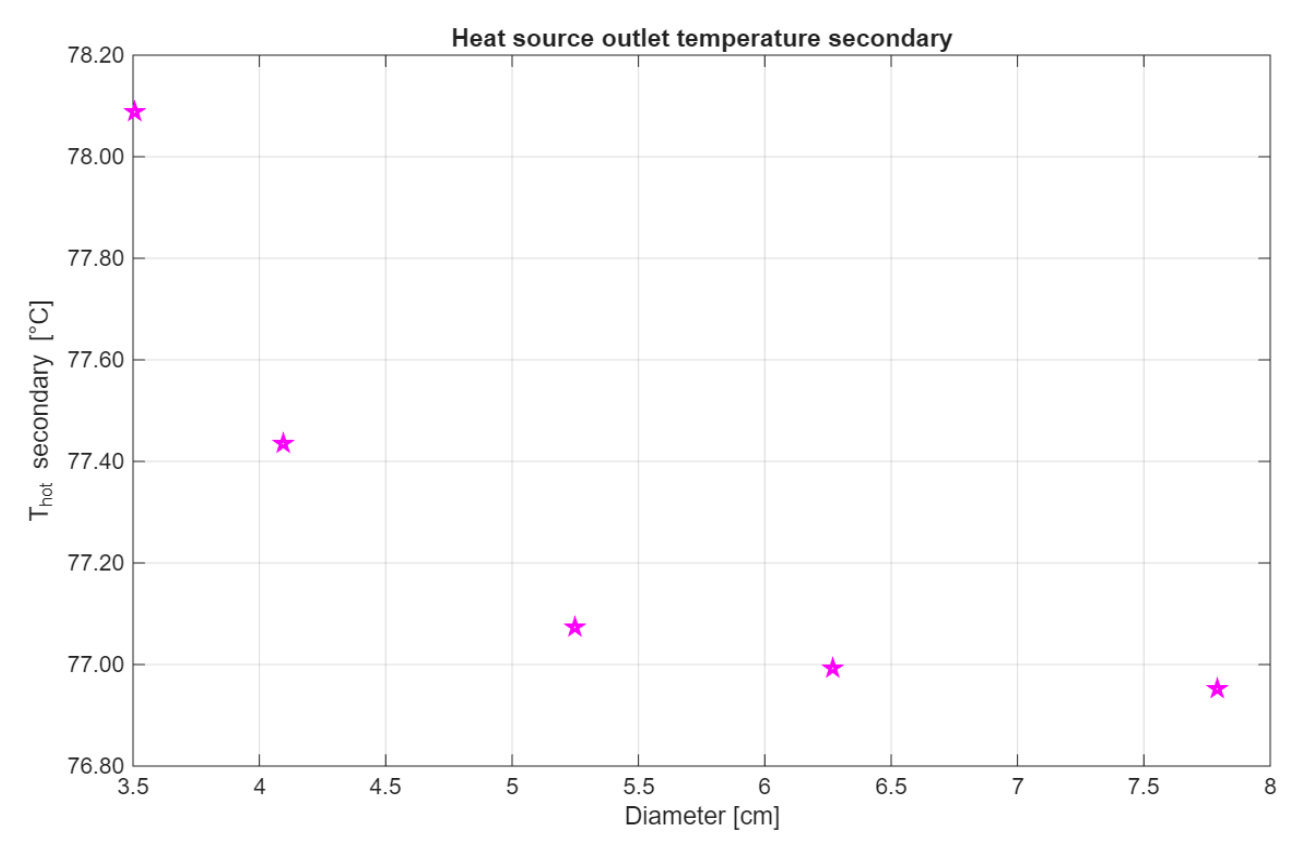


Figure 31. CHX outlet temperature on secondary side for different diameters at 2 bar.

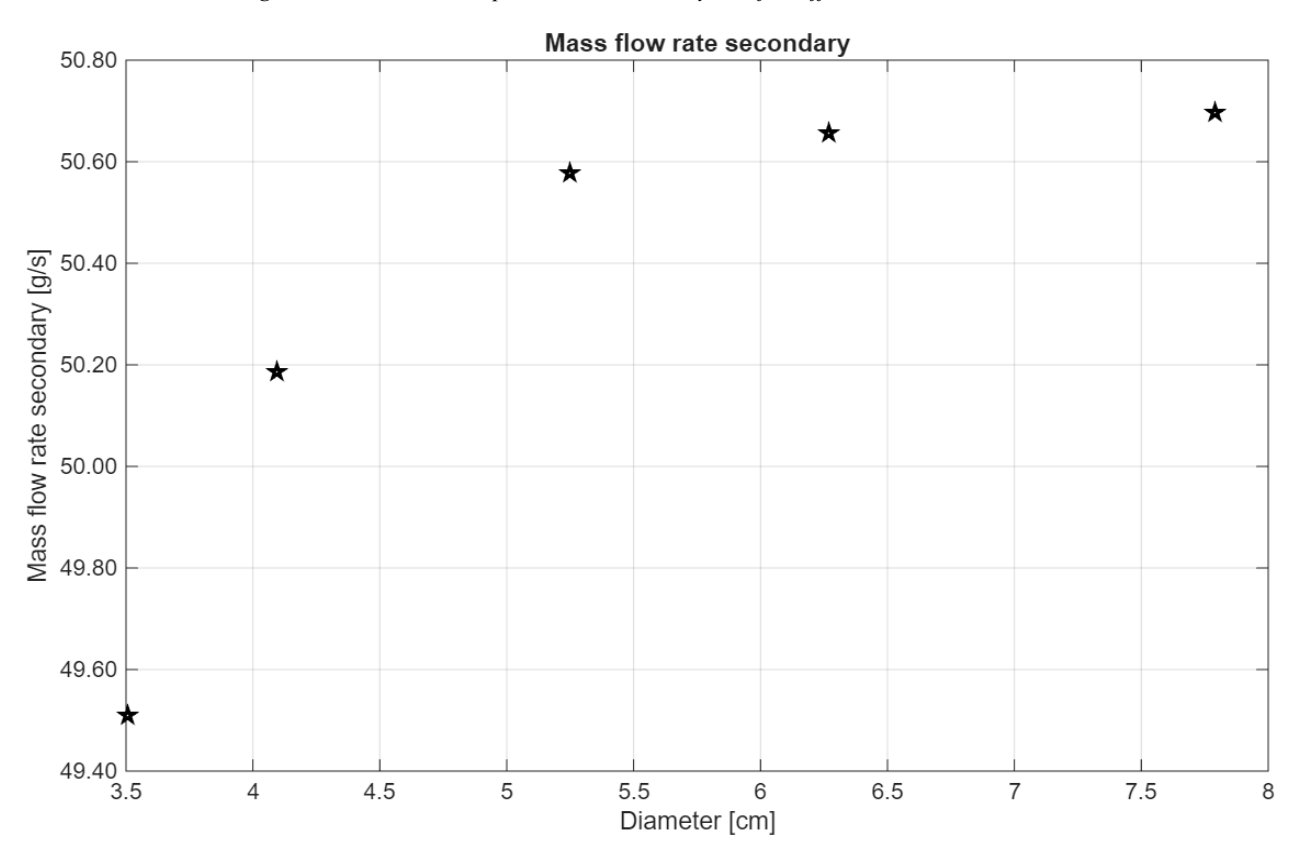


Figure 32. Secondary loop mass flow rate for different diameters at 2 bar.

The trend of primary loop variables is the same of the primary-loop-only case, with the only difference of a small increase in temperature and mass flow rates values (with an increase in values below 1% for primary loop and around 2% for secondary). The increase in

temperatures is directly connected to the introduction of the secondary loop that substitutes the constant temperature hypothesis of the previous case. The higher temperature difference between inlet and outlet of the heat source has brought to a reduced mass flow rate.. *Table 19* compares the value of this ΔT in this and the previous case.

Diameter	ΔT in primary-loop-only system	ΔT in coupled primary- secondary system
1.25	59.36	58.68
1.5	59.09	58.37
2	58.91	58.24
2.5	58.87	58.21
3	58.85	58.20

Table 19. Comparison of primary loop ΔT .

For what concerns the secondary loop, the hot temperature shows a decreasing trend, while the mass flow rate increases with diameter. This is caused by the reduction of friction pressure losses brought by larger diameters, which caused a reduction in temperature difference between inlet and outlet of CHX.

The behavior of high-pressure conditions is shown in the graphs below (Figure 33, Figure 34, Figure 35, Figure 36 and Figure 37).

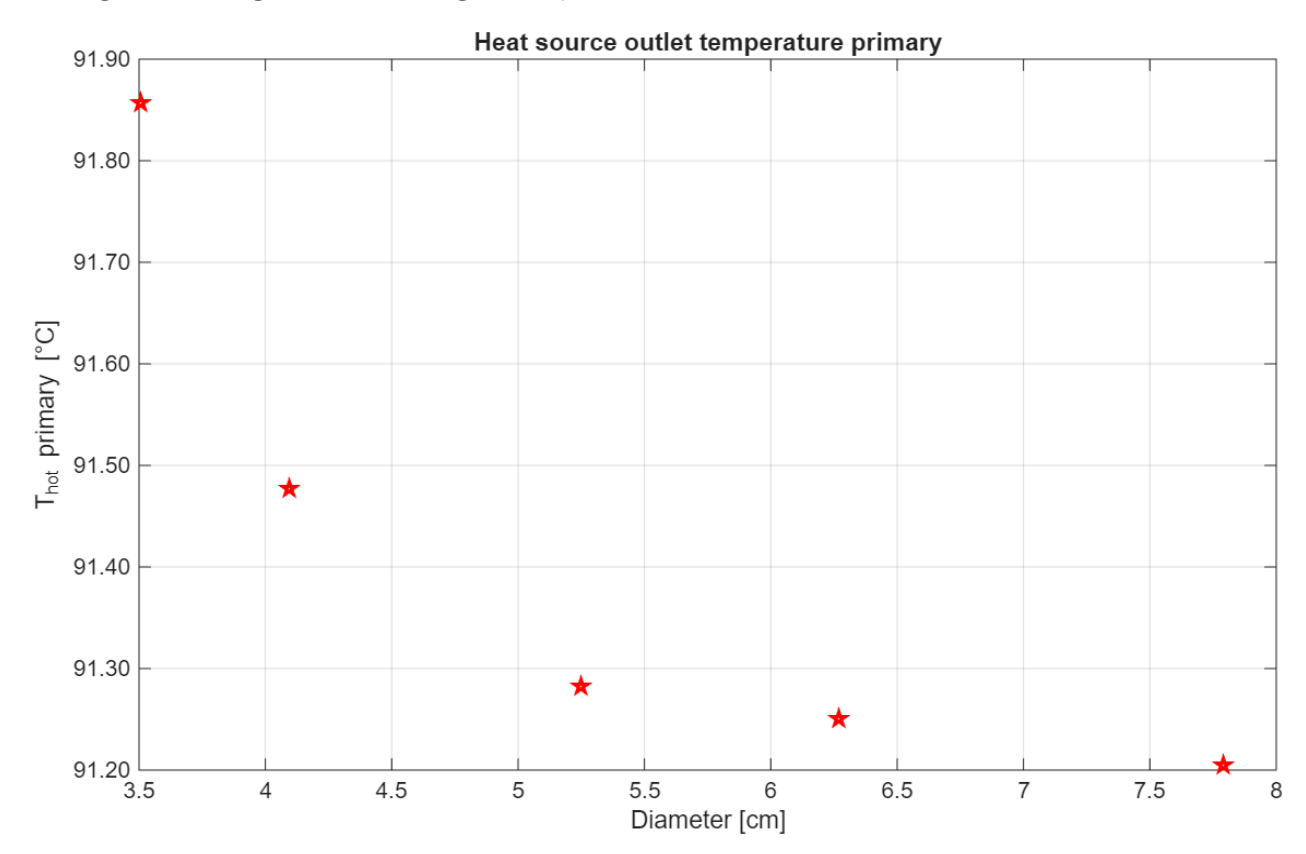


Figure 33. Heat source outlet temperature for different diameters at 150 bar.

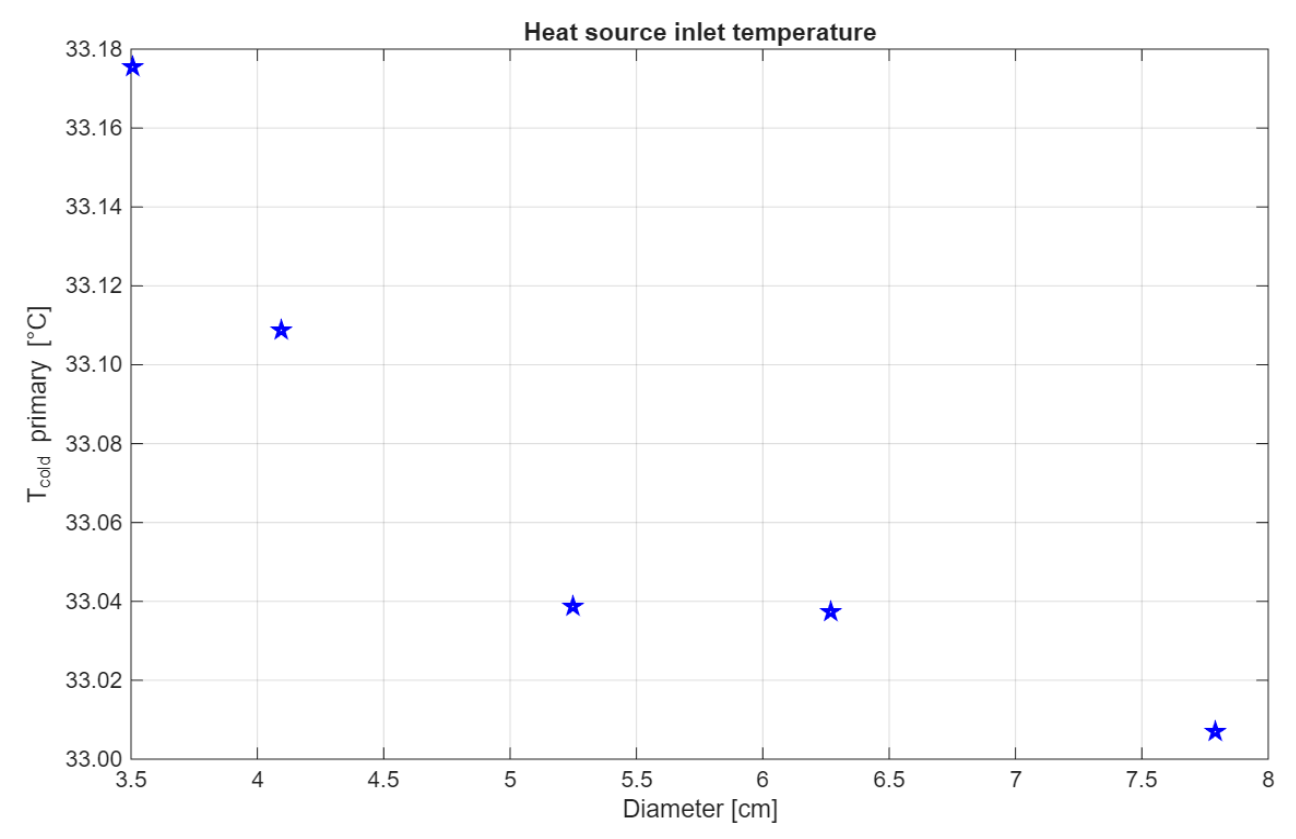


Figure 34. Heat source inlet temperature for different diameters at 150 bar.

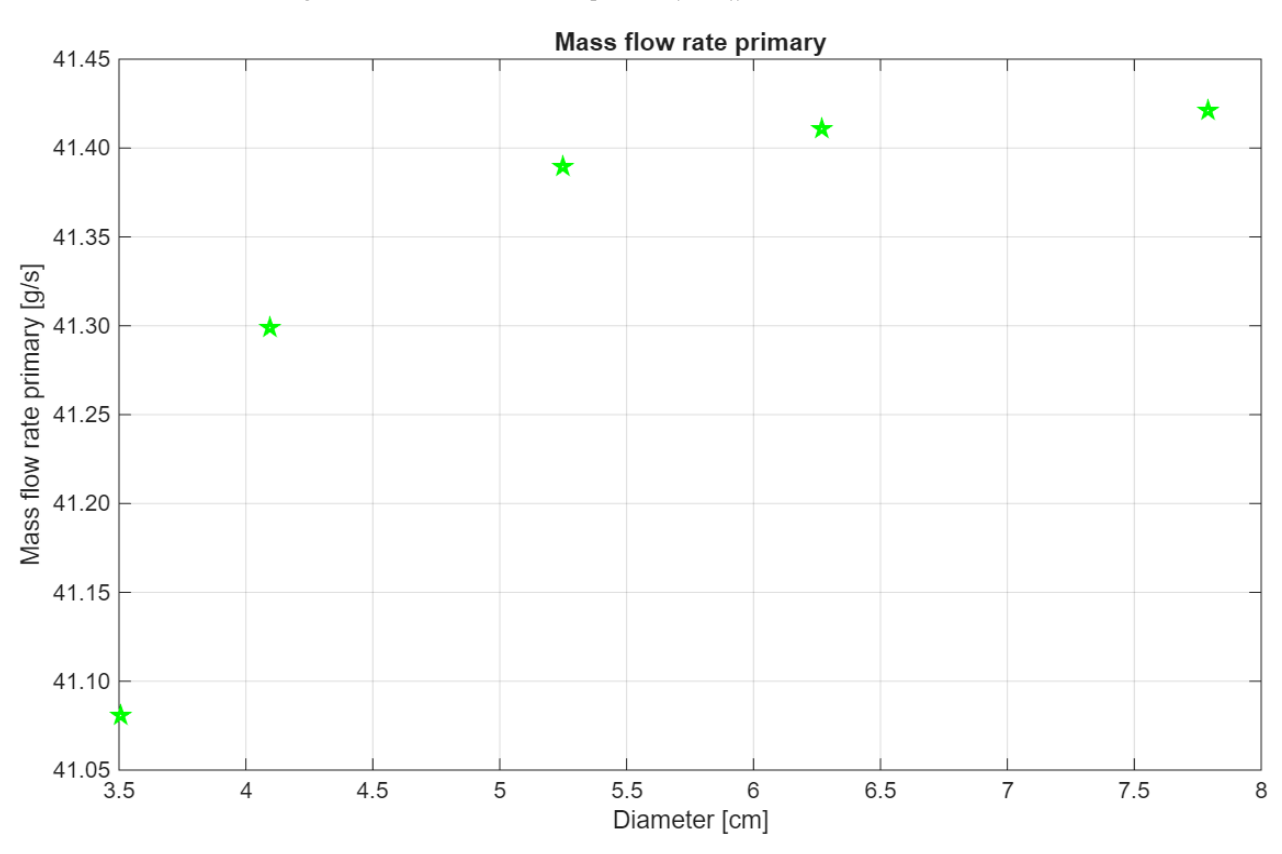


Figure 35. Primary loop mass flow rate for different diameters at 150 bar.

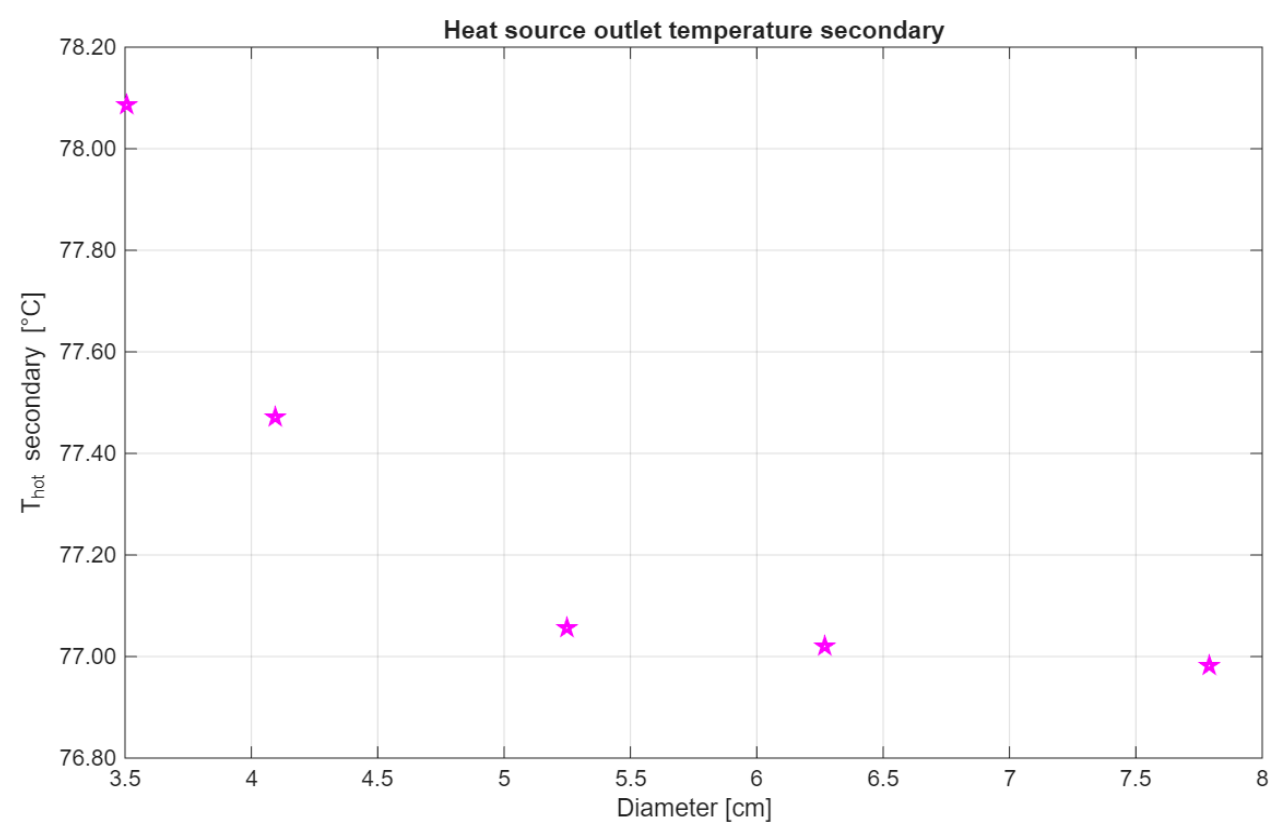


Figure 36. CHX outlet temperature on secondary side for different diameters at 70 bar.

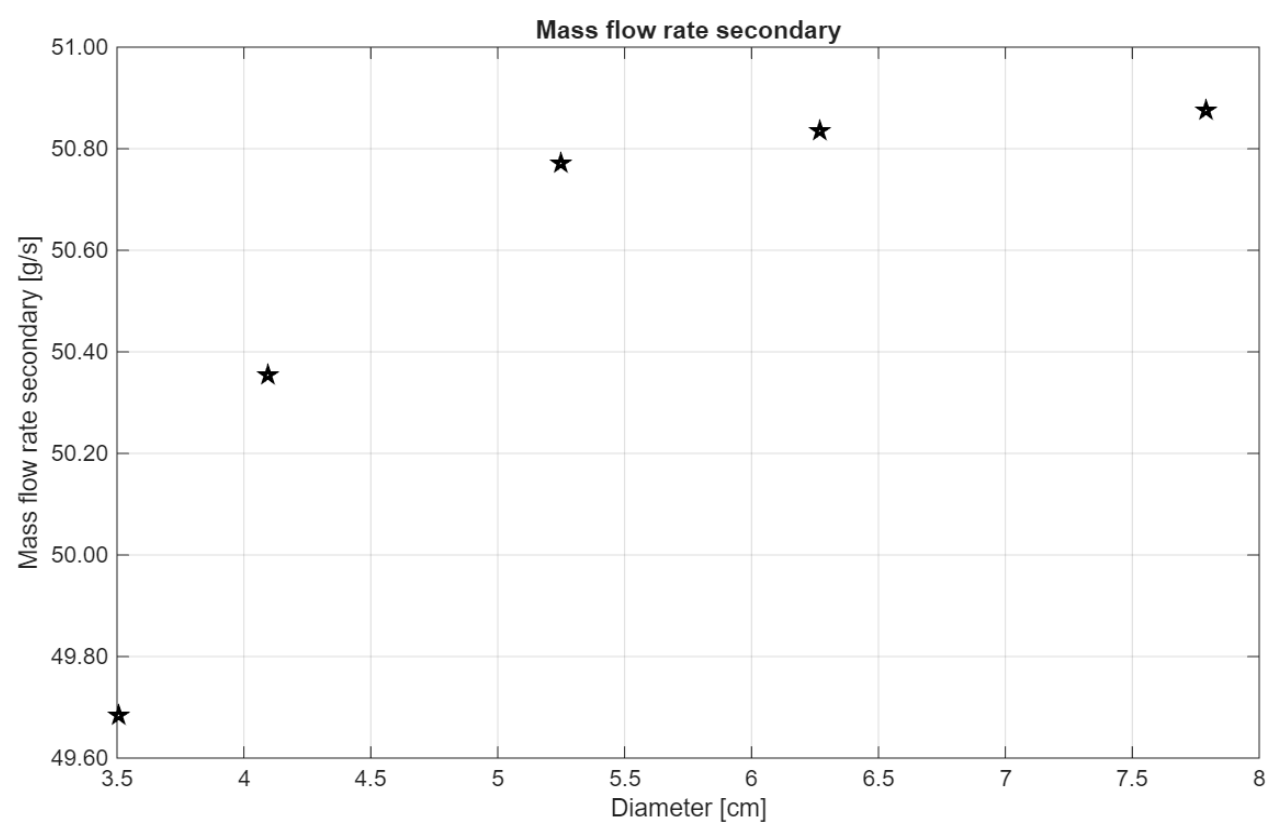


Figure 37. Secondary loop mass flow rate for different diameters at 70 bar.

As expected, the results are subjected to very small variations induced by the change in thermal properties.

4.2.2. Variation in thermal power

In this subsection the effects of the variation of thermal power have been analyzed. To proceed with the tests, pipes constant diameter and HX pressure losses have been assumed. The technical and geometrical parameters involved are shown in *Table 20*.

Parameter	Value	Unit measure
Primary/Secondary inner diameter	5.248	cm
Primary/Secondary inner diameter	2	in
Primary loop pressure	150	bar
Primary loop total height	6	m
Heat source-sink thermal centers height difference	5.145	m
Power	[10 15 20 25 30]	kW
HX pressure losses	1.5	kPa
Secondary loop pressure	70	bar
Secondary loop source-sink height difference	7	m

Table 20. Parameters used in variable thermal power analysis.

The results obtained are illustrated here below (Figure 38, Figure 39, Figure 40, Figure 41 and Figure 42).

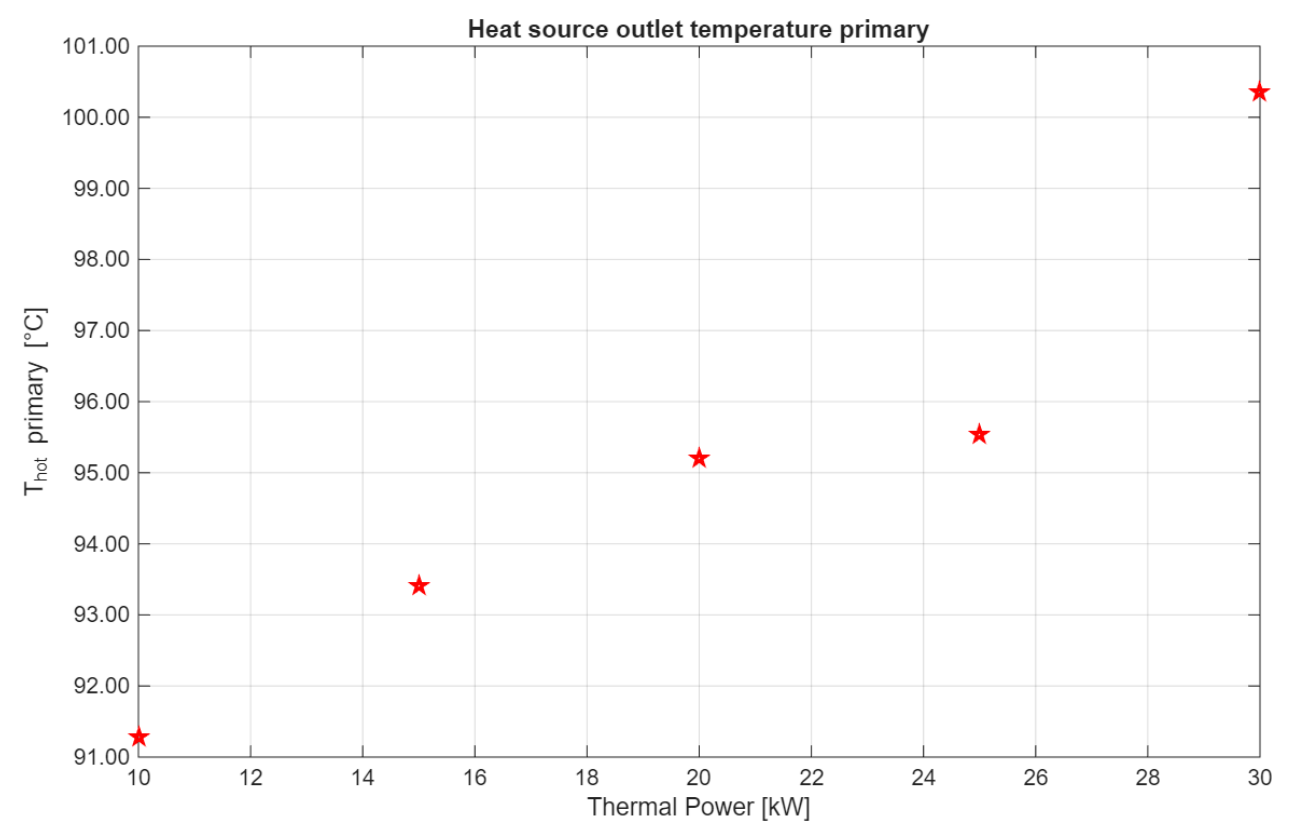


Figure 38. Heat source outlet temperature for different thermal powers.

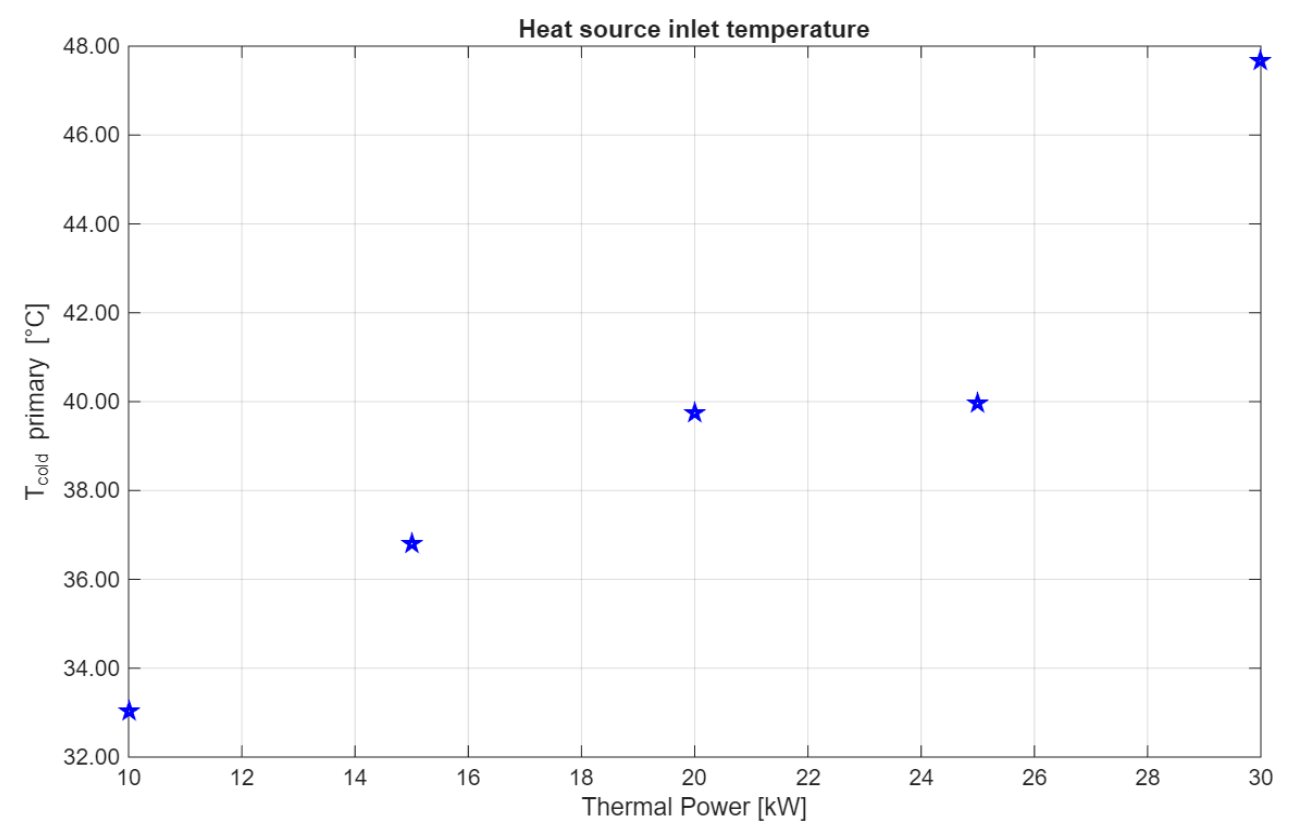


Figure 39. Heat source inlet temperature for different thermal powers.

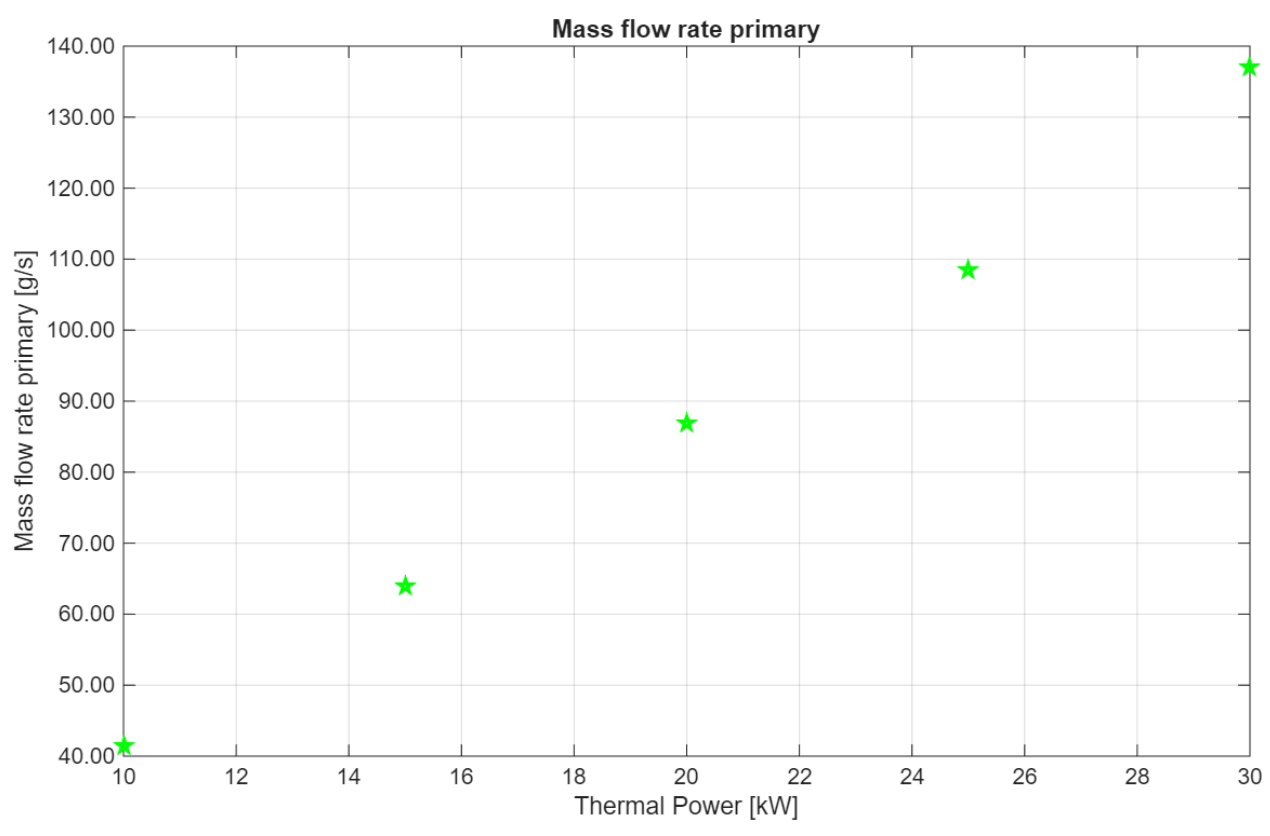


Figure 40. Primary loop mass flow rate for different thermal powers.

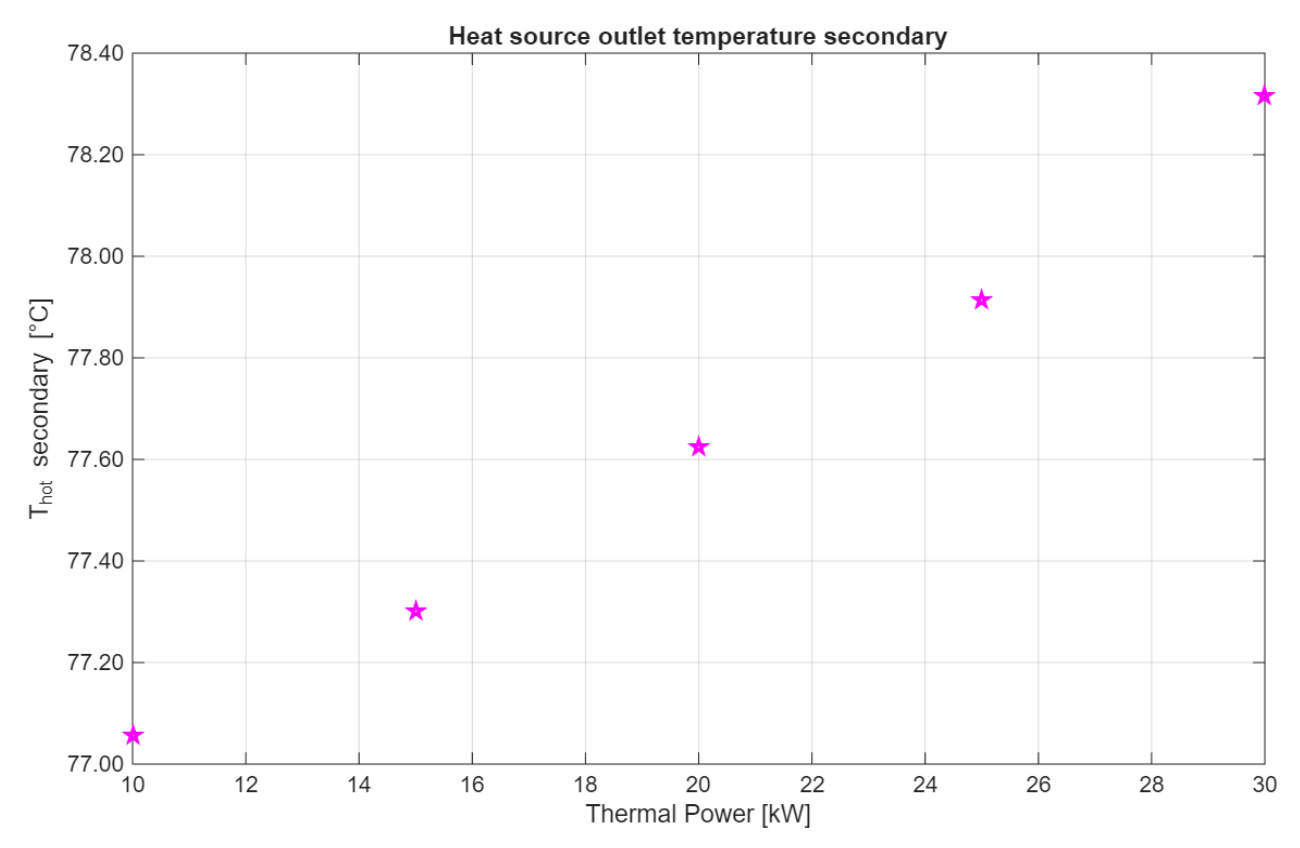


Figure 41. CHX outlet temperature on secondary side for different thermal powers.

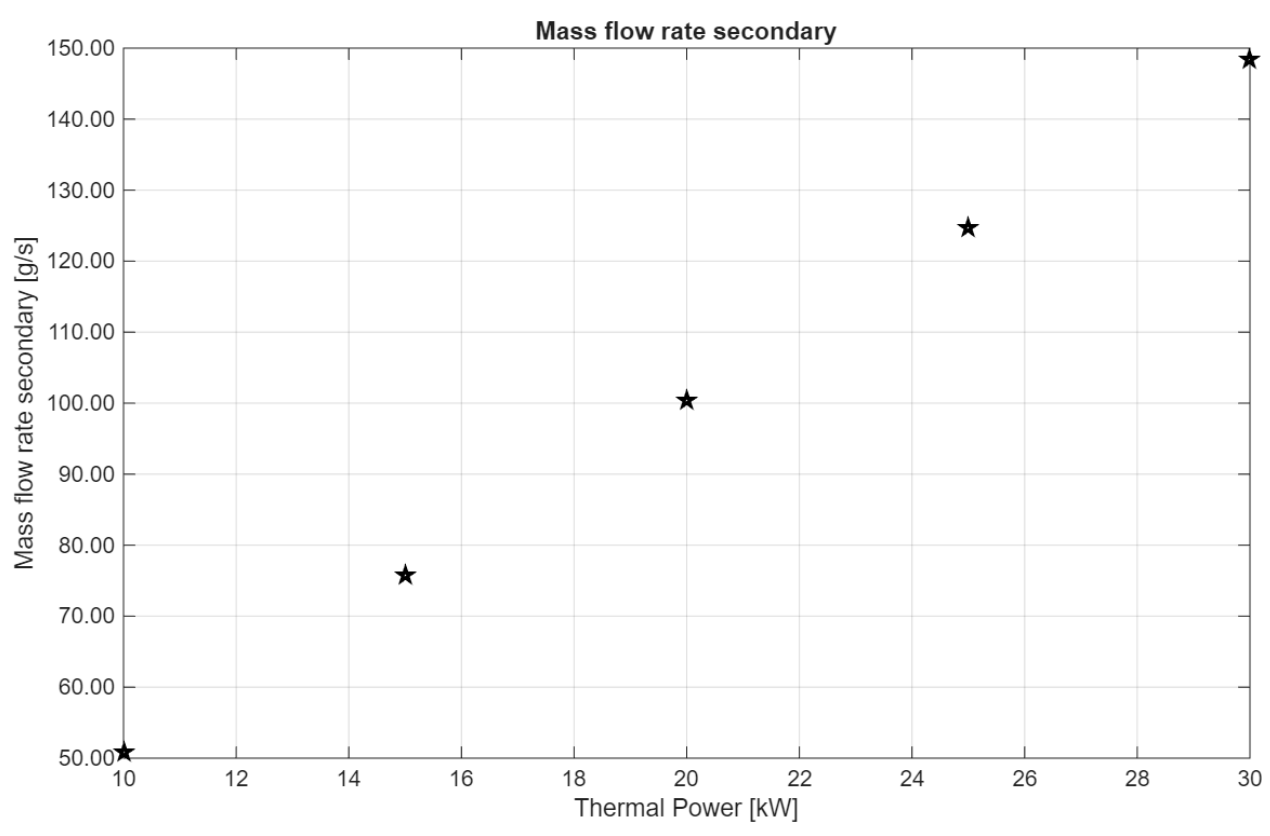


Figure 42. Secondary loop mass flow rate for different thermal powers.

All variables show an increasing trend, as chapter 4.1.4. showed for a primary loop only system. The simulation has been conducted, however, with a power upper threshold of 30 kW. This number comes from specific test that have shown that, whenever the thermal load

imposed is higher, the simulation fails. This may be caused by two-phase flow formation (during the iterative process) that leads to the overall simulation failure.

4.2.3. Variation in HX pressure losses

Similarly to the previous case, the effects of CHX pressure losses have been studied regarding both primary and secondary loop. The tests have been performed in two different operative conditions: low-pressure and high-pressure conditions, each with a separate goal. In the first case, a low-pressure system was assumed, with the aim to prove the maximum sustainable CHX pressure loss capable of guaranteeing single-phase flow in both loops. The second case assumed, instead, a high-pressure system and aimed to show the effects on loops variables caused by CHX flow resistance.

Let's now discuss the results obtained in a low-pressures system. The technical and geometrical parameters are summarized in *Table 21*.

Parameter	Value	Unit measure
Primary/Secondary inner diameter	5.248	cm
Primary/Secondary inner diameter	2	in
Primary loop pressure	8	bar
Primary loop total height	6	m
Heat source-sink thermal centers height difference	5.145	m
Power	10	kW
HX pressure losses	[1.5 2 2.5 3 3.5]	kPa
Secondary loop pressure	2	bar
Secondary loop source-sink height difference	7	m

Table 21. Parameters used in variable CHX pressure losses analysis at low-pressure conditions.

The choice of the values of HX pressure losses coefficient is not casual but comes after several attempts which fixed its maximum acceptable value to 3.5 kPa. Whenever the pressure losses at the heat exchanger are assumed to be higher than this value, two-phase flow forms and MATLAB is no longer able to obtain reasonable results. Even though the tested pressure losses are not significantly different, the results are shown in the following pictures (*Figure 43, Figure 44, Figure 45, Figure 46* and *Figure 47*).

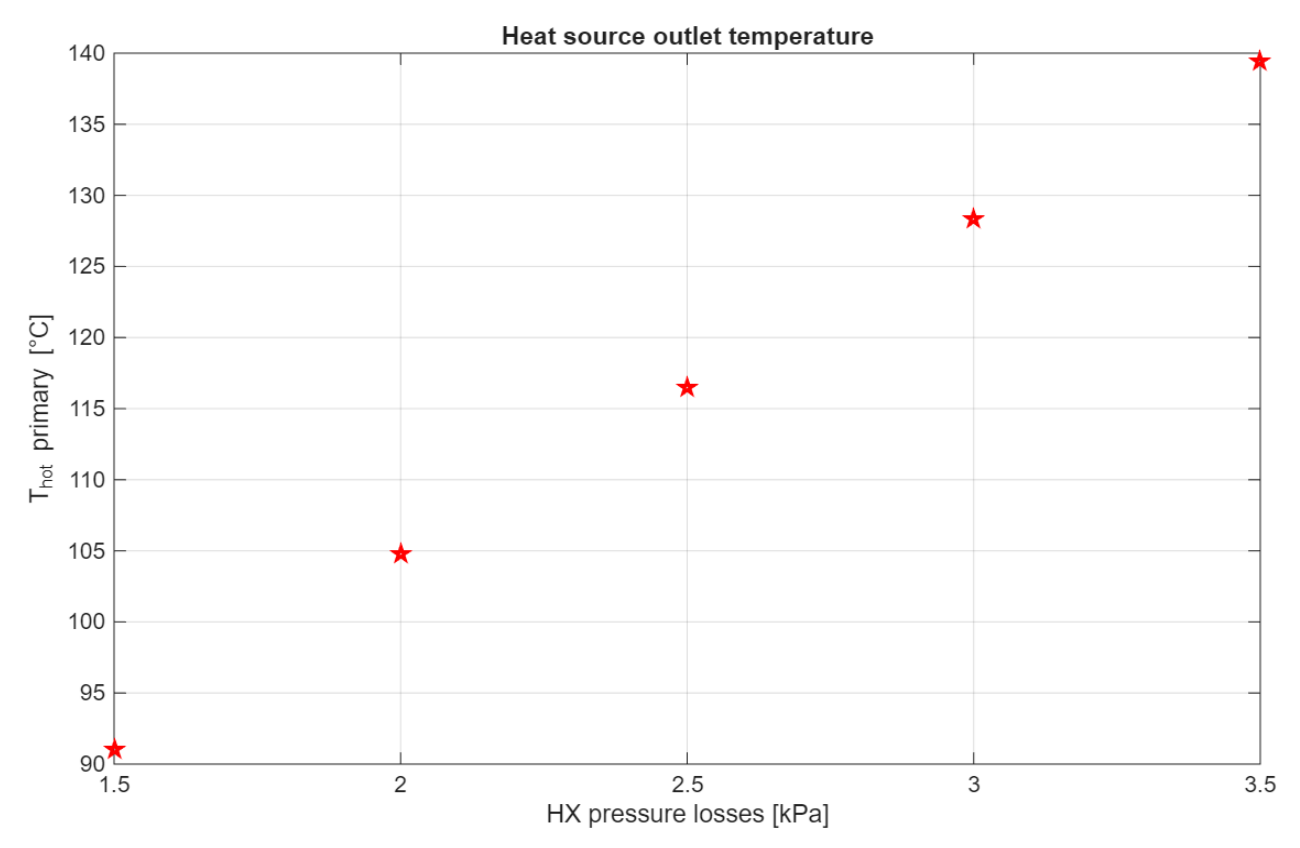


Figure 43. Heat source outlet temperature for different CHX pressure losses at 8 bar.

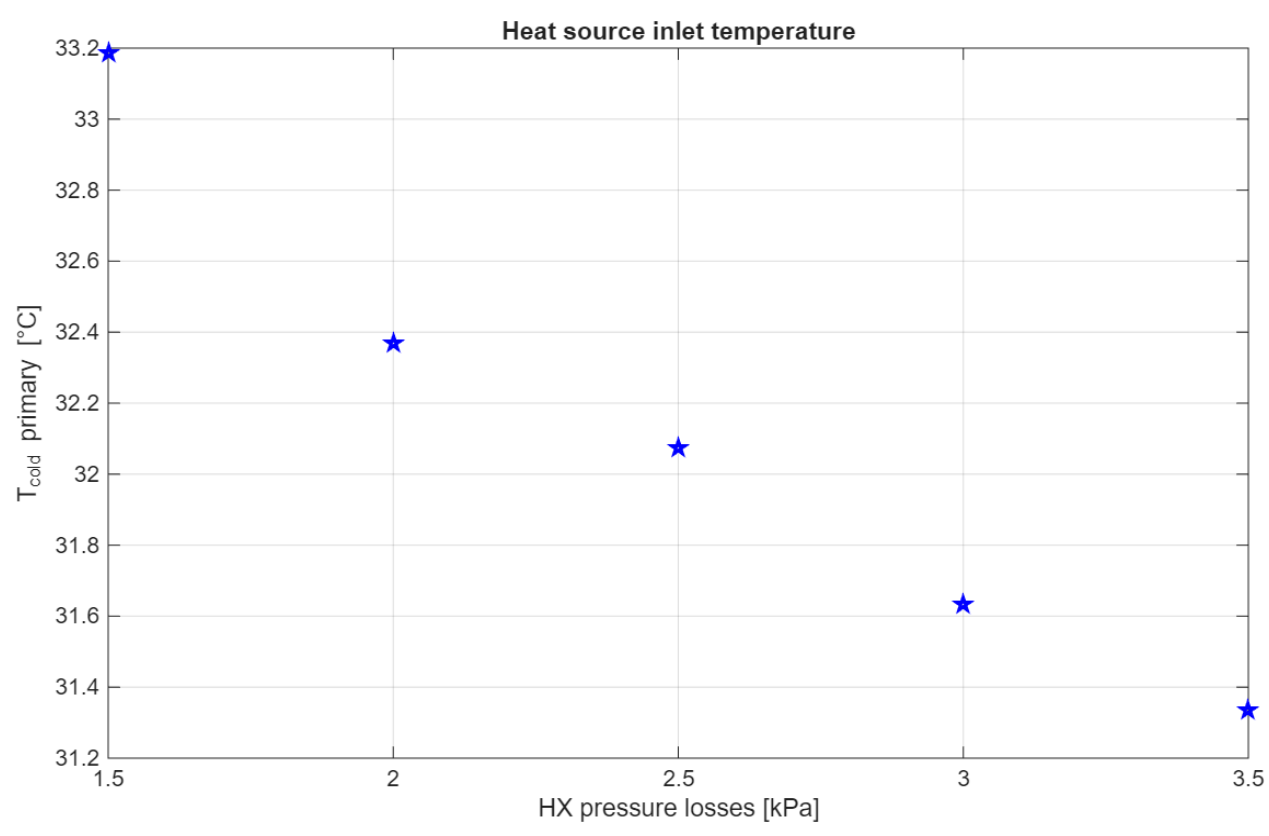


Figure 44. Heat source inlet temperature for different CHX pressure losses at 8 bar.

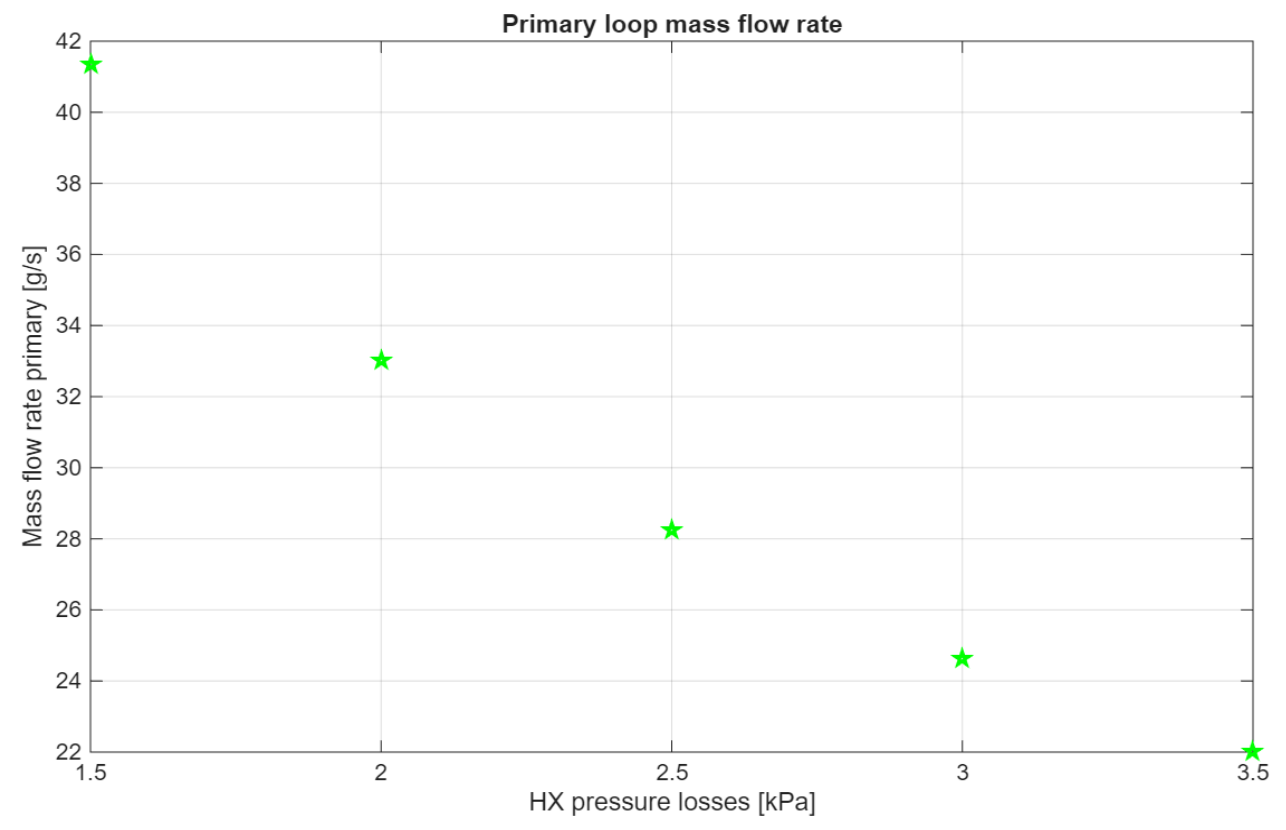


Figure 45. Primary loop mass flow rate for different CHX pressure losses at 8 bar.

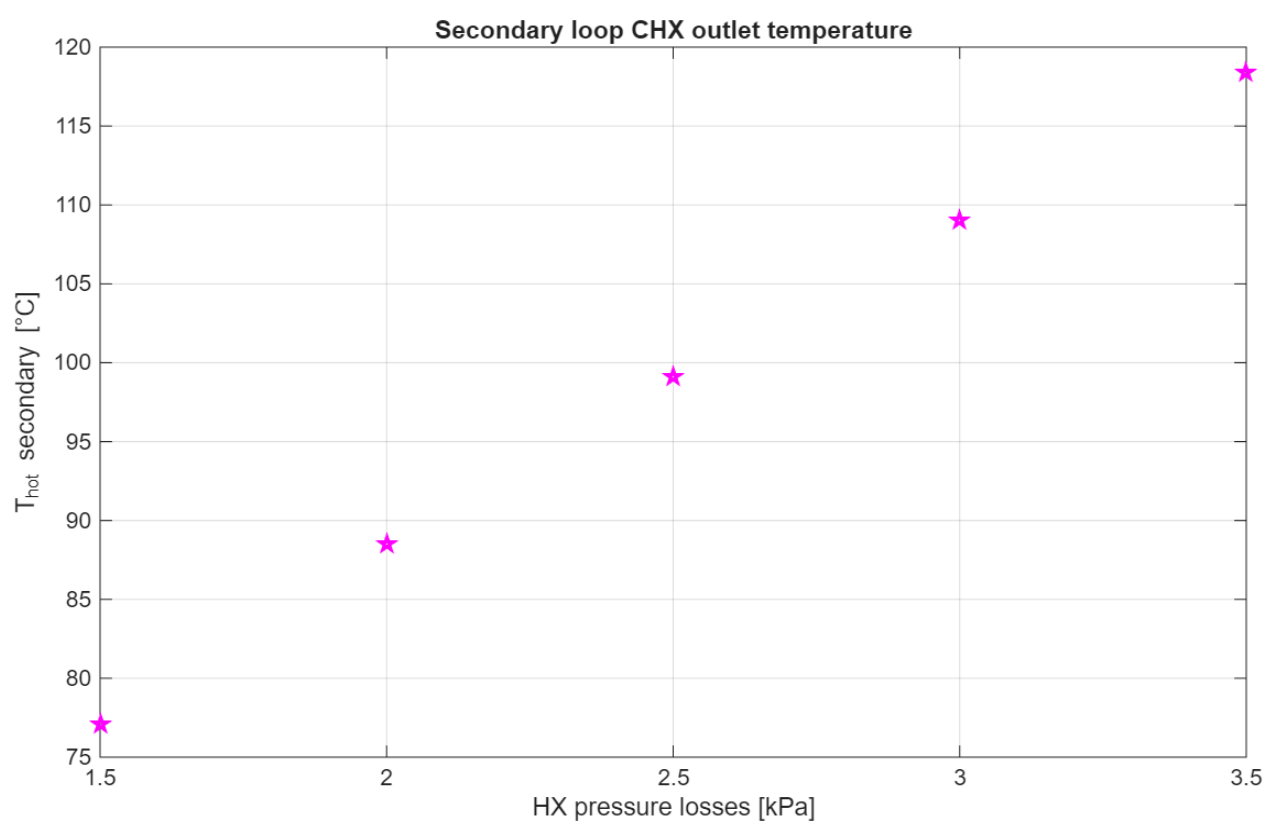


Figure 46. CHX outlet temperature on secondary side for different CHX pressure losses at 2 bar.

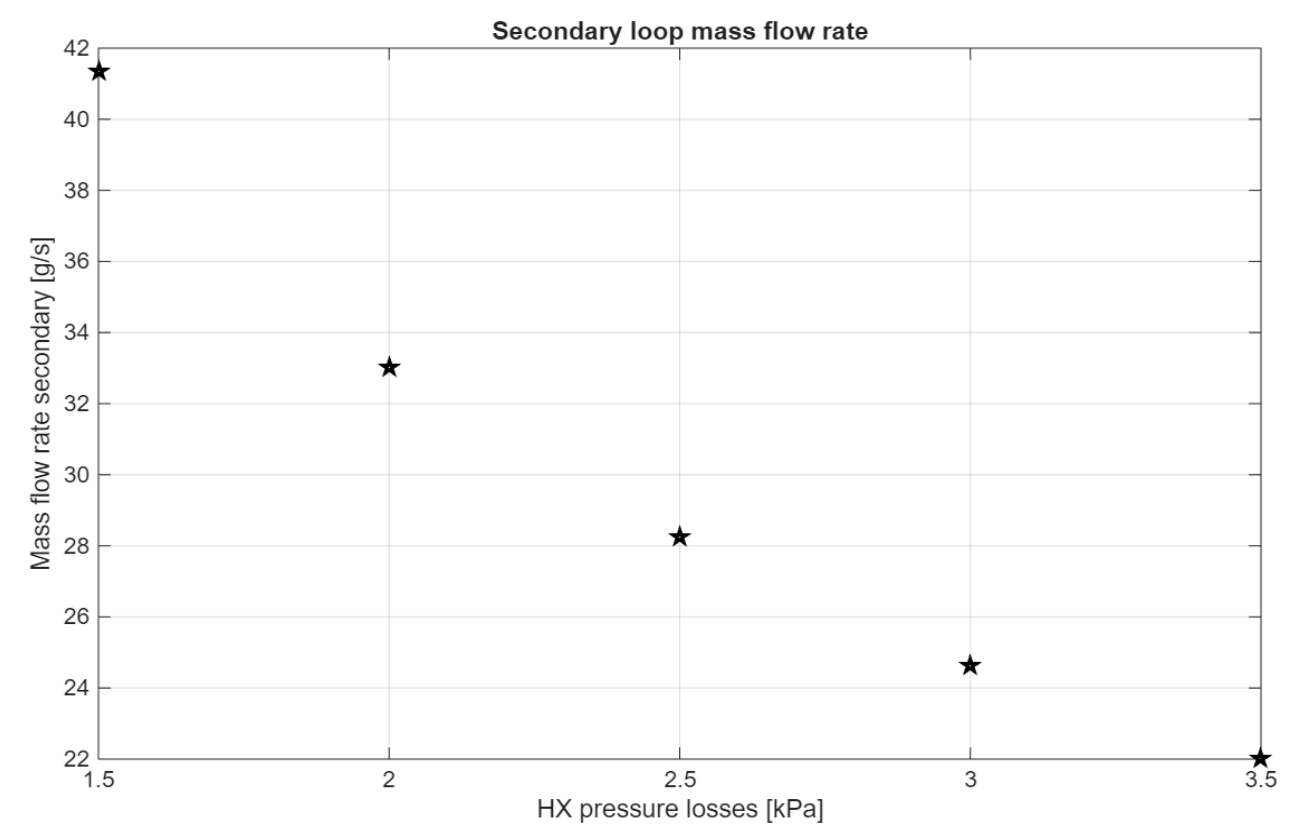


Figure 47. Secondary loop mass flow rate for different CHX pressure losses at 2 bar.

The effects follow the same trend of chapter 4.1.5., where hot temperatures are seen to increase due to longer heat source residence time, cold temperatures slightly decrease and mass flow rates decrease due to larger temperature differences. The threshold on the value of the pressure loss coefficient is imposed by the saturation temperature at secondary loop, whose value slightly overcomes 120 °C (120.21°C). The differences in temperatures and mass flow rates are significant, despite the small variation of the HX parameter.

A high-pressure system analysis has been conducted, with the objective to show how CHX pressure resistance affects a real condition coupled loop. The data used are shown in *Table 22*.

Parameter	Value	Unit measure
Primary/Secondary inner diameter	5.248	cm
Primary/Secondary inner diameter	2	in
Primary loop pressure	150	bar
Primary loop total height	6	m
Heat source-sink thermal centers height difference	5.145	m
Power	10	kW
HX pressure losses	[1.5 3 5 10 15]	kPa
Secondary loop pressure	70	bar
Secondary loop source-sink height difference	7	m

Table 22. Parameters used in variable CHX pressure losses analysis at high-pressure conditions.

The graphs show the results obtained for both primary and secondary loop (*Figure 48, Figure 49, Figure 50, Figure 51* and *Figure 52*).

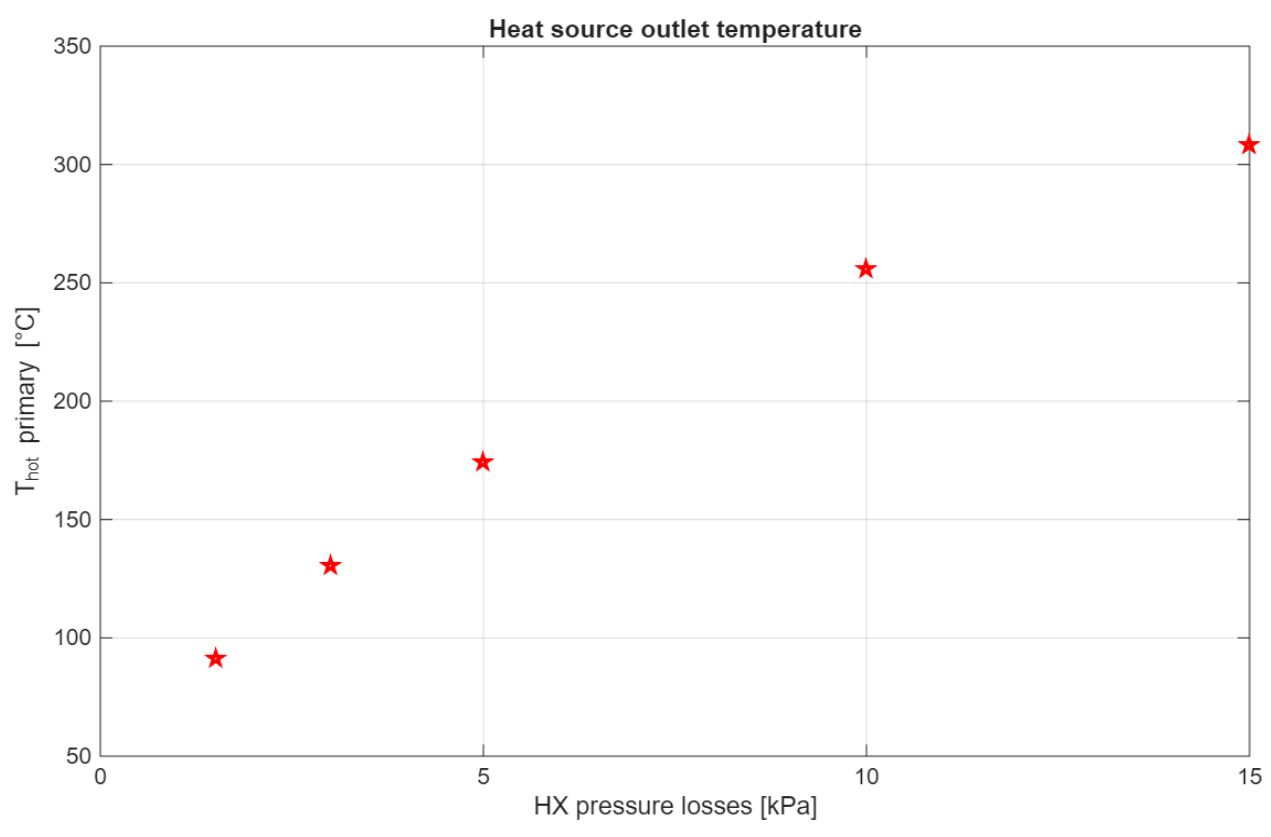


Figure 48. Heat source outlet temperature for different CHX pressure losses at 150 bar.

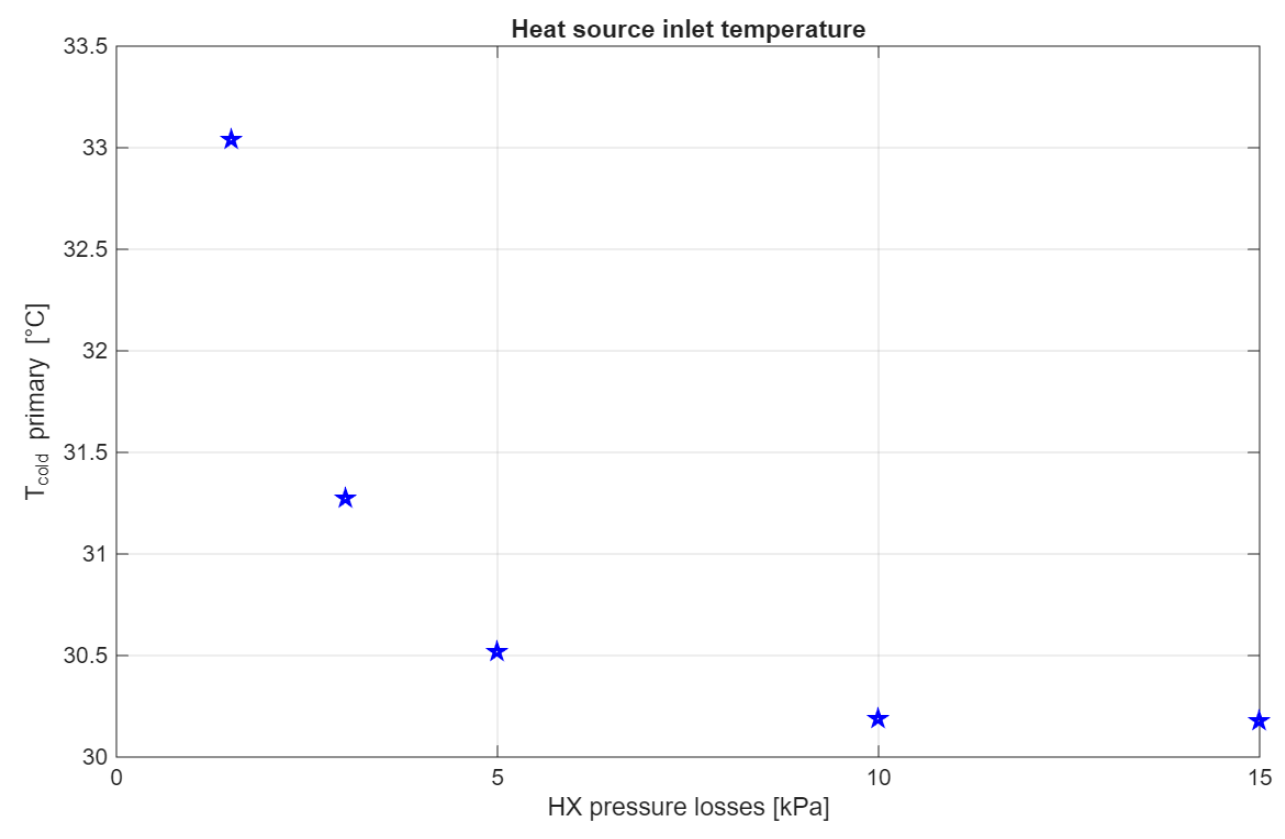


Figure 49. Heat source inlet temperature for different CHX pressure losses at 150 bar.

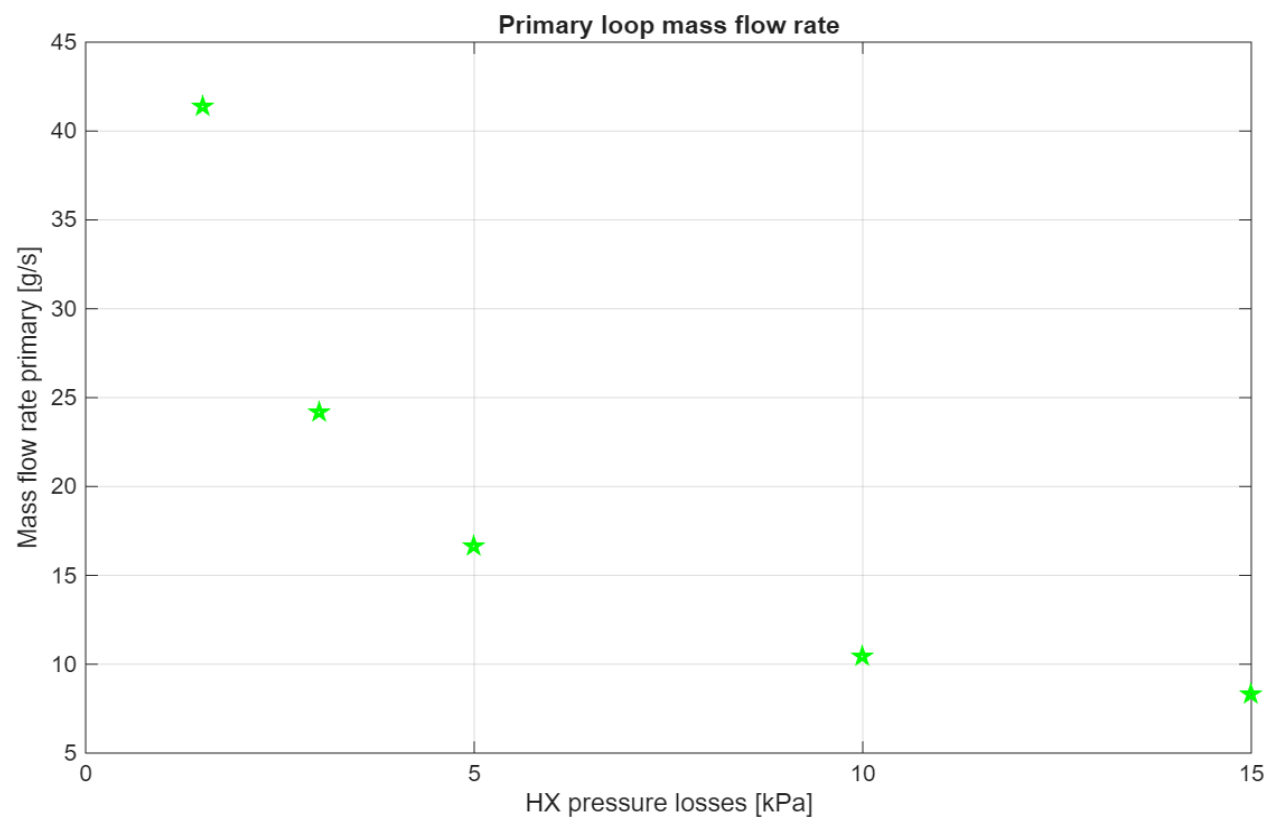


Figure 50. Primary loop mass flow rate for different CHX pressure losses at 150 bar.

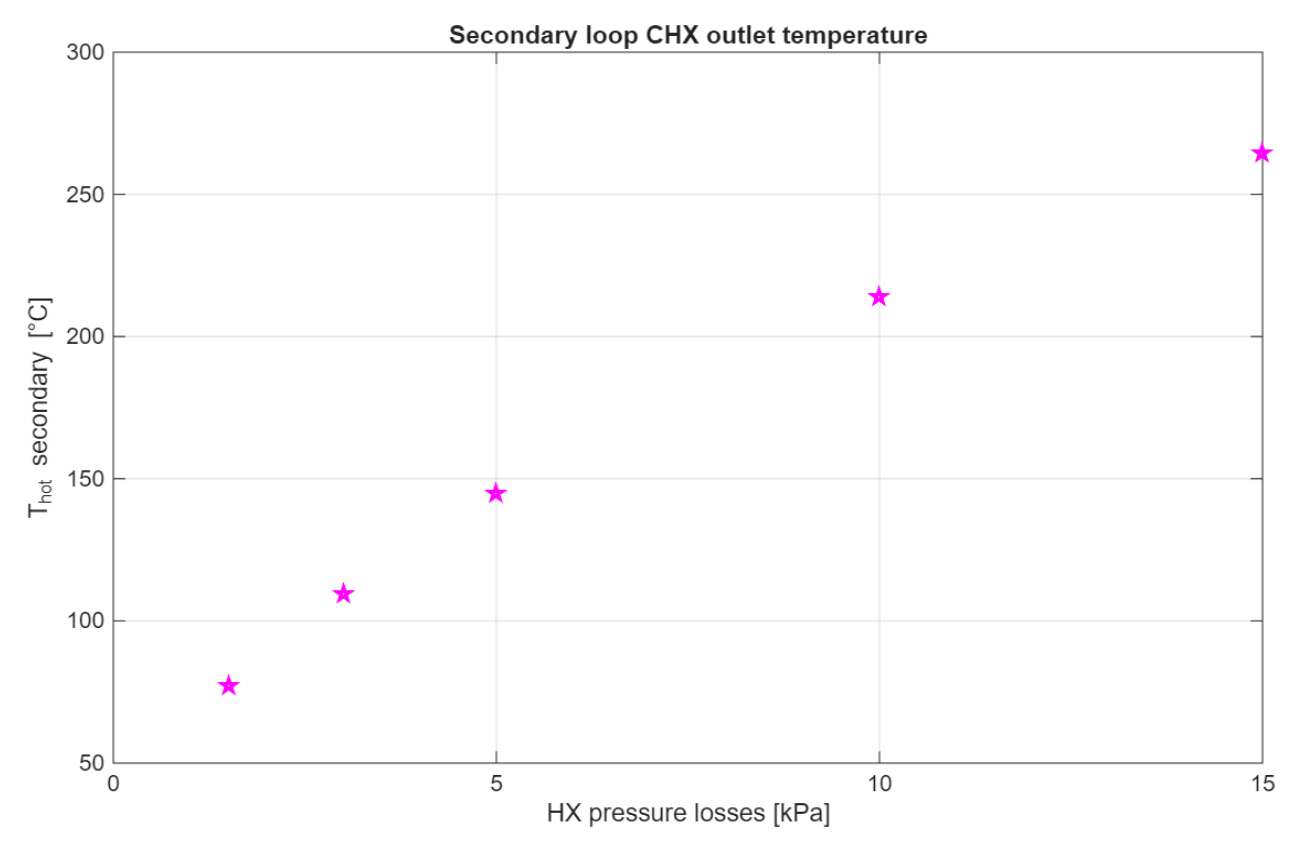


Figure 51. CHX outlet temperature on secondary side for different CHX pressure losses at 70 bar.

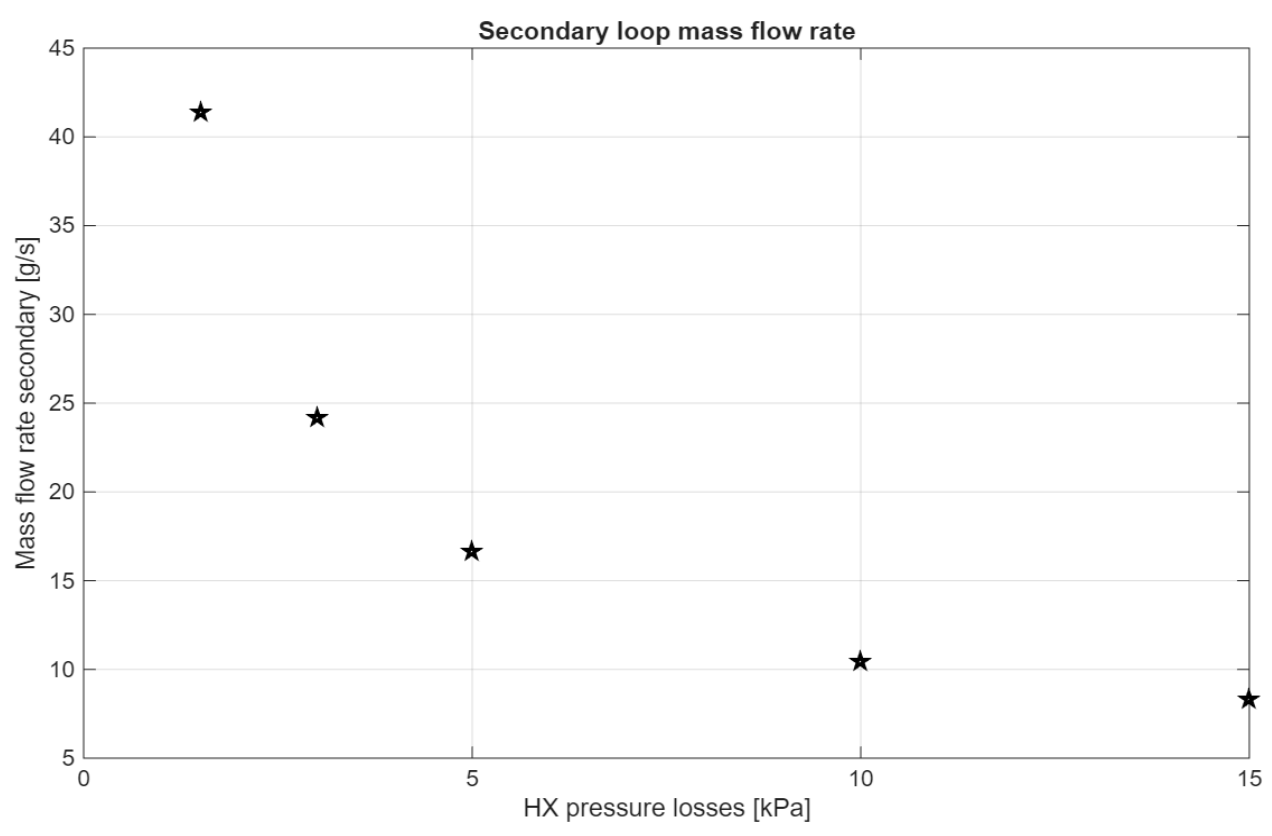


Figure 52. Secondary loop mass flow rate for different CHX pressure losses at 70 bar.

The trend of the curves is the same as low-pressure conditions, but the variations in temperatures are significantly larger. The tested power is too low to even get close to saturation conditions, so no significant limitations to this loop can be seen.

Considering the simulations carried out and the results discussed, a cross analysis can be conducted. The analysis has been conducted in high-pressure conditions only. *Table 23* presents the parameters involved.

Parameter	Value	Unit measure
Primary/Secondary inner diameter	[3.508 4.094 5.248 6.268 7.792]	cm
Primary/Secondary inner diameter	2	in
Primary loop pressure	150	bar
Primary loop total height	6	m
Heat source-sink thermal centers height difference	5.145	m
Power	10	kW
HX pressure losses	[1.5 3 5 10 15]	kPa
Secondary loop pressure	70	bar
Secondary loop source-sink height difference	7	m

Table 23. Parameters used in variable diameter and CHX pressure losses analysis.

The figures below show the effects on both loops of different diameters and different pressure losses on the parameters (*Figure 53, Figure 54, Figure 55, Figure 56* and *Figure 57*).

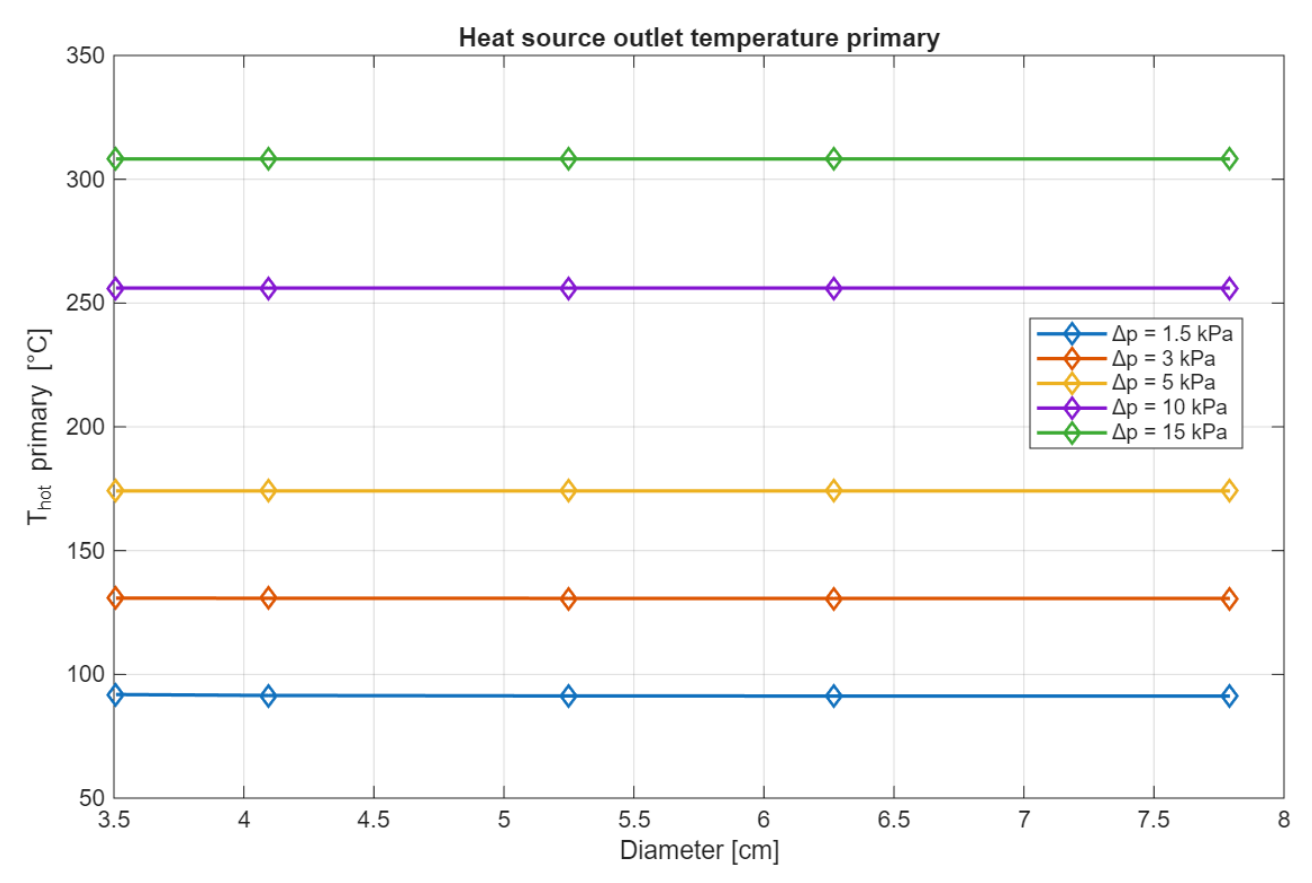


Figure 53. Heat source outlet temperature for different diameters at different CHX pressure losses.

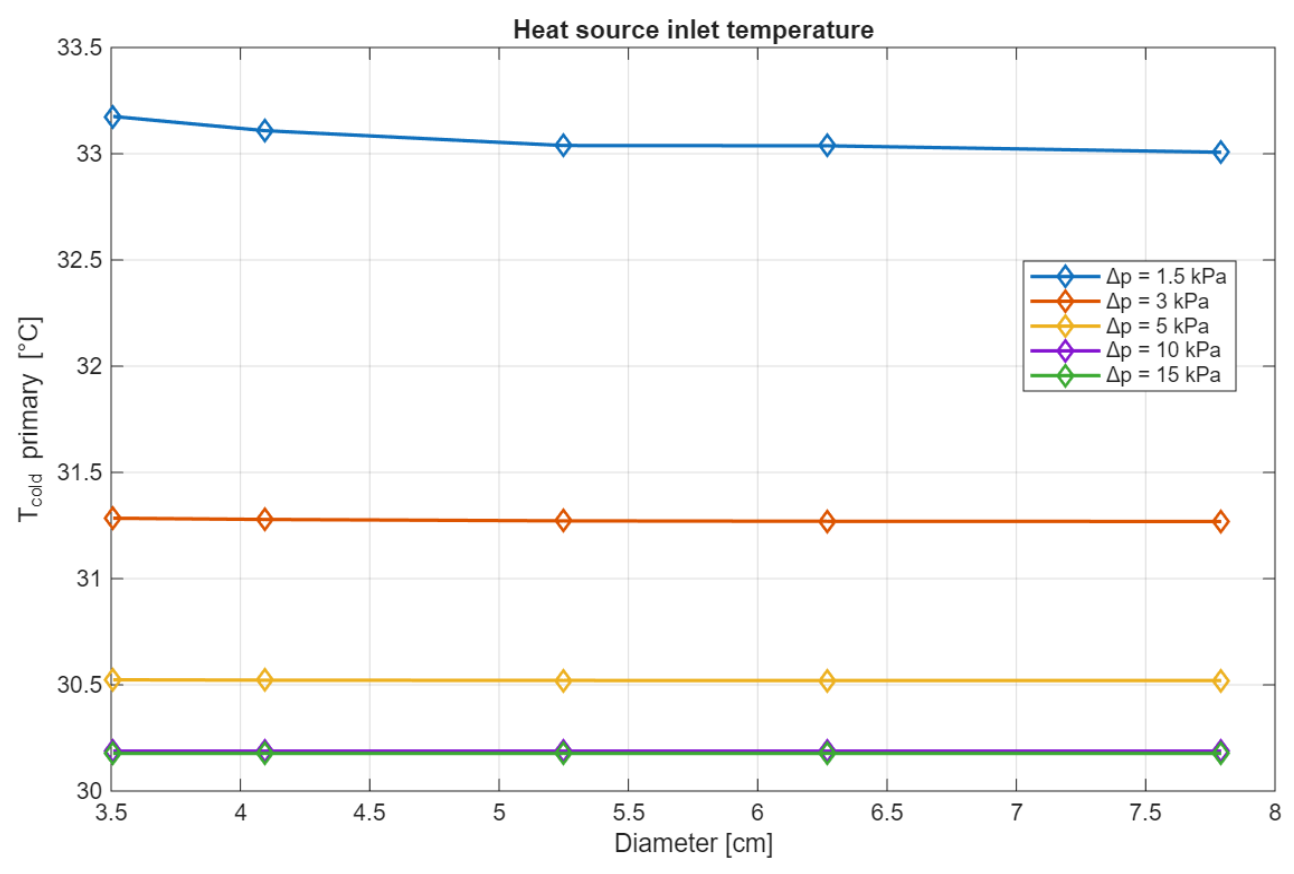


Figure 54. Heat source inlet temperature for different diameters at different CHX pressure losses.

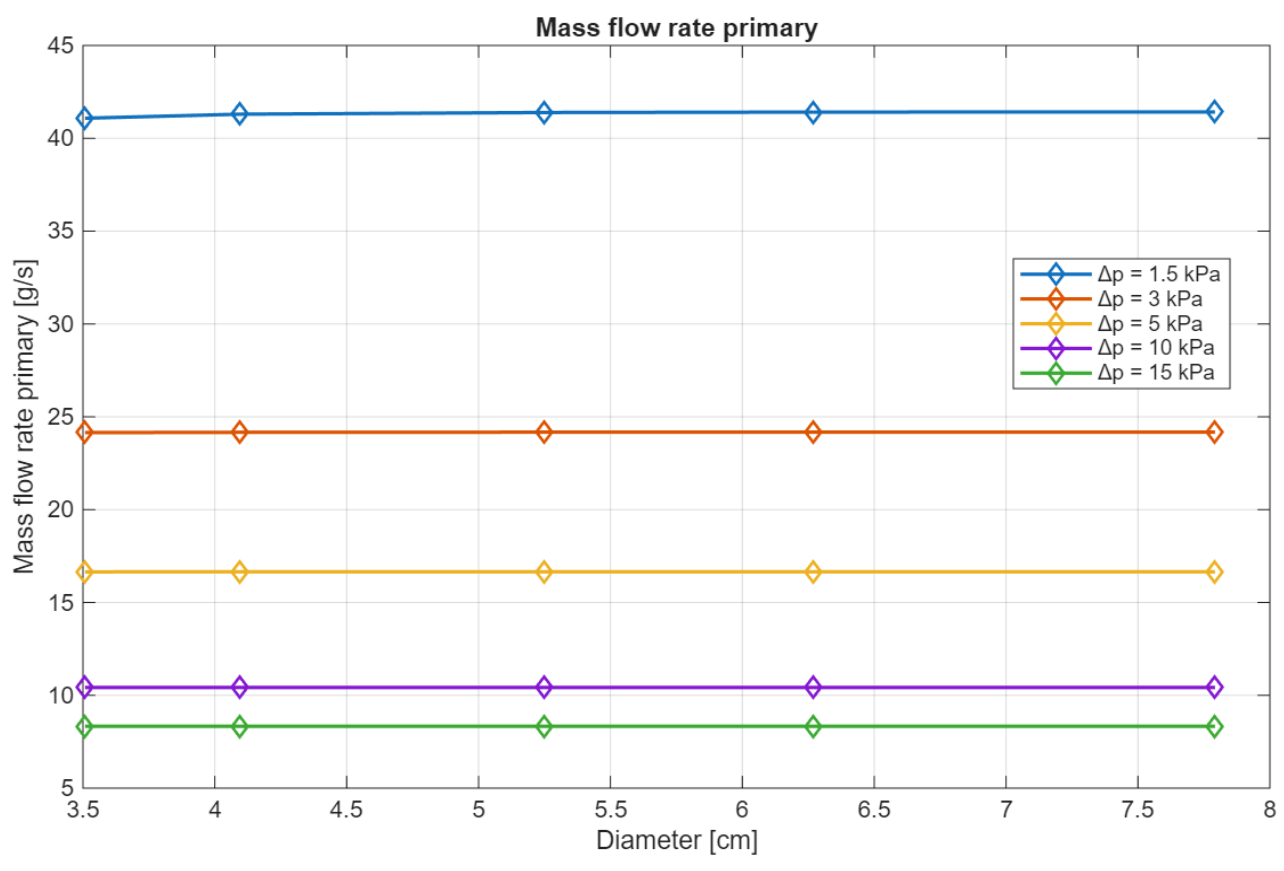


Figure 55. Primary loop mass flow rate for different diameters at different CHX pressure losses.

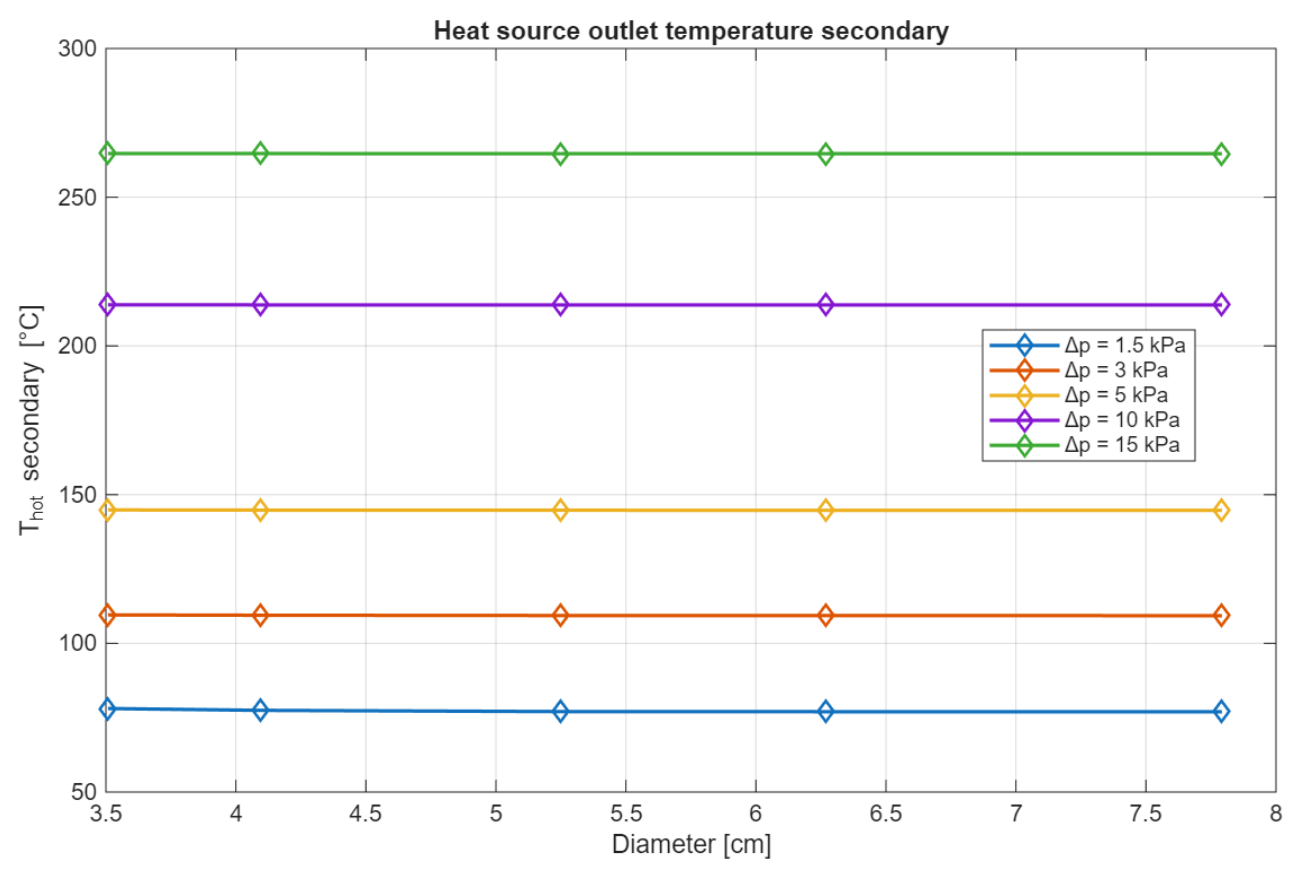


Figure 56. CHX outlet temperature on secondary side for different diameters at different CHX pressure losses.

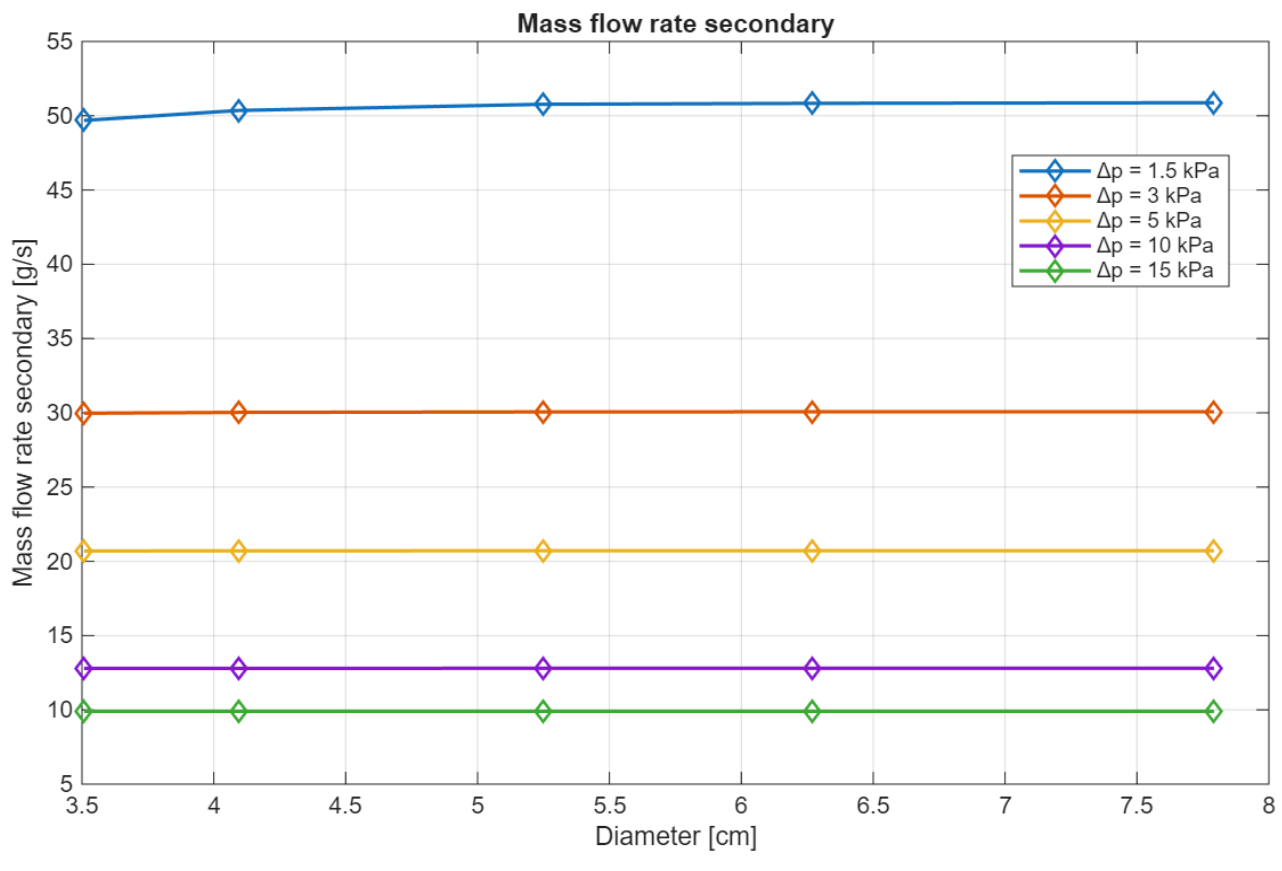


Figure 57. Secondary loop mass flow rate for different diameters at different CHX pressure losses.

The graphs show how the HX pressure loss dominates on the obtained results, while diameter have almost negligible effects. On the other hand, secondary loop has shown more visible effects regarding the diameters change for low HX pressure drops.

Moving forward, the final tests aimed to show the effects of crossed conditions of HX pressure loss and thermal power variations. The imposed values are shown in *Table 24*.

Parameter	Value	Unit measure
Primary/Secondary inner diameter	5.248	cm
Primary/Secondary inner diameter	2	in
Primary loop pressure	150	bar
Primary loop total height	6	m
Heat source-sink thermal centers height difference	5.145	m
Power	[10 15 20 25 30]	kW
HX pressure losses	[1.5 3 5 10 15]	kPa
Secondary loop pressure	70	bar
Secondary loop source-sink height difference	7	m

Table 24. Parameters used in variable thermal power and CHX pressure losses analysis.

Here below the behavior of the variables (Figure 58, Figure 59, Figure 60, Figure 61 and Figure 62).

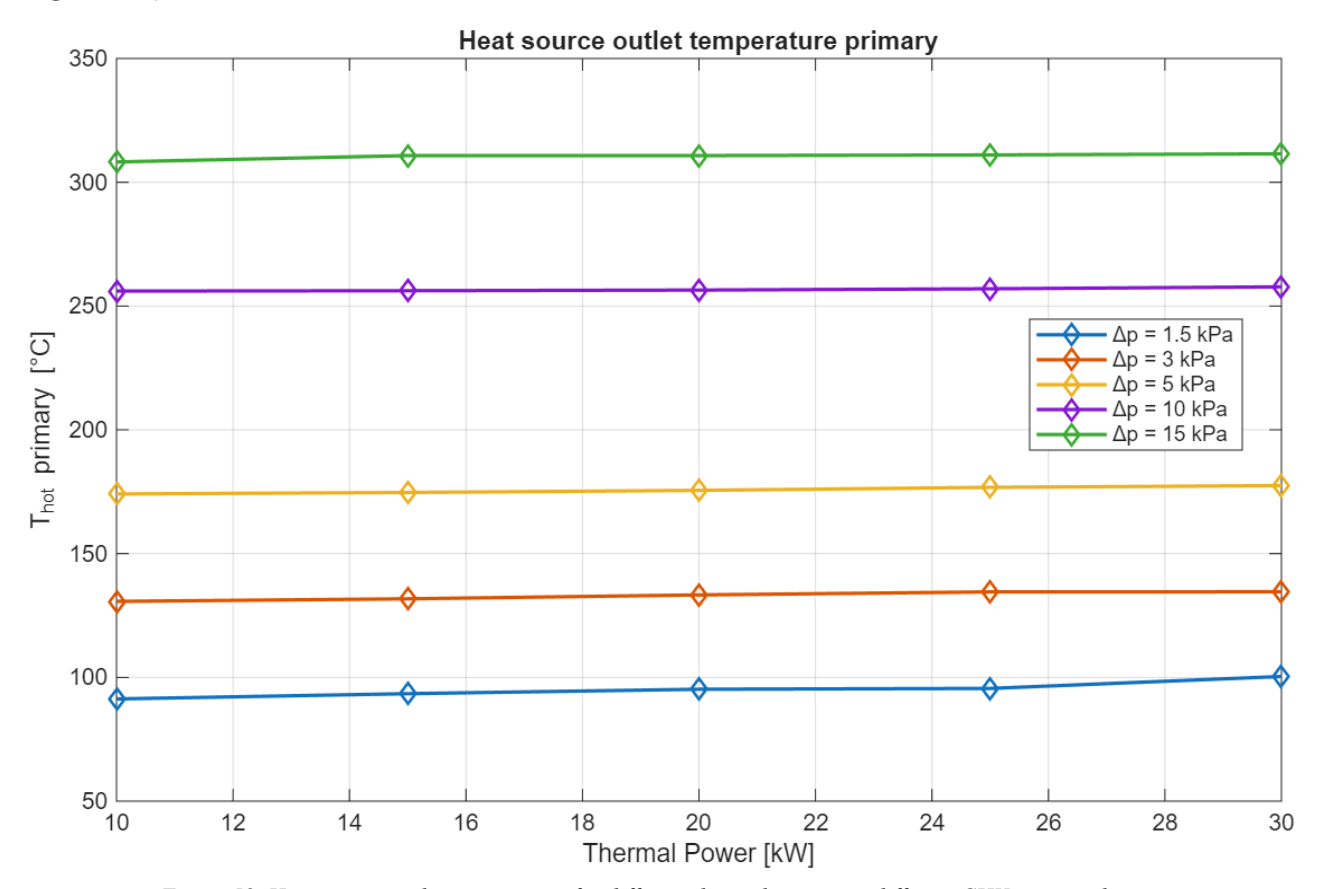


Figure 58. Heat source outlet temperature for different thermal powers at different CHX pressure losses.

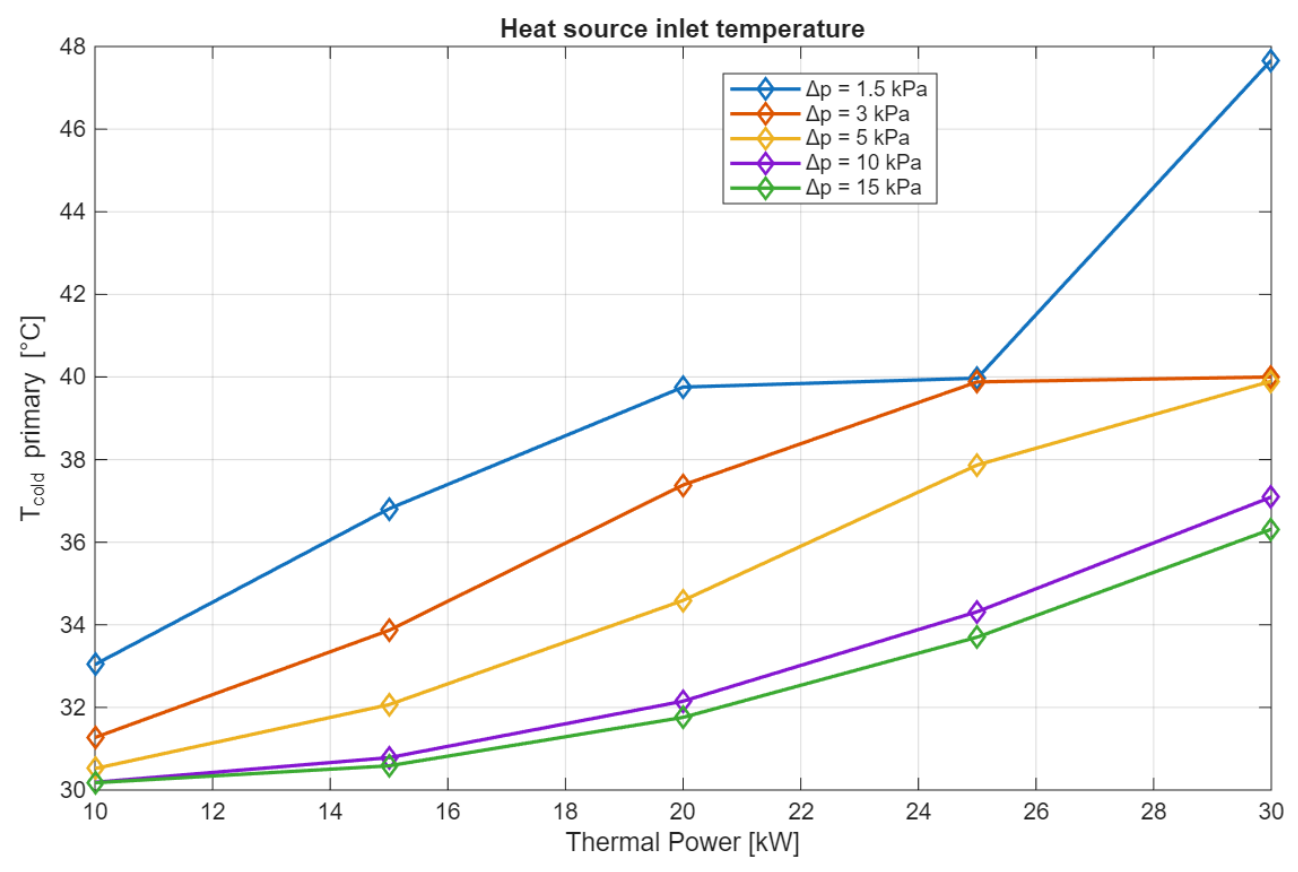


Figure 59. Heat source inlet temperature for different thermal power at different CHX pressure losses.

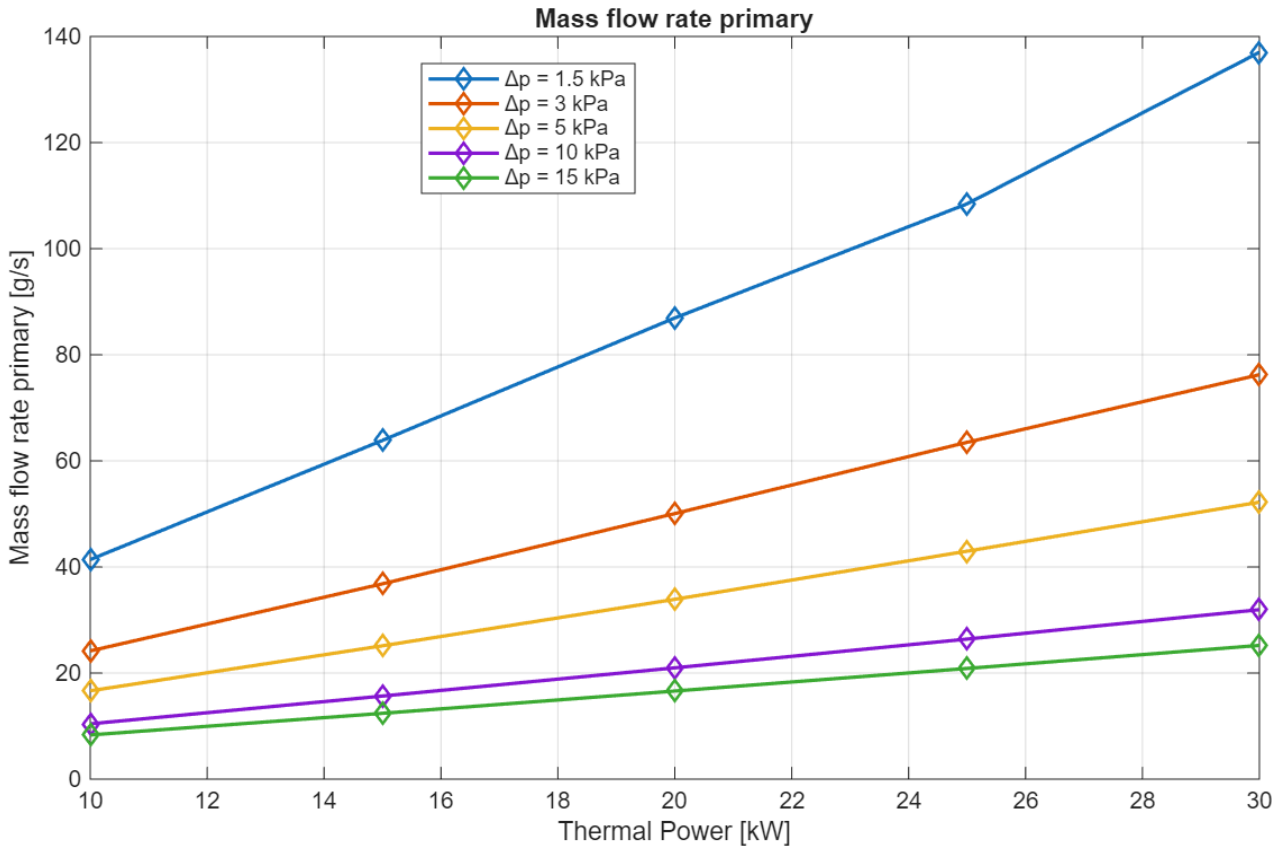


Figure 60. Primary loop mass flow rate for different thermal power at different CHX pressure losses.

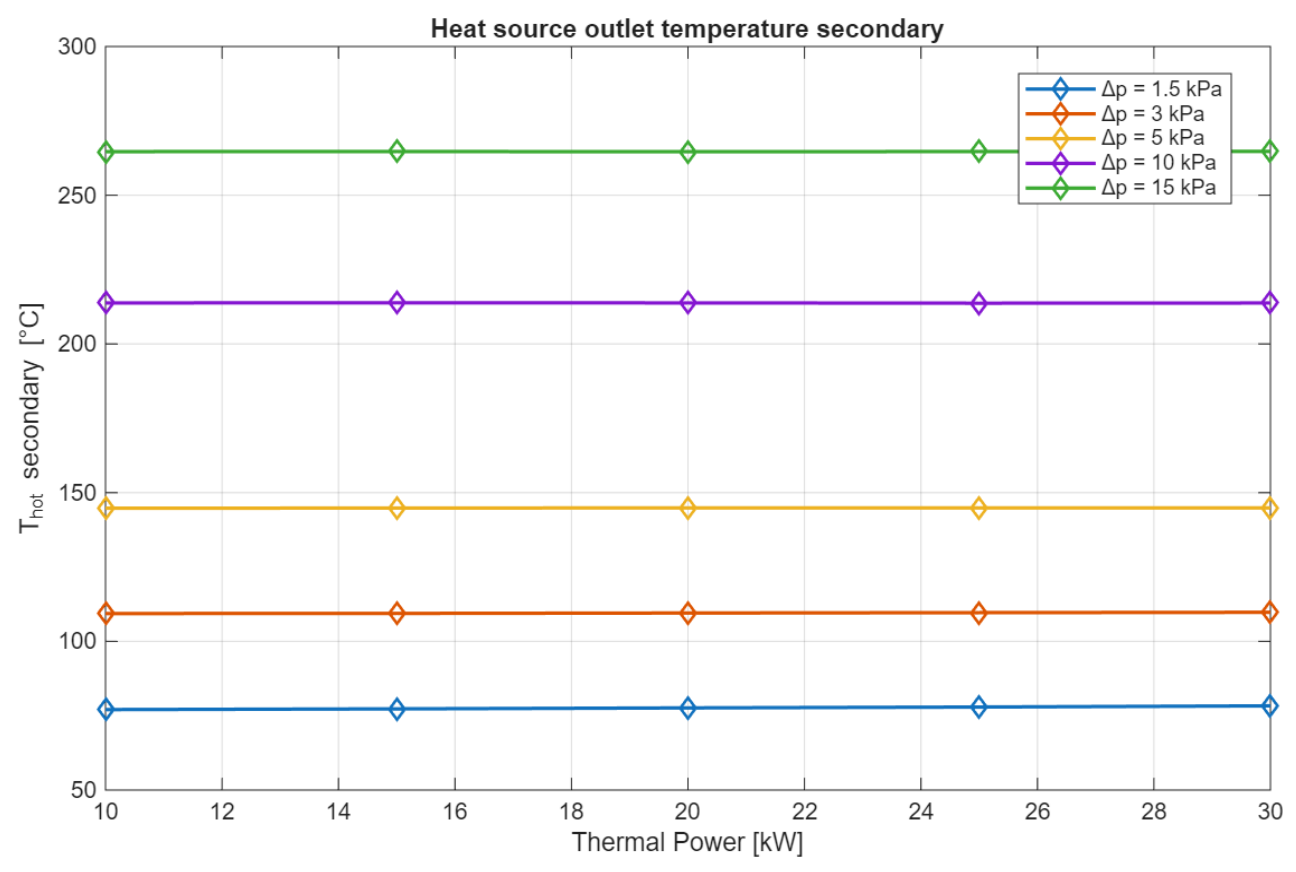


Figure 61. CHX outlet temperature on secondary side for different thermal power at different CHX pressure losses.

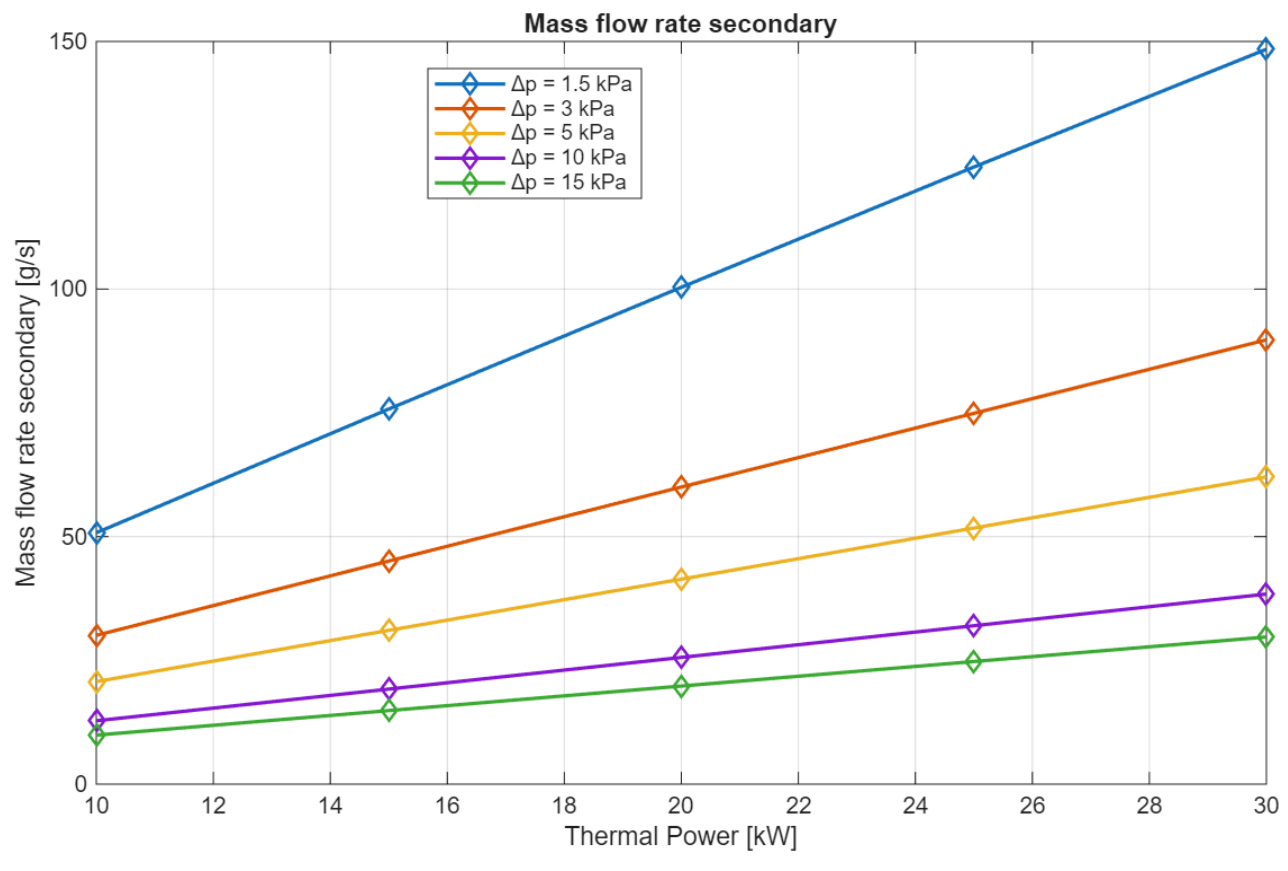


Figure 62. Secondary loop mass flow rate for different thermal power at different CHX pressure losses.

The trend of the curve is rising for all of them, but it's clear that thermal power has strong influence on the loop along with the HX pressure losses. More in detail, while "hot" temperatures haven't showed significant changes, primary "cold" temperatures have, especially for low pressure losses. Mass flow rates seem to follow a linear increase along with power and the lower the pressure drop and the steeper the curve is.

5. Comparison between ATHLET and MATLAB simulations

This last paragraph focuses on the comparison of the results obtained for the primary-looponly system with MATLAB coding language and system code ATHLET.

ATHLET (Analysis of THermal-hydraulics of LEaks and Transients) is an advanced thermal-hydraulic simulation code used to analyze and describe cooling systems in a NPP during transients in both nominal and emergency situations. It presents a modular structure, which comprises:

- Thermo-Fluid dynamics (TFD) module concerning the resolution of the selected equation system for the fluid volumes.
- Heat Conduction and Heat Transfer (HECU) module which models the heat transfer between fluid volumes and heat structures.

Regarding TFD module, ATHLET can solve fluid's equations using two different models, both valid for single-phase and two-phase flows:

1) 5-equation model.

It solves continuity and energy conservation equations for each phase separately, whereas the momentum conservation equation is a single equation valid for a mixture of the two phases, thus assuming that the relative velocity between the phases is null.

2) 6-equations model (or Two-fluid model)

It solves continuity, momentum and energy conservation for each phase separately. This model reduces the approximations since considers two phase separately (each with a specific velocity) and it's used for a better accuracy in two-phase flows.

Since the case analyzed deals only with one phase (e.g. liquid water), the 5-equation model was selected to reduce the computational cost. Spatial discretization is achieved with a finite-volume staggered grid approach. Each element is discretized based on the number of nodes imposed on the input file. Time discretization is based on a linear-implicit Euler method and the proper timestep is selected automatically by the code.

For what concerns HECU module, ATHLET evaluates the heat transfer through heat conduction objects (HCOs) based on the selected material properties. Fluid's heat transfer coefficient (HTC) is calculated, instead, by means of correlations depending on the flow regime. In the case analyzed, where only subcooled liquid water is present, ATHLET calculates the HTC as the maximum between Dittus-Boelter and McAdams correlations, both for heating and cooling wall surfaces.

5.1. Geometry description

The loop has been modelled keeping its rectangular shape and it presents all the elements named in previous simulations, with the addition of a control volume (CV1) connected to a time dependent volume (TDV1). These two elements guarantee constant pressure in all the system. The representation of ATHLET's loop is shown in *Figure 63*.

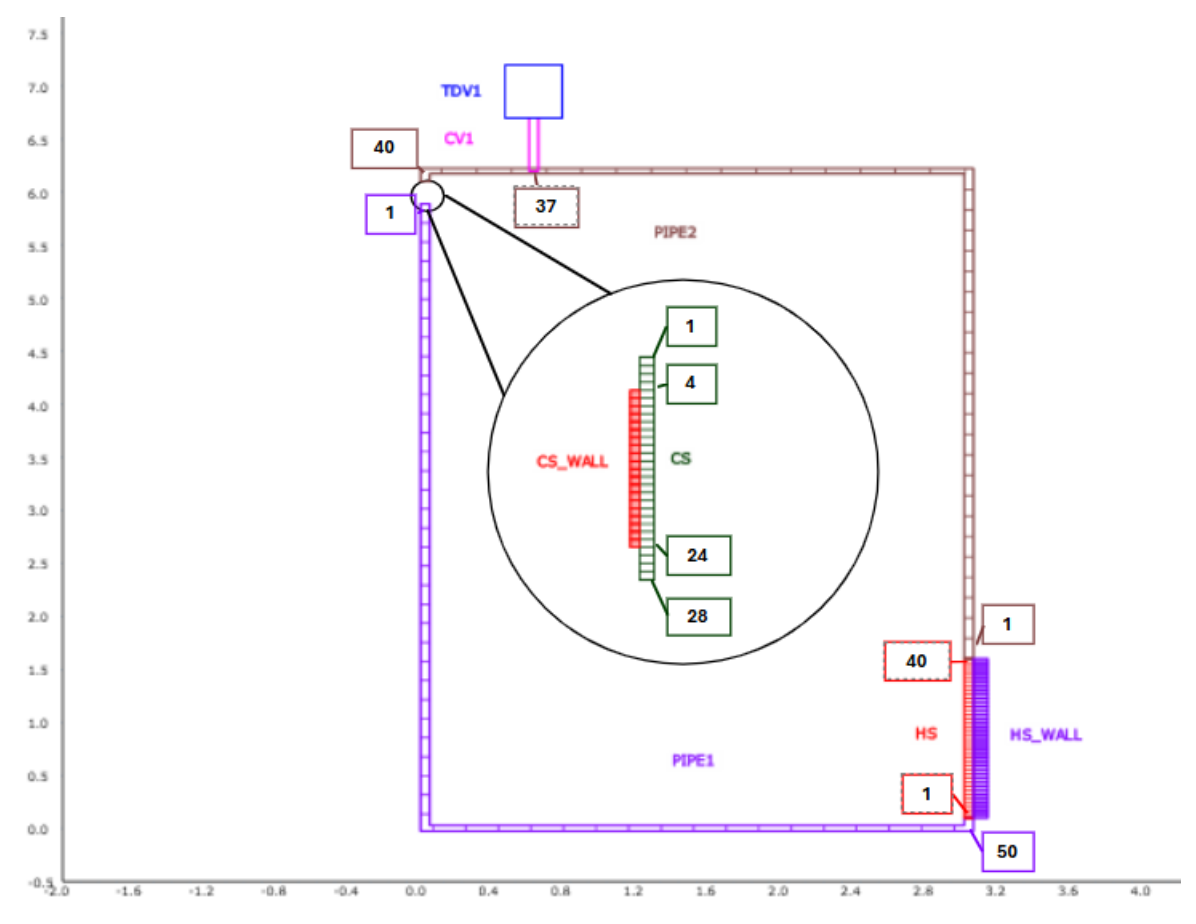


Figure 63. ATHLET's schematic design of primary loop.

The location of CV1 and TDV1 is arbitrary. The numbers represent the initial and final node number of each structure.

Four small sections have been added in rising/falling vertical segments right at the corners of the geometry. While MATLAB model assumed the heat source and the heat sink to begin right after the horizontal sections, for simplicity in the analysis, ATHLET required the addition of small segments right before the two components, causing a small increase in the overall height of the loop. This change simplifies the connection between the volumes of two different elements, that would be harder to set if they were placed exactly at the corners. The effects on the results are minimum. The height distance between heat source outlet and CHX inlet has been kept equal to MATLAB case. The elements in the picture are classified as:

- HS/HS WALL → heat source
- PIPE2 → riser
- CS/CS WALL → Compact Heat Exchanger
- PIPE1 → downcomer

There is a main difference inside ATHLET between HS and HS WALL and between CS and CS WALL: while the first ones regard the geometrical length of the associated structures, the second are connected to the effective length involved in the heat exchange process. In other words, CS WALL and HS WALL are the CHX and the heat source set of computational volumes involved in the heat transfer mechanism with the fluid. CS and HS are the CHX and heat source set of computational volumes where the fluid is assumed to flow. While HS and HS WALL have the same length, CS and CS WALL don't. This discrepancy in the heat exchanger comes from CHX geometry model. The CHX has been modeled as a set of parallel microchannels, 1365 in total (number obtained multiplying the number of flow passages and the number of microchannels in a flow passage as shown in Table 26). Each microchannel presented an hydraulic diameter equal to the one set in MATLAB simulations, a total length equal to the total height of the CHX, an effective heat transfer length equal to the microchannel length (obtained by MATLAB simulations). The cross section has been set equal to the sum of the cross sections of all microchannels. The total heat transfer area was set equal to the heat transfer area of a plate, multiplied by the number of plates (as in MATLAB model). Since not all CHX total length is involved in the heat exchange process, the excessive fluid in those sections had to be removed for the overall loop mass evaluation.

The length of the additional segments placed at the four vertical sections is 0.1 m each. Inside ATHLET's input file, the CHX pressure losses were imposed and fixed. *Table 25* shows the main parameters in the loop.

Parameter	Value	Unit Measure
Loop's total height	6.2	m
Loop's horizontal section	3	m
Heat source/sink height difference	4.5	m
PIPE1/PIPE2 inner diameter	5.248	cm
CS length	0.210	m
CS_WALL length	0.148	m
HS length	1.5	m
PIPE1 number of nodes	50	_
PIPE1 number of nodes	40	-
HS number of nodes	40	-
CS number of nodes	28	-
CS WALL number of nodes	20	-

Table 25. ATHLET loop dimensions.

Table 26 shows the dimensions used to model the microchannels.

Parameter	Value	Unit Measure
Diameter	1	mm
Heat exchange length	14.8	cm
# of channels per plate	105	-
# of channels per plate repetition	13	-
# tot. of channels	1365	-

Table 26. ATHLET CHX parameters.

5.2. Operative conditions

The system is set to operate at constant pressure. As for MATLAB simulations, the CHX pressure losses have been imposed. The secondary loop is not included in the simulation, however it was necessary to fix its mass flow rate (considered equal to the one imposed in single-loop only-simulations with MATLAB). All the values used are shown in *Table 27*.

Parameter	Value	Unit measure
Operative pressure	150	bar
Thermal power	10	kW
CHX pressure losses	1.5	kPa
Secondary loop mass flow rate	0.2	kg/s

Table 27. ATHLET operative parameters.

To proceed with the simulations, specific initial conditions and boundary conditions have been set. The chosen initial conditions, shown in *Table 28*, are the same used in MATLAB simulations.

Parameter	Value	Unit
		Measure
Primary loop temperature	30	°C
Primary loop pressure	150	bar
Primary loop mass flow rate	0	kg/s

Table 28. ATHLET initial conditions.

The choice of these parameters aimed to reduce the time required by the simulation to reach the steady state and the time required by ATHLET to complete the simulations. The main goal was not to verify the effects of a real-facility initial conditions. Regarding the boundary conditions, the simulation imposed:

- Uniform thermal power production in HS WALL.
- Adiabaticity in riser and downcomer.
- Imposed heat transfer coefficient of $2200 \frac{W}{m^2 K}$ and temperature at 30°C on the left-hand side of CS WALL (correspondent to secondary-loop side).
- Pressure boundary condition imposed by TDV1 presence that fixes the operative pressure at 150 bar.

5.3. Results

The comparison regarded the temperatures at the inlet and outlet of the heat source, the mass flow rate and the exported mass in the expansion tank. To proceed with the study, both systems had to be in steady state. While MATLAB simulations already assumed a steady state system, ATHLET results were taken after a transient of $5 \cdot 10^4$ seconds. The outlet heat source temperature and mass flow rate in time are shown in *Figure 64*.

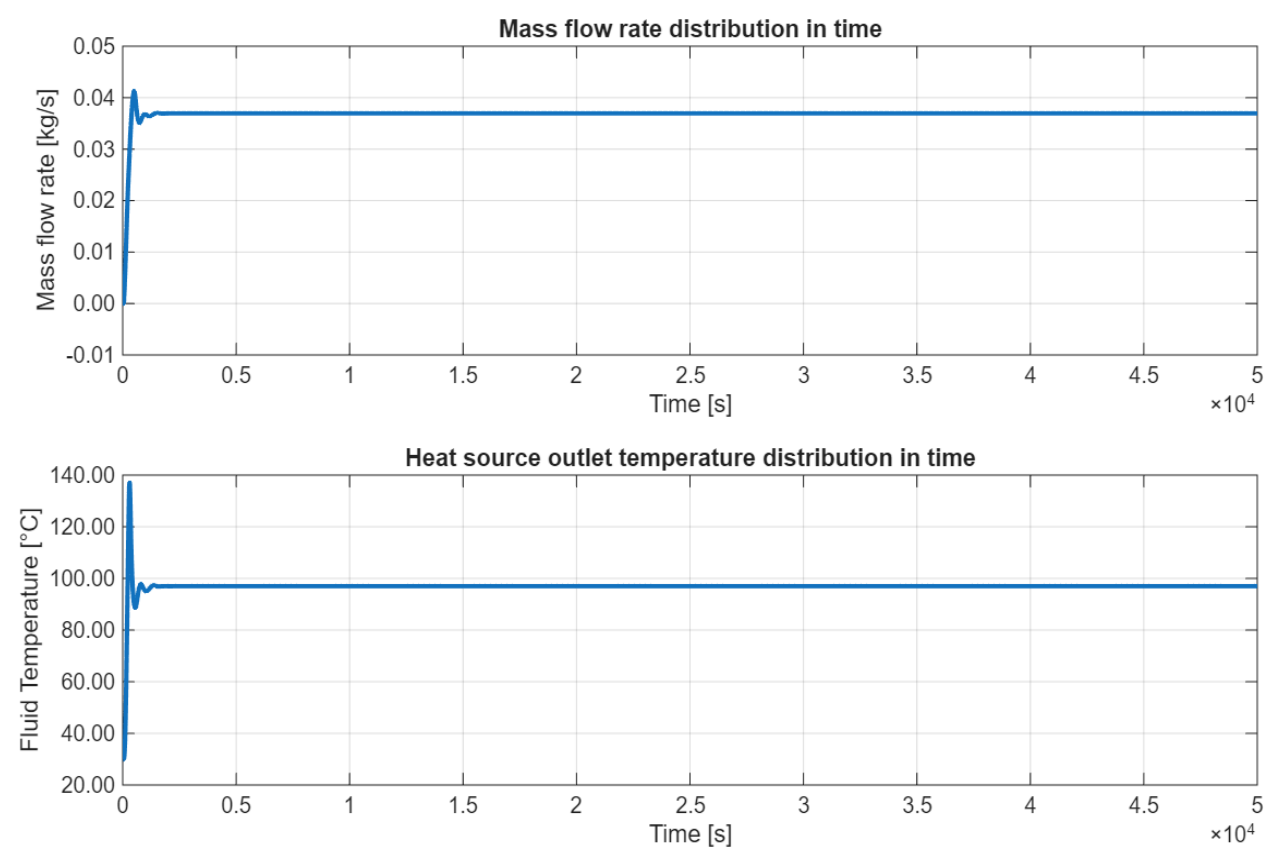


Figure 64. Mass flow rate distribution in time (top) and heat source outlet temperature distribution in time (bottom).

It is possible to notice how the variables reach steady state at around 3000 seconds. To simplify the comparison, MATLAB model included a 1-D model in the heat source.

The evaluation of the extracted mass required a more detailed analysis. For what concerns MATLAB model, its values have been already presented in Eq. (42)-(43)-(44). For ATHLET's results instead, the initial and final values of the loop mass have been retrieved from the output file, along with temperatures. The masses extracted extracted from the output file were 39.52 kg for the initial loop mass and 38.95 kg for the final loop mass. In these values are comprehended the contributes of:

- The four vertical segments (0.86 kg in the initial case and 0.84 from the final value).
- The fluid mass of the CHX nodes not involved in the heat transfer process (0.93 kg in the initial mass and 0.92 kg in the final mass).
- The loop mass in riser and downcomer, in the CHX microchannel involved in the heat transfer mechanism and the mass in the heat source (whose value is showed in *Table 29*).

Table 29 reports the numerical values of the temperatures and mass flow rates with the percentage deviation of the MATLAB variables relative to the ATHLET reference values.

Parameter	MATLAB	ATHLET	Variation [%]
Heat source outlet temperature [°C]	88.93	97.03	8.3
Mass flow rate [g/s]	40.86	36.98	10.5
Initial mass [kg]	38.72	38.59	0.3
Final mass [kg]	38.20	38.03	0.4
$\Delta m [kg]$	0.52	0.56	7.1

Table 29. Comparison between ATHLET and MATLAB results.

The difference in total loop's height are minimum, while the main cause come from the different libraries used for water properties. As a demonstration, *Table 30* shows the values of water density at 30°C and 150 bar retrieved from MATLAB's XSteam and ATHLET's library TAS/TFA (based on "IFC formulation 1967").

XSteam [kg/m ³]	TAS/TFA [kg/m³]
1002.2	997.56

Table 30. Comparison of water densities.

Considering this density difference, it was possible to retrieve a new ATHLET initial mass adding the contribute from properties discrepancies. This contribute is expressed in Eq. (54).

$$\Delta m = \Delta \rho \cdot V = (\rho_{MATLAB} - \rho_{ATHLET}) \tag{54}$$

As final result, the initial ATHLET mass becomes 38.77 kg, compared with 38.73 kg in MATLAB.

6. Conclusions

Natural circulation heat removal systems have become one of the main topics in passive safety systems for NPP. While some plants already implemented this type of systems, many experimental facilities continuously proceeds with the analysis of transient scenarios from natural circulation systems operation.

This master thesis focused on the introduction of the design of a new experimental facility in Politecnico of Turin, set to operate with two single-phase CHX-coupled loops in natural circulation for passive heat removal process. After introducing the geometry and the physics behind the topic, the elaborate presented a series of tests on MATLAB R2025a based on the variation of the operative parameters (for a single loop at first and for the whole system then) as loop's diameter, heat source-sink thermal centers height difference, operative pressure and compact heat exchanger pressure losses. Above all, the compact heat exchanger demonstrated to be the most critical component in the loop. Its pressure losses have the most dominant effects on the results, followed by the height difference between the thermal centers of the heat source and the heat sink. The simulations have also defined specific thresholds and ranges in which the operative imposed requirements are fulfilled. The validation of the tests on a single-loop system has been confirmed by ATHLET code system.

From the performed simulations it has been possible to identify the parameters that mostly affect the operative temperatures and mass flow rates in the loop, along with the least incisive.

The loop diameter is arbitrary in the geometry, but the analysis has shown that its effect on the result is minimum, both for primary-loop-only system and global system..

The operative pressure has no relevant effects on the results, but it sets the saturation temperature in the loop, which has been used as upper limit for the maximum operative temperature in the simulations to maintain single-phase flow.

The height difference between the thermal centers of the heat source and the heat sink plays instead a crucial role. As presented in the model and verified with the simulations, its increase leads to higher mass flow rate and lower values of maximum temperatures in the loop. The limitations in the use of large height differences comes from the structural limits imposed by the construction site.

The thermal power has also shown significant impact on the results. High thermal powers cause the rising of heat source inlet and outlet temperatures, along with mass flow rates. The operative thresholds of this parameter in the elaborate were governed by the necessity to guarantee single-phase flow, keeping the maximum loop temperature below saturation.

Lastly, CHX pressure losses have proved to be the most relevant parameter in the simulations. High pressure losses cause a significant reduction in mass flow rate, with a consequent increase in the heat source outlet temperatures. It is fundamental to keep this parameter as low as possible, in order to reduce the maximum loop temperatures.

This elaborate provides a preliminary study aimed at the design of the experimental facility. The results obtained up to now are promising and demonstrate the feasibility based on the imposed thresholds and parameters. Despite the single-phase flow imposition, the system is expected to operate in both single-phase and two-phase flow. For future studies, an ATHLET's validation regarding the two loops system is fundamental followed by the analysis of the two-phase flow system.

7. References

- [1] Surip W., Putra N. & Antariksawan A. R. (2022). Design of passive residual heat removal systems and application of two-phase thermosyphons: A review. *Progress in Nuclear Energy*, *154*, 104473. https://doi.org/10.1016/j.pnucene.2022.104473
- [2] Pallippattu K. V., Arun K.N. & Naveen K. Single-Phase, Two-Phase and Supercritical Natural Circulation Systems. Woodhead Publishing. Elsevier
- [3] Adinarayana K. N. V., Mangarjuna Rao P. & Ali S. M. (2023). Analysis of coupled two-phase natural circulation loops by developing HEM and DFM based numerical models. *International Journal of Thermal Sciences*, *194*, 108584. https://doi.org/10.1016/j.ijthermalsci.2023.108584
- [4] Adinarayana K. N. V., Mangarjuna Rao P. & Mansoor Ali S. (2024). Numerical investigations on the performance of coupled NCL based passive heat removal system of an IPHWR. *Progress in Nuclear Energy*, *176*, 105378. https://doi.org/10.1016/j.pnucene.2024.105378
- [5] Haag M., Dolganov I. & Leyer S. (2025). Modified Evaporation Model for ATHLET System Code in a Passive Containment Cooling System for Nuclear Safety. *Nuclear Technology*, 211(1), 111–126. https://doi.org/10.1080/00295450.2024.2319933
- [6] Ali S. M., Anumandla S. R. & Singh S. S. (2022). Effect of geometrical and operating parameters on performance of a rectangular two-phase natural circulation loop. *International Communications in Heat and Mass Transfer*, *135*, 106126. https://doi.org/10.1016/j.icheatmasstransfer.2022.106126
- [7] Telkkä J., Riikonen V., Kouhia V., Puustinen M., Pyy L., Räsänen A., Kotro E. & Hyvärinen J. (2024). Experiments on open loop passive cooling of nuclear reactor containment: Quasi-steady-state heat removal, dynamic loads, and feasibility of practical periodic testing. *Nuclear Engineering and Design*, 424, 113317. https://doi.org/10.1016/j.nucengdes.2024.113317

- [8] Dené P., Montout M., Garcia E., Telkkä J., Riikonen V. & David F. (2024). Frequency and amplitude of flashing-induced instability in an open natural circulation loop. *Nuclear Engineering and Design*, 424, 113279. https://doi.org/10.1016/j.nucengdes.2024.113279
- [9] zhang S., Lin W., Meng Z., Sun Z. & Zhang N. (2025). Experimental study on the influence of gas injection on flashing in open natural circulation systems under stable boundary conditions. *Progress in Nuclear Energy*, *180*, 105541. https://doi.org/10.1016/j.pnucene.2024.105541
- [10] Yu J., Zhang Y., Song H., Lu H., Zhao X., Chen P., Su G., Tian W. & Qiu S. (2026). Visualization experiments of the heat transfer and pressure drop characteristics during the particle bed flooding. *International Journal of Thermal Sciences*, *219*, 110245. https://doi.org/10.1016/j.ijthermalsci.2025.110245
- [11] Shi M., Duan Z., Zhao X., Wang Z., Liu S. & Xue H. (2024). Experimental investigation on two-phase flow instability induced by direct contact condensation in open natural circulation. *Energy*, 292, 130547. https://doi.org/10.1016/j.energy.2024.130547
- [12] Kumar B., Soni A. & Singh S. N. (2018). Effect of geometrical parameters on the performance of chevron type plate heat exchanger. *Experimental Thermal and Fluid Science*, *91*, 126–133. https://doi.org/10.1016/j.expthermflusci.2017.09.023
- [13] Kumar H. (1988). Plate Heat exchangers. Hemisphere Publishing Corporation
- [14] Munson B. R., Okiishi T. H., Huebsch W. W., Rothmayer A. P. (2016). *Meccanica dei fluidi* (Cittastudi, Ed.; Prima).
- [15] Jin, Y., Fourspring, P., & Shirvan, K. (2024). Compact steam generator thermal-hydraulic and structural assessment. *Nuclear Engineering and Design*, *428*, 113514. https://doi.org/10.1016/j.nucengdes.2024.113514
- [16] Ferri, R., Achilli, A., Congiu, C., Marcianò, S., Gandolfi, S., Marengoni, M., Bersani, A., & Passerin D'Entreves, A. (2023). ELSMOR European Project: Experimental Results on an Innovative Decay Heat Removal System Based on a Plate-Type Heat Exchanger. *Science and Technology of Nuclear Installations*, 2023. https://doi.org/10.1155/2023/6672504

- [17] Kouhia, V., Riikonen, V., Kauppinen, O. P., Telkkä, J., & Hyvärinen, J. (2021). PASI A test facility for research on passive heat removal. *Nuclear Engineering and Design*, *383*. https://doi.org/10.1016/j.nucengdes.2021.111417
- [18] Montout, M., Herer, C., & Telkkä, J. (2024). PASTELS project overall progress of the project on experimental and numerical activities on passive safety systems. In *Nuclear Engineering and Technology* (Vol. 56, Issue 3, pp. 803–811). Korean Nuclear Society. https://doi.org/10.1016/j.net.2023.08.021
- [19] Deliverable 3.1: PKL & SACO Technical Description & Design Review Report. (n.d.).
- [20] Bertani, C., Bersano, A., de Salve, M., & Sobrero, G. (2021). Experimental analysis of the start-up of a natural circulation loop in single and two-phase flow. *Nuclear Engineering and Design*, 385. https://doi.org/10.1016/j.nucengdes.2021.111532
- [21] Todreas, N. E., & Kazimi, M. S. (n.d.). *Nuclear Systems II Elements of Thermal Hydraulic Design*.
- [22] pid-legend. (n.d.). https://www.edrawsoft.com/pid/images/pid-legend.pdf